THE UNIVERSITY
of EDINBURGH

Modelling Synucleinopathies with Human Neurons Derived from Embryonic Stem Cells Over-expressing α-Synuclein

Ratsuda Yapom

Thesis submitted for the degree of Doctor of Philosophy

The University of Edinburgh

2015

Declaration

I declare that the thesis was composed by me, and the work presented is of my own unless otherwise stated.

The work has not been submitted for any other degree or professional qualification.

Ratsuda Yapom

Acknowledgements

I would like to thank my supervisors, Dr. Tilo Kunath and Prof. Siddharthan Chandran, for giving me the opportunity to undertake this work in their research groups and for their support, guidance and encouragement. Particularly I thank Dr. Tilo Kunath for his kindness and incredible patience with me during writing time. I also thank my committee members, Prof. Peter Brophy and Prof. Josh Brickman, for advice during my first year.

I sincerely thank all the members of my supervisor's lab groups for comments and friendship. In particular, I would like to thank Dr. William Hamilton for assisting with plasmid construction and FACS experiments, Dr. Agnieszka Paca for teaching me Western blotting, Dr. Masumi Nagano for MTS assay and cell culture help. Also thanks to Dr. Bilada Bilican and Dr. Andrea Serio for knowledge transfer and sharing techniques in cell culture and immunocytochemistry. Thanks to David Story for his support and kindness.

Thanks to my collaborators at the Institute of Neurology UCL, Dr. Andrey Abramov and Dr. Sonia Gandhi for help with ROS and cell death assays, and Dr. Michael John Devine for sharing iPS cell lines.

My sincere thanks also go to all of my colleagues at the SCRM, for giving me technical help and friendship. In particular, I would like to thank the Lowell lab group, for giving me antibodies and help with Western blotting. I thank Dr. Guillaume Blin for imaging analysis help. Also I thank Nick Mullin for advice about Western blotting. Tissue culture staff, I thank you for your hard work and help.

Thanks to all the friends I made in SCRM, especially, Dr. Nicola Drummond for friendship, care and love. Dr. Niamh Fanning, I thank you and your family for friendship and kindness; you all made my away-from-home time a happy one.

For my family, I would like to thank you all for your understanding, love and consistent support. Most of all, I would like to thank my mother for her time, love and kindness. She was always there when I needed her.

Finally, I would like to thank the Royal Thai Government Scholarship for giving me the opportunity to study and undertake this research.

Lay Summary

Parkinson's disease (PD) is a common neurological disorder that causes problems in motor control as well as non-motor symptoms, such as dementia. Although the majority of PD cases are sporadic, at least 10% of cases are caused by a genetic defect and therefore inherited. The first mutation identified to cause PD was in a gene named *SNCA*, which makes a protein called α-synuclein (αSyn). This protein is also implicated in dementia with Lewy bodies and multiple system atrophy. Although the first mutation identified in αSyn caused a change of one amino acid, subsequent familial mutations were characterised to be a duplication or triplication of the *SNCA* gene. Patients with *SNCA* triplication mutations were always more severity affected by PD than patients with *SNCA* duplication mutations, such as an earlier age of onset and more rapid progression of disease. This clinical information demonstrated that disease severity is positively correlated with *SNCA* gene copy number.

In an attempt to model this αSyn dose-dependent affect on PD severity with human neurons, I have established a collection of genetically-engineered (transgenic) human embryonic stem cell (hESC) lines that over-express different levels of αSyn. I first showed that elevated αSyn expression does not affect the ability of hESCs to grow in a culture dish, and it does not affect their ability to make neurons when instructed to do so. I identified two transgenic hESC lines with different levels of αSyn expression – one line had high αSyn expression and the second line had normal αSyn expression. I first transformed both lines into forebrain (cortical) neurons using an established method, and then compared the rate of reactive oxygen species (ROS) production in high versus normal αSyn expressing nerve cells. High levels of ROS production indicate unhealthy nerve cells. I observed a significantly elevated level of ROS production in αSyn over-expressing neurons in less mature neurons suggesting they are in an unhealthy state. However, when I examined more mature neurons I did not observe a difference in ROS production between the high and normal αSyn expressing nerve cells. This suggests that either the immature nerve cells had died and were no longer present in later cultures, or they had recovered from the high levels of ROS production and were now producing normal levels of ROS.

Abstract

α-Synuclein (αSyn) is a small intrinsically disordered protein that drives the progression of a group of neurological disorders known of synucleinopathies, including Parkinson's disease, dementia with Lewy bodies and multiple system atrophy. Increased expression of αSyn due to gene duplication or triplication causes familial forms of these diseases, of which the severity is positively correlated with the gene copy number. Despite extensive efforts using various models, the precise mechanisms of αSyn toxicity in neurons have not been elucidated. This could be partly due to biological differences between the models and authentic human neurons.

In an attempt to model synucleinopathies with human neurons, I have established a collection of transgenic human embryonic stem cell (hESC) lines over-expressing αSyn. I first showed that elevated αSyn expression does not affect hESC proliferation and their differentiation potential towards neurons. Then I identified transgenic hESC lines that maintained high αSyn expression in differentiated neurons and compared the rate of reactive oxygen species (ROS) production in high versus normal αSyn expressing cortical neuronal cultures. I observed a significantly elevated level of ROS production in αSyn over-expressing neurons in less mature neurons; however, there was no difference observed in more mature neurons. The possible reasons that lead to this difference are discussed.

This is the first report of stable αSyn overexpressing hESC lines, which can provide an unlimited source of human neurons for studying the mechanism underlying neuronal cell death in synucleinopathies, which in turn could lead to the development of potential therapeutics.

Abbreviations

αSyn	α-synuclein, alpha-synuclein
AD	Alzheimer's disease
AST	Alpha-synuclein triplication (iPS cell line)
ATP	Adenosine triphosphate
βSyn	β-synuclein, beta-synuclein
γSyn	γ-synuclein, gamma-synuclein
BDNF	Brain-derived neurotrophic factor
BMP	Bone morphogenetic protein
cDNA	Complementary DNA
CNS	Central nervous system
DLB	Dementia with Lewy bodies
DMEM	Dulbecco's modified eagle's medium
DNA	Deoxyribose nucleic acid
DTT	Dithiothreitol
EDTA	Ethylenediaminetetraacetic acid
FACS	Fluorescence-activated cell sorting
FCS	Foetal calf serum
FGF2	Fibroblast growth factor 2
GDNF	Glial-derived neurotrophic factor
GFAP	Glial fibrillary associated protein
GFP	Green fluorescent protein
HBSS	Hank's buffered saline solution
hES	Human embryonic stem (cell)
hESC	Human embryonic stem cell
HRP	Horseradish peroxidase
ICM	Inner cell mass
iPS	Induced pluripotent stem (cell)
IRES	Internal ribosome entry site
KSR	Knockout serum replacement media
LBs	Lewy bodies
mES	Mouse embryonic stem (cell)
MPTP	1-methyl 4-phenyl 1, 2, 3, 6-tetrahydropyridine

MSA	Multiple system atrophy
MTS assay	CellTiter 96® AQ_{ueous} One Solution Reagent assay
NAC	Non-amyloid component
NAS	Normal Alpha-Synuclein (iPS cell line)
OCT4	Octamer-binding transcription factor 4, POU class 5 homeobox 1
OTX2	Orthodenticle homologue 2
PAX6	Paired box gene 6
PBS	Phosphate buffered saline
PD	Parkinson's disease
ROS	Reactive oxygen species
RNA	Ribose nucleic acid
RPM	Revolutions per minute
ROCK	Rho-associated protein kinase
RT-qPCR	Reverse transcriptase quantitative polymerase chain reaction
SDS	Sodium dodecyl sulphate
SNARE	Soluble N-ethylmaleimide–sensitive factor attachment protein receptor
SNCA	Synuclein, alpha (non A4 component of amyloid precursor)
SOX7	SRY (sex determining region Y)-box 7
SOX17	SRY-box 17
TGFβ	Transforming growth factor beta
TuJ1	β-III-tubulin antigen

List of Figures

List of Tables

Table of Contents

Chapter 1

Introduction

1.1 Thesis introduction

The protein α-synuclein (αSyn) has gained considerable research interest in recent years due to its strong association with a group of incurable, progressive neurodegenerative diseases collectively known as synucleinopathies. The protein is a major component of LBs (Spillantini et al., 1997), a pathological hallmark of Parkinson's disease (PD) and dementia with Lewy bodies (DLB), and its mutant forms can cause familial PD (Kruger et al., 1998; Polymeropoulos et al., 1997; Singleton et al., 2003; Zarranz et al., 2004). These findings suggest that αSyn may have a key role in governing the mechanism underlying the aetiology and progression of neurodegeneration in these conditions. However, the pathogenic mechanism caused by αSyn has not been fully understood, hindering the development of therapeutic approaches.

Lack of an experimental model that fully recapitulates key features of the diseases is a central problem in this research area. As access to patient tissue is limited, most *in vitro* studies rely on animal tissue, human cancer cell lines or primary cell lines, such as fibroblasts. These models lack either neuronal aspects or human genetic background, which may contribute to failure in manifestation of the disease phenotypes. To sum up, since current available models have not provided a clear understanding of the disease mechanism, the development of new models is needed.

Human embryonic stem (hES) cells are pluripotent cell lines isolated from the inner cell mass (ICM) of blastocysts (Thomson et al., 1998). Their capacity to differentiate into neurons and self-renew *in vitro* presents an unlimited experimental resource to study neurodegenerative conditions at the cellular level. The advantage of hES cells is that they are amendable to genetic modification, providing an opportunity to model genetic forms of synucleinopathies.

This thesis presents transgenic human embryonic stem cell (hESC) lines as a tool for modelling synucleinopathies. Specifically, the focus is on increased WT-*SNCA* expression, which represents one form of genetic PD. In human, *SNCA* triplication or duplication causes

PD inherited in autosomal dominant manner (Ibanez et al., 2004; Singleton et al., 2003). Clinically, the severity of disease is positively correlated with the *SNCA* gene dosage (Fuchs et al., 2007); however, this correlation has not been proven *in vitro*. Induced pluripotent cell (iPS) cells derived from patients with *SNCA* triplication recently have been established (Devine et al., 2011). However, whether the models exhibit disease phenotypes remains to be elucidated. Also, like other forms of PD, the pathogenesis caused by increased WT-*SNCA* is poorly understood.

Employing random insertional transgenesis using plasmid DNA, a set of clonal transgenic Shef4 hESC lines constitutively expressing different levels of αSyn were established. The models were evaluated for differentiation potential toward cortical neurons and phenotypes were investigated by determining levels of reactive oxygen species (ROS) production and cell death. The analyses revealed promising results supporting the potential of the models to be very useful in PD research in the future. To my knowledge, this is the first demonstration of the use of transgenic *SNCA*-hESC lines as a tool for modelling synucleinopathies *in vitro*. However, as some limitations were encountered, the thesis suggests future experiments to be undertaken to get more out of the models and ways to overcome these limitations.

The thesis begins with a chapter of literature review of the protein αSyn and its association with synucleinophaties. The later part of the chapter reviews the technology of random insertional transgenesis of hES cells using plasmid DNA, and a brief summary of currently used protocols for *in vitro* neural differentiation of hES cells. Chapter 2 describes materials and methods used in the research. Chapter 3 presents data on the generation of transgenic Shef4 hESC lines, which begins with construction of the expression plasmids. When the transgenic Shef4 hES cell lines were obtained, they were characterised for *SNCA* expression, gene silencing during hESC propagation, and rate of cell proliferation. Chapter 4 presents further characterisation of the transgenic lines and phenotypic analysis of neurons derived from selected transgenic hES cell lines. The characterisation includes neural differentiation potential and transgene expression during neural differentiation. The later part of this chapter presents ROS production and cell death analysis of neurons derived from selected transgenic hESC lines. The final chapter discusses limitations of the work and future experiments to further evaluate the models. It also suggests how to get the most out of the current models and ways to construct improved versions to overcome some of the limitations presented.

1.2. Thesis hypothesis and aims

I aim to answer the question of whether transgenic hESC lines stably over-expressing αSyn can be used to generate neurons for modelling synucleinopathies.

My hypothesis is that αSyn over-expressing hES cells can efficiently differentiate into neurons and will exhibit elevated ROS production and cell death, which is part of the pathogenic phenotype of synucleinopathies.

Aims:

1. To establish a collection of transgenic hESC lines with different levels of *SNCA* expression.
2. To characterise the transgenic hESC lines by means of
    a. The stability of transgene expression during hESC propagation and during neural differentiation.
    b. The impact of increased *SNCA* expression on differentiation potential towards the neural lineage.
3. To produce cortical neurons from the transgenic hESC lines.
4. To investigate ROS production and cell death in the neurons derived from the transgenic hESC lines.

1.3 αSyn gene and protein

1.3.1 Discovery

In 1980, antiserum against highly purified cholinergic vesicles extracted from electric rays was generated and shown to bind synaptic vesicles (Carlson and Kelly, 1980). In an attempt to identify the gene encoding the synaptic-specific protein, the serum was used to screen a cDNA expression library generated from electromotor nuclei of *Torpedo californica* (Maroteaux et al., 1988). Using this approach, a neuron-specific gene was identified, and further immunostaining showed its protein product to be localized on the nuclear envelope and presynaptic nerve terminal. This unique expression pattern led the authors to name it synuclein.

In 1993, a protein precursor of Non-Aβ-Amyloid Component (NAC), a component of amyloid plaques of Alzheimer's disease (AD) was identified, and named NACP (Ueda et al., 1993). NACP and αSyn were known to be the same protein when synucleins were identified in human. Human α- and β-synuclein (βSyn) were first isolated from human brain samples with sizes of 134 and 140 amino acids, respectively (Jakes et al., 1994) whereas γ-synuclein (γSyn) was identified later with size of 127 amino acids (Ji et al., 1997).

1.3.2 Protein structures and domains

The synuclein family is currently classified into 3 groups; α-, β-, and γSyn. The proteins are characterised by imperfect repeats, which have a core consensus of KTKEGV present mainly in a highly conserved N-terminus. The acidic C-terminal domain is divergent, and this distinguishes each synuclein member (Figure 1.1A). Human αSyn is more closely related to βSyn than to γSyn (Figure 1.1B and Figure 1.1C).

αSyn can be divided into 3 major domains; amphipathic domain, NAC region (residues 61-95) and acidic tail. Only the first two domains participate in formation of α-helical structures when interacting with lipids whereas the acidic part stabilizes the binding. NAC domain, known as a component of amyloid plaques, has an essential role *in vitro* fibrillization of αSyn (Giasson et al., 2001). The domain contains a hydrophobic stretch of 12 amino acids (residues 71-82), of which deletion abolishes αSyn fibrillization.

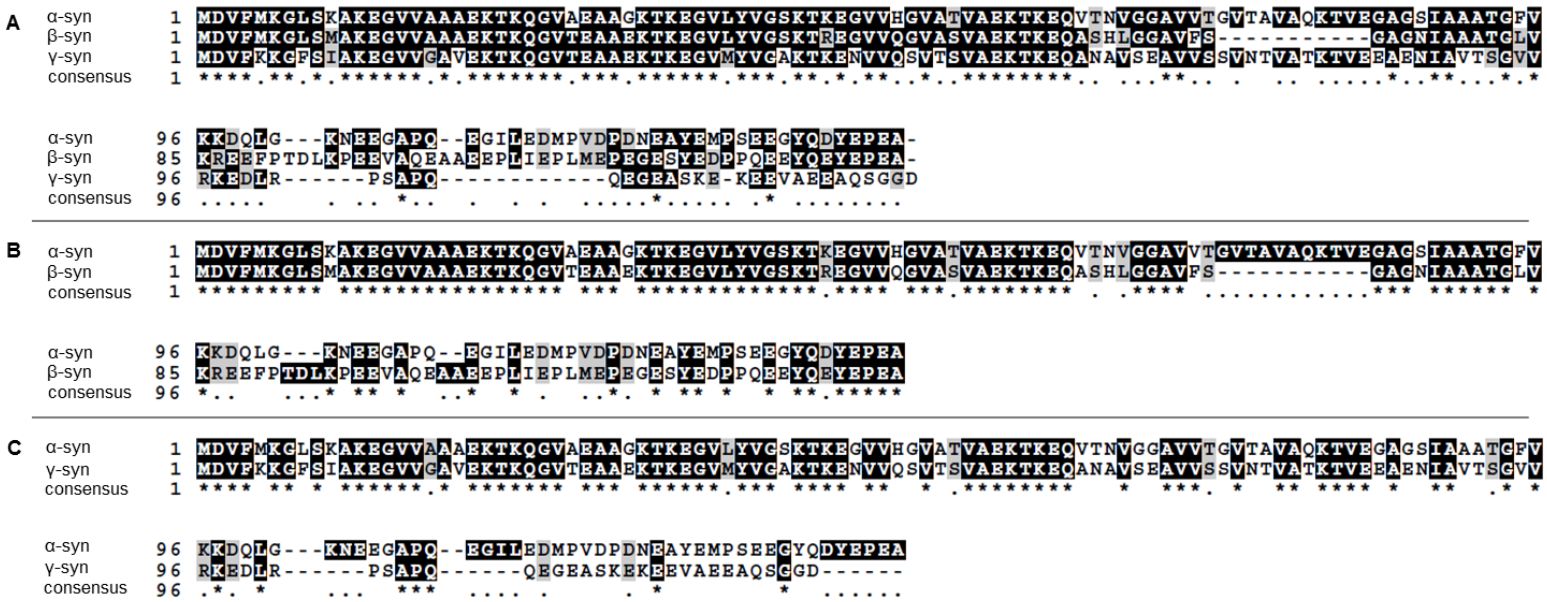

Figure 1.1 Amino acid sequence alignments of human synucleins.

A) α-, β- and γ-synucleins

B) α- and β-synucleins

C) α- and γ-synucleins

Box shaded as black and grey indicate consensus sequences in all three and that in two classes of synucleins, respectively. Note that the N-terminus is conserved among the synucleins, and that αSyn is more related to βSyn than to γSyn.

Due to its association with synaptic vesicles, αSyn was believed to bind to vesicle membranes as part of its normal function. Upon binding to lipid, αSyn acquires α-helical structure from residues 9-89, which includes the 7 imperfect repeats of 11 amino acids (Figure 1.2A) (Alderson and Markley, 2013). The amino acids in this region form an amphipathic α-helix with polar and charged amino acids on one face of the helix and apolar amino acids on the opposite face (Figure 1.2B). The polar face is exposed to the aqueous environment of the cytosol while the apolar face interacts with hydrophobic lipid tails of the phospholipid bilayer. The lysine residues in the repeat domains reside at the polar-apolar interface, interacting with lipid head groups of the phospholipid bilayer.

Based on studies using membrane mimics, two helical conformations of αSyn have been proposed; the two broken helices and a single extended helix. The conformations of αSyn are affected by the size and content of membrane, and solution condition. It is likely that membrane size affects αSyn conformation as it determines the curvature of membrane surface. When binds to membrane with more curvature, such as a micelle, αSyn exists as a broken-helix (Figure 1.2C). However, with larger and less curvature membrane, such as vesicle, αSyn adopts a single extended helix (Alderson and Markley, 2013). Similar to membrane size that influence αSyn conformation via determining the curvature of membrane, lipid content and SDS concentration determines the shapes of micellar SDS to be either high-curvature spherical or low-curvature cylindrical micelles (Ferreon et al., 2009; Georgieva et al., 2010). Moreover, with a certain range of ratio of lipid- or SDS-to-protein (αSyn), αSyn can interconverts between the two conformations, which results in coexisting of broken-helix and extended helix conformations (Ferreon et al., 2009; Georgieva et al., 2010). This conformational conversion of αSyn may mediate its function on vesicle fusion (Georgieva et al., 2010).

Apart from lipid-bound, free αSyn has been studied extensively (Alderson and Markley, 2013). Initial studies agreed that αSyn was intrinsically disordered existing mostly as random coils and lack of secondary structure in solution. However, later studies demonstrated that free αSyn can partially fold, having internal interaction between residues in the N- and C-termini. A recent controversial proposal is that αSyn exists natively as tetramer conformation, (Bartels et al., 2011).

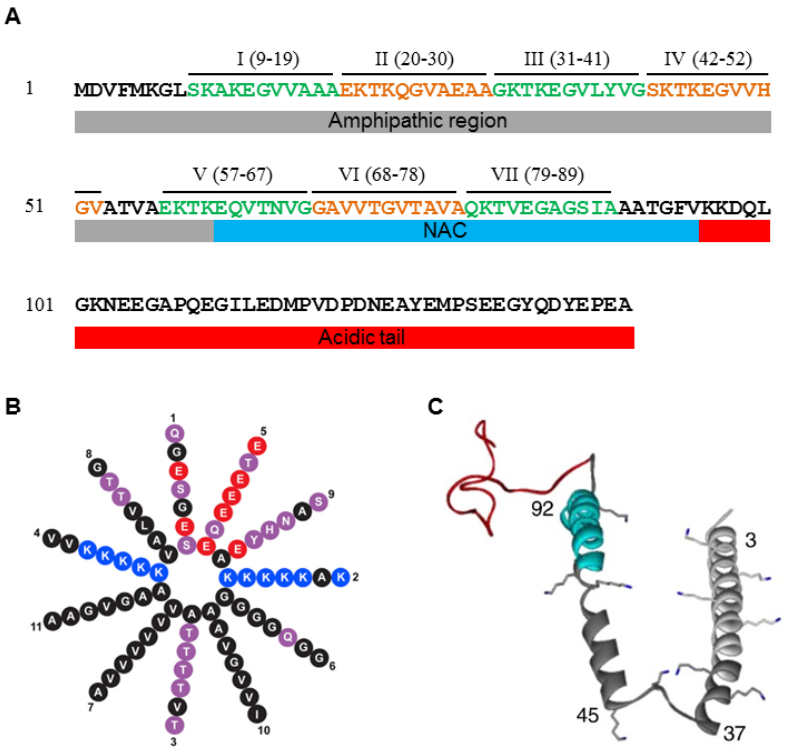

Figure 1.2 Amino acid sequences, domains and a proposed structure of human αSyn.

A) Amino acid sequences and domains. The 7 imperfect repeats of 11-amino acids are highlighted in orange and grenn. Each repeat is given a Roman numeral. The shaded boxes under the sequences indicate 3 domains of the protein; the amphipathic domain (grey), NAC (light blue), and the acidic domain (red). (Adapted from Anderson and Markley, 2013).

B) The α-helical wheel of the 7 imperfect repeats. The wheel is separated radially into a polar domain and a hydrophobic domain by lysine residues. The polar domain is proposed to face the cytosol whereas the other is buried in the hydrophobic environment of the phospholipid bilayer. The positively charged residue, lysine, is believed to bind to the negatively charged head groups of the bilayer. Numbers indicate positions within the repeats. Colours indicate properties of the amino acid side chains; blue: basic, red: acidic, purple: polar uncharged, black: nonpolar. (Adapted from Bendor et al., 2013).

C) Two broken-helical structure of αSyn. While binding to micelles, αSyn adopts two anti-parallel helices, which are formed by the amphipathic domain and NAC. The colours correspond to protein domains shown in A). (Adapted from Pfefferkorn et al., 2012).

1.3.3 Expression of αSyn

αSyn is encoded by the gene *SNCA* located on chromosomes 4q22.1 (Chen et al., 1995). It is well documented that αSyn is enriched in the brain. Purified human αSyn is present in the cytosolic fraction of the brain homogenate with apparent molecular mass of approximately 19 kDa (Jakes et al., 1994; Ueda et al., 1993), which is higher than a calculated molecular mass, ~14.7 kDa (Jakes et al., 1994). The higher apparent molecular mass is believed to be caused by the negatively charged carboxyterminal of the protein (Jakes et al., 1994).

Beside intense expression in the brain, αSyn is also distributed in other tissues. *SNCA* mRNA is detected in a significant level in placenta, low level in kidney, heart, lung, red blood cells and skeleton muscle and no detectable in liver (Scherzer et al., 2008; Ueda et al., 1993). The protein is also observed in sensory system during early mouse embryonic development (Zhong et al., 2010).

In human, αSyn is detected as early as 11-week gestation in cortical plate whereas in mouse, the protein is found at E9.5 in the midbrain/hindbrain junction (Raghavan et al., 2004; Zhong et al., 2010). Zhong and colleagues show that in various regions of the embryonic mouse brain, αSyn expression follows a spatio-temporal pattern that matched the neuronal migratory pathway and the formation of synaptic connections (Zhong et al., 2010). For example, in cerebral cortex, where neuron migration happens during preplate division into two discrete layers; marginal zone (MZ) and subplate (SP), αSyn, which is initially detected at E12.5 in preplate, is sequentially expressed strongly in MZ and SP, where synapses are formed (Zhong et al., 2010). The results are consistent with a steep increase of αSyn when synaptophysin is increasing. This interval coincides with redistribution of the protein from neuronal cell body to the nerve terminal (Hsu et al., 1998).

During early brain development, αSyn exhibits dynamic subcellular localisation (Zhong et al., 2010). In early embryonic stages of mouse, the protein is found in the nuclei as well as in the cytoplasm and the processes of neurons. Then, in later stages, most of the αSyn is localized in the non-nuclear compartments (Raghavan et al., 2004; Zhong et al., 2010). Consistent with this, developing human brain also exhibited changes of αSyn subcellular localisation (Raghavan et al., 2004).

Nuclear localisation of the αSyn suggested that it might have a transcriptional regulatory role in neuronal nuclei. It is worth nothing that nuclear and cytoplasmic αSyn seems to have

different molecular structures (Yu et al., 2007; Zhong et al., 2010). Yu and colleagues have generated two antibodies that recognised different epitopes of αSyn (Yu et al., 2007). Both antibodies can detect nuclear and cytoplasmic αSyn by western blotting. However, only one of them can detect nuclear αSyn by immunofluorescence. The results implied that nuclear αSyn may have a structure that limits access of the antibody to the epitopes, which were revealed by denaturing in western blotting (Yu et al., 2007).

1.3.4 Physiological function of αSyn

Neurotransmission and synaptic plasticity

While presynaptic localization of αSyn is well documented, its function on this site is not as dramatic as expected. Mice lacking αSyn exhibited normal basic synaptic function with minor neurological deficits (Abeliovich et al., 2000; Cabin et al., 2002; Chandra et al., 2004). αSyn is only required for some synaptic activities in particular circumstances, for example, in response to extensive stimulations or during aging (Burre et al., 2010; Cabin et al., 2002), and may work redundantly with the two other synucleins (Chandra et al., 2004; Vargas et al., 2014).

αSyn appears to be implicated in modulating the nigrostriatal dopamine system. αSyn alone or together with βSyn was demonstrated to be required for maintaining normal DA levels in the striatum. In one study, αSyn null mice displayed a reduction in nigrostriatal DA (Abeliovich et al., 2000) whereas similar result was observed only in double αSyn/ βSyn knockout mice, but not in individual αSyn or βSyn knockout mice (Chandra et al., 2004); thus, suggesting functional redundancy of these two synucleins. As there was no change in the degradation rate of DA, it was likely that a reduction of DA level was a result of decreased synthesis or storage (Abeliovich et al., 2000; Chandra et al., 2004). Moreover, neurons lacking αSyn exhibited increased DA release in response to paired stimuli; thus, suggesting an inhibitory role of αSyn in DA release under this condition (Abeliovich et al., 2000).

Several mechanisms have been proposed to explain how αSyn may modulate the DA system. αSyn has been implicated in regulating synaptic vesicle biology, including vesicle endocytosis, exocytosis, and trafficking. During vesicle exocytosis to release neurotransmitter, αSyn promotes SNARE complex assembly. Deletion of CSPα resulted in inhibition of SNARE complex assembly, which could be rescued by transgenic expression of

αSyn (Chandra et al., 2005). A recent study further demonstrated that αSyn promotes SNARE complex assembly by direct binding to a SNARE-protein synaptobrevin2/ vesicle-associated membrane protein2 (VAMP2) (Burre et al., 2010). Sustaining SNARE complex assembly by αSyn appeared important for neurological function during aging, but not in early development. Triple-knockout of all synucleins caused severe neurodegeneration in aging mice, which subsequently died prematurely. These animals did not have an obvious phenotype when they were young, despite a significant reduction in SNARE complex assembly (Burre et al., 2010).

αSyn may regulate neurotransmission by modulating synaptic vesicle endocytosis, which is a process for vesicle recycling at presynaptic nerve terminals. Recent studies demonstrated that αSyn enhanced synaptic vesicle endocytosis. (Ben Gedalya et al., 2009; Vargas et al., 2014). In this process, synucleins work redundantly, by which individual expression of each synuclein member could rescue defective endocytosis in triple synuclein-null neurons (Vargas et al., 2014) .

αSyn may modulate neurotransmission by altering release probability of neurotransmitters. More specifically, αSyn may regulate the number of vesicles available for neurotransmitter release by governing the mobilization of synaptic vesicles from reserve pool to readily releasable pool, for example, by controlling the size of reserve pool and/or resting pool (Cheng et al., 2011). Suppression of αSyn using antisense oligonucleotides in rat hippocampal neurons resulted in significant reduction in distal synaptic vesicle pool without affecting docked vesicles (Murphy et al., 2000). Similar results were observed in the hippocampal neurons of αSyn-deficient mice (Cabin et al., 2002).

Brain lipid metabolism and mitochondrial functions

αSyn may modulate turnover and incorporation of fatty acid in brain phospholipids (Golovko et al., 2007). In mice lacking αSyn, incorporation rates of two major Polyunsaturated Fatty Acids (PUFA) in the brain is altered (Golovko et al., 2005; Golovko et al., 2007). Consistent with this, another study showed that loss of αSyn leads to alterations in fatty acid content and metabolism of brain phospholipids, and in biophysical properties of cellular membranes (Ellis et al., 2005) .

Interestingly, lack of αSyn also resulted in decreased cardiolipin, a mitochondrial membrane associated phospholipid, while other major phospholipids were unchanged (Ellis et al., 2005). Moreover, the mice exhibited impaired complex I/III function. Taken together with the fact that cardiolipin is enriched in the mitochondrial inner membrane, where electron transport takes place, the results suggest that αSyn may affect the function of the electron transport chain. Indeed, it has been demonstrated that αSyn is associated with mitochondrial membrane in basal conditions (Devi et al., 2008a; Li et al., 2007) . Its interaction with mitochondria is believed to occur via a direct binding to cardiolipin (Nakamura, 2013). However, the detailed function of αSyn in mitochondria is still mostly unknown.

1.3.5 Link to disease

In 1993 Ueda et al. identified a component of Alzheimer's amyloid plaques to be αSyn, known as NAC precursor (NACP) at the time (Ueda et al., 1993). It raised the question of whether αSyn was involved in other neurodegenerative diseases. In 1997 Polymeropouros and colleagues demonstrated for the first time that a point mutation in the *SNCA* gene is linked to a familial form of Parkinson's disease (PD) (Polymeropoulos et al., 1997). This work suggested αSyn could initiate or potentiate the pathogenesis of PD. This hypothesis is supported by the finding that αSyn is a major component of Lewy bodies (LBs), a pathological hallmark of PD. Spillantini and colleagues showed that LBs from PD and DLB could be identified using antibodies raised specifically against αSyn (Spillantini et al., 1997), which later replaced the conventional methods relying on staining for ubiquitin and neurofilament. After that, detailed descriptions of αSyn aggregates in LBs (Baba et al., 1998; Spillantini et al., 1998), and more mutations in *SNCA* have been reported (Fujioka et al., 2014). Currently, it is known that aggregated αSyn is also a component of multiple pathological structures in several neurological conditions.

1.4 Synucleinopathies

1.4.1 Description and common pathologies

Synucleinopathies is a group of progressive neurodegenerative disorders, which share common pathological lesions characterized by αSyn aggregates in neurons and glia. Parkinson's disease (PD), DLB and multiple systems atrophy (MSA) are common synucleinopathies, which mainly affect the aging population. Despite common αSyn pathology, they differ in the affected brain regions and neural cell types, which results in different clinical symptoms.

αSyn pathology is present in various forms in different locations within the cell or even extracellular locations. LBs, the histological hallmark of PD and DLB, are in the cytoplasm of neurons, but can be extracellular, whereas glial cytoplasmic inclusions (GCIs) are found primarily in oligodendrocytes of MSA. LBs can be classified into 2 types; classical brainstem LBs, which have dense core and halo, and less-defined structure cortical LBs. These αSyn deposits are present in variable density with different distribution patterns in the brain.

Parkinson's disease (PD)

PD is the most common neurodegenerative movement disorder clinically characterized by a failure in movement control including resting tremor, bradykinesia, rigidity and postural instability. In addition to motor symptoms, PD patients also manifest non-motor symptoms, such as cognitive dysfunction and sleep disturbance (Jankovic, 2008). Dementia is common in severe cases, which could lead to misdiagnosis of DLB. To distinguish PD with dementia (PDD) from DLB, a diagnosis of PDD is only given to PD patients whose dementia develops at least one year after parkinsonism motor symptoms begin. However, recent consensus criteria suggest using the collective term Lewy body disease to describe PDD, and DLB, since they are on the same spectrum of disease (McKeith et al., 2005).

Pathologically, PD is characterized by the loss of dopaminergic neurons in the nigrostriatal pathway, which is important for motor function, and the presence of brainstem LBs. However, as the disease progresses, LBs are also present in the cerebral cortex (Braak and Del Tredici, 2009) (Figure 1.3C-D).

Dementia with Lewy bodies (DLB)

DLB is the second most common neurodegenerative dementia after AD. It is clinically characterized by progressive dementia with three core features including fluctuating cognition, recurrent visual hallucination and spontaneous parkinsonism.

The pathological hallmark of DLB is LBs (Figure 1.3E-G), which spread in variable regional patterns and can be pathologically classified into brainstem predominant, limbic or transitional, and diffuse neocortical type pathology (McKeith et al., 2005). The incidence of limbic and diffuse neocortical type pathology is much higher than the brainstem predominant type (Fujishiro et al., 2008; Weisman et al., 2007). AD lesions in the form of senile plaques

and neurofibrillary tangles are frequently present in the cortical region, limbic area, and amygdala. However, the topographic stages of the lesions do not fit with DLB clinical symptoms. Studies showed that clinical features of DLB are positively correlated with Lewy-related pathology, and inversely related with the severity of AD pathology (Fujishiro et al., 2008; Merdes et al., 2003).

Multiple system atrophy (MSA)

MSA is a progressive neurodegenerative disease with oligodendroglial degeneration. The clinical manifestations include cerebellar and paramidal dysfunction (ataxia), parkinsonism and autonomic dysfunction.

Accompanied with neurodegeneration in brainstem, olivopontocerebellar, striatonigral, and autonomic systems, pathological characteristic of MSA is αSyn -immunoreactive GCIs in oligodendroglia (Papp et al., 1989; Papp and Lantos, 1994). Not uncommon, abnormal αSyn aggregates are also present in the nuclei of glia, cytoplasm (NCIs) and nuclei (NNIs) of neurons, and dystrophic neurites (Figure 1.3A-B) (Papp and Lantos, 1994; Yoshida, 2007). GCIs are widely distributed throughout the central nervous system, especially in the white matter, where most affected areas include paramidal, extraparamidal, limbic and corticocerebellar, and the supraspinal autonomic system (Papp and Lantos, 1994; Yoshida, 2007).

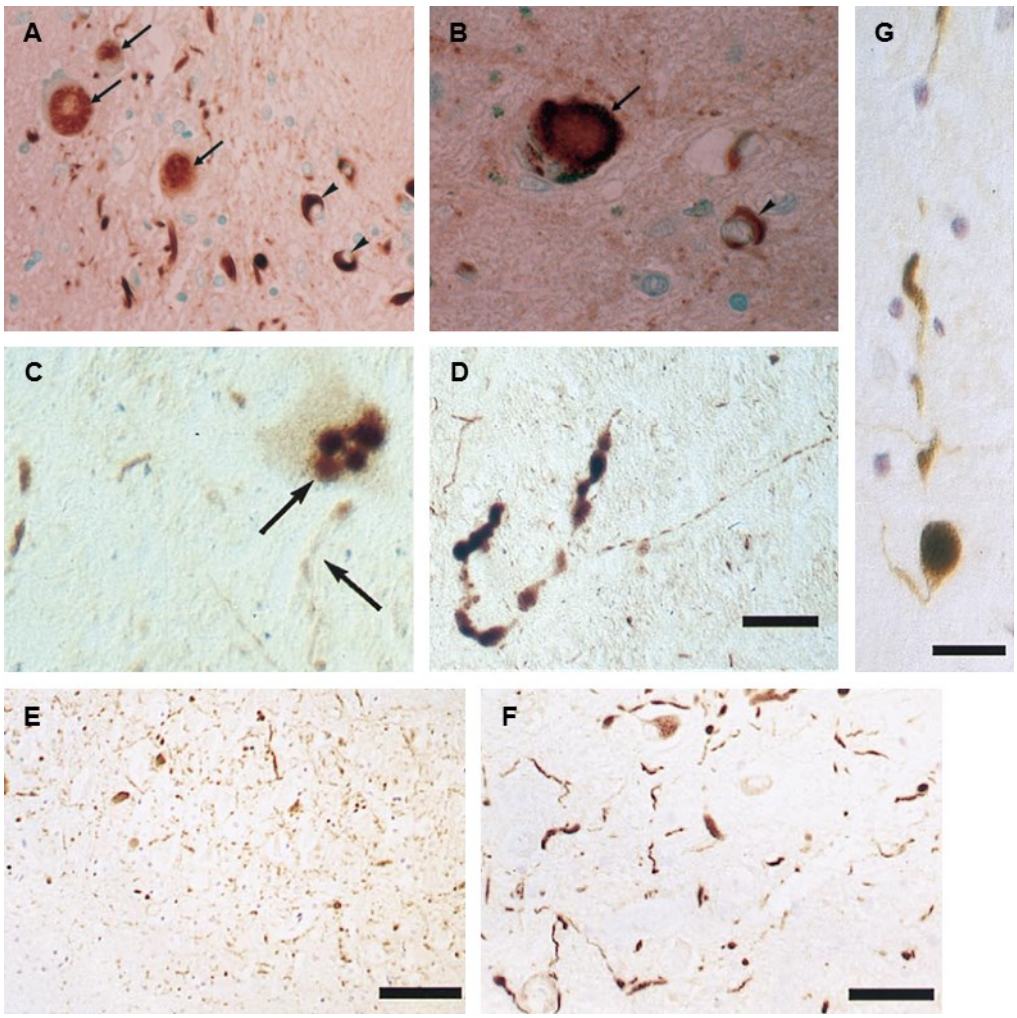

Figure 1.3 Pathological αSyn aggregates in MSA, PD and DLB.

A) - B) Brain tissues from patients with MSA immunostained for αSyn. αSyn-immunoreactive GCIs (arrowheads) and neuronal intracytoplasmic inclusions (arrows) in substantia nigra (A) and pontine nucleus (B). (Adapted from Wakabayashi et al.,1998).

C) - D) Substantial nigra from patients with PD immunostained for αSyn. Lewy neurites and a nerve cell with four cytoplasmic LBs. Scale bars are equivalent to 30 µm in C and 90 µm in D. (Adapted from Spillantini et al., 1998).

E) -G) Brain tissues from patients with DLB immunostained for αSyn. αSyn-immunoreactive LBs and Lewy neurites in hippocampus (E) and substantia nigra (F and G). Scale bars are equivalent to 80 µm in E, 100 µm in F and 40 µm in G. (Adapted from Spillantini et al., 1998).

1.4.2 *SNCA* Point mutation cases

In the last 20 years, several missense mutations in the *SNCA* gene have been identified (Table 1.1). The A53T, A30P and E46K missense mutations were identified first, and are well recognized to cause rare forms of autosomal dominant inherited PD (Kruger et al., 1998; Polymeropoulos et al., 1997; Zarranz et al., 2004).

The first mutation, A53T, was identified in two large kindreds descending from the same ancestors in Italy, and in three Greek kindreds (Polymeropoulos et al., 1997). A single nucleotide substitution at position 209 from G to A results in amino acid change from alanine to threonine at amino acid residue 53. The mutation segregates with PD phenotypes with 85% penetrance. Patients with this mutation had clinical features similar to sporadic PD except with an early age of onset (average 46 years), and a rapid disease progression (Polymeropoulos et al., 1997).

A year later, the A30P mutation was identified in a family of German origin (Kruger et al., 1998). The average disease age onset caused by the mutation (59.7 years) is slightly younger than idiopathic PD, but with a similar rate of progression, suggesting a milder phenotype than the A53T mutation (Kruger et al., 2001; Kruger et al., 1998).

Unlike the first two mutations, the E46K mutation causes phenotypes resemble DLB except that dementia develops in two or more years after disease onset (Zarranz et al., 2004). The affected individuals manifested parkinsonism, dementia, and visual hallucinations of variable severity. Postmortem examination revealed atrophy of the substantial nigral and numerous LBs in cortical and subcortical area, which is consistent with DLB (Zarranz et al., 2004).

Other recently identified mutations include H50Q, G51D and A53E mutations (Appel-Cresswell et al., 2013; Kiely et al., 2013; Lesage et al., 2013; Pasanen et al., 2014; Proukakis et al., 2013) (Table 1.1). The mutations caused rare forms of hereditary autosomal dominant PD.

Animal models have confirmed the toxicity of the A53T, A30P, and E46K mutations as reviewed by Dawson T. et al. (Dawson et al., 2010). Moreover, *in vitro* studies demonstrated that the mutations cause secondary structural changes and altered physicochemical properties of the protein. For example, the A53T mutation accelerates

Table 1.1 Clinical and pathological characteristics of familial PD caused by missense mutations of *SNCA*. (Adapted from Fujioka et al., 2014).

Mutation	AAO/MDD (years)	Clinical phenotype	Pathology	Reference
A30P	54–76	PD (sustained response to L-dopa therapy), hallucination[a]	LB, Tau	Krüger et al. 1998, Krüger et al. 2001
E46K	50–69	PD, cognitive impairment, visual hallucination[a], REM sleep behaviour disorder	LB	Zarranz et al. 2004
H50Q	60–71/12	PD, cognitive impairment, psychiatric symptoms	LB, Tau	Appel-Cresswell et al. 2013, Proukakis et al. 2013
G51D	19–60/11	PD (early-onset, rapidly progressive), pyramidal signs, psychiatric symptoms	LB, Tau, TDP-43	Lesage et al. 2013, Kiely et al. 2013
A53E	32-62/ 24	Atypical PD (early-onset), MSA, profound spasticity, myoclonic jerks, anxiety, panic disorder	LB , TDP-43, GCIs	Pasanen et al. 2014
A53T	20–85/12	PD (early-onset, rapidly progressive), dementia, dysautonomia[a], myoclonus[a], psychiatric symptoms[a]	LB , Tau , TDP-43	Polymeropoulos et al. 1997

AAO, age at onset; MDD, mean disease duration; LB, Lewy body; MSA, Multiple system atrophy; GCIs, glial cytoplasmic inclusions

[a]Uncommon in sporadic PD.

fibril formation of the protein *in vitro* (Conway et al., 2000b). Unlike A53T, the A30P αSyn mutant has a slower fibrillization rate but exhibits rapid formation of spherical oligomers (Conway et al., 2000a). These structural alterations would interfere with normal physiological functions of the protein as well as confer gain-of-function toxicity.

1.4.3 *SNCA* Multiplication cases

In 1998, Muenter et al. described the pathological and clinical characteristics of the autosomal dominant hereditary parkinsonism with dementia in a family known as "the Iowa kindred" (Muenter et al., 1998). This hereditary PD is markedly characterised by severe parkinsonism, very young age onset, rapid disease progression and dementia. Neuropathological examination revealed profound pathology including severe degeneration of the substantia nigra, of which one autopsy had more that 90% nerve cell loss, wide spread occurrence of subcortical and cortical LBs, vacuolation of the cortex in the temporal lobe, and unusual nerve cell loss in the hippocampus. Five years later, Singleton and colleagues demonstrated co-segregation of heterozygous *SNCA* triplication with parkinsonism in affected members in this family (Singleton et al., 2003). Expression of all four *SNCA* alleles resulted in a doubling in amount of α-syuclein protein and mRNA in blood and brain of the affected members (Farrer et al., 2004; Miller et al., 2004). One year later, *SNCA* triplication was reported in an unrelated Swedish-American descent family with comparable neuropathology and clinical features to that of the Iowa kindred (Farrer et al., 2004). Early ages of disease onset, dementia and cornu ammonis 2/3 hippocampal degeneration were common features of this form of PD (Farrer et al., 2004).

Ibáñez et al. identified *SNCA* heterozygous duplication in two PD patients with familial history of PD (Ibanez et al., 2004). Compared to the triplication cases, these patients had later ages of disease onset (46 and 56 years), subtle clinical features, such as mild parkinsonism and mental impairment without any atypical symptoms. Disease progression is slow considering that their mothers, who were also reported to have parkinsonism, survived until the age of 80 years.

These observations suggested that clinical features might be influenced by the *SNCA* gene dosage; the more *SNCA* alleles, the more severe symptoms would be. Nonetheless, there was a concern of whether *SNCA* was indeed a causative gene of the disease phenotype. In other words, the phenotype severity might depend on other genes within the multiplied region. Regarding this concern, there is a report on a family with *SNCA* duplication, of which the

multiplication region contains no other genes but *SNCA*. PD in this family is autosomal dominant inherited, and has phenotype similar to idiopathic PD. This finding proved that multiple copies of *SNCA* alone can cause PD (Ibanez et al., 2009).

To investigate the relationship between *SNCA* dosage and clinical severity, direct comparison of the disease manifestation between affected families was difficult in early time due to variation in genetic background and multiplication region. However, when more cases of familial *SNCA* multiplication were reported, the notion of *SNCA* dosage effect on disease phenotypes appeared to be true. Fuchs et al. investigated clinical phenotype of a carrier of *SNCA* triplication and that of *SNCA* duplication, all carriers shared the same region of genetic multiplication (Fuchs et al., 2007). The probands were from two kindreds that were inherited the multiplied genetic region from a common ancestor known as the "Lister family complex". As expected, a proband with *SNCA* triplication had more severe clinical features than that with duplication.

Similar to the Lister family complex descents, *SNCA* gene dosage effect was demonstrated in a large Japanese family, of which the members carried heterozygous *SNCA* duplication (3 alleles of *SNCA*) or homozygous *SNCA* duplication (4 alleles of *SNCA*) (Ikeuchi et al., 2008). Gene multiplication this family occurred within the same genetic region due to consanguineous marriage. The proband with homozygous *SNCA* duplication showed similar clinical manifestations to that of *SNCA* triplication, and manifested more pronounce phenotypes than the heterozygous probands.

Moreover, disease penetrance caused by *SNCA* triplication is clearly higher than that caused by duplication (85% vs 33-50%) indicating increased aggressiveness of *SNCA* triplication compared to *SNCA* duplication (Muenter et al., 1998; Nishioka et al., 2009).

Genetic background and environmental factors are likely to have considerable contribution to the phenotype of this form of PD (Nishioka et al., 2009). In *SNCA* duplication cases, clinical manifestations variable between the carriers including no symptoms, parkinsonism, MSA, PDD, and DLB (Fuchs et al., 2007; Ibanez et al., 2009; Nishioka et al., 2009; Uchiyama et al., 2008). Some *SNCA* duplication carriers did not show any sign of parkinsonism despites their ages were beyond the mean age of disease onset (Ibanez et al., 2009; Nishioka et al., 2009). Ages of disease onset are also considerably variable among affected individuals (Ibanez et al., 2009). The number of genes in genetic multiplied region or the size of multiplication is unlikely to correlate to the age of disease onset as two

asymptomatic individuals were identified in a family, of which duplication region was estimated to contain 23-25 genes within a region of approximately 3.5 Mb (Ibanez et al., 2009).

1.4.4 Effect of αSyn on cellular ROS production

Oxidative stress is an imbalance state of ROS production and cellular detoxification (Dias et al., 2013). When the level of ROS is beyond the ability of cell to cope with, the cell is under oxidative stress. Oxidative stress could lead to damage to cellular components. Moreover, feed-forward scenarios could happen when the damage occurs to a key cellular pathogenic protein that in turn causes more ROS production (Dias et al., 2013).

The link of oxidative stress and neurodegeneration is suggested by the evidence of oxidative damages in the SNs of PD patients. These damages include the increase in amount of lipid peroxidation (Floor and Wetzel, 1998), protein oxidation (Alam et al., 1997; Floor and Wetzel, 1998), and nucleic acid damage (Zhang et al., 1999).

ROS and αSyn aggregation have impacts on each other; aggregated αSyn increases ROS production, and ROS exacerbates αSyn aggregation. This could happen through a feed-forward mechanism, which eventually could result in more ROS production and α-increased susceptibility of cells to oxidative stress (Dias et al., 2013). *In vitro*, aggregation of αSyn can be induced by oxidative reactions (Hashimoto et al., 1999; Paxinou et al., 2001), and adding of antioxidants eliminates the inhibitory effect of catecholamine on fibril formation (Conway et al., 2001). On the other hand, overexpression of WT αSyn or its mutant resulted in increased intracellular ROS level (Junn and Mouradian, 2002; Parihar et al., 2009) and cell susceptibility to oxidative stress (Jiang et al., 2007). Transgenic mice expressing A30P mutant exhibited increased protein carbonyl, a marker for protein oxidation (Poon et al., 2005).

Several cellular processes have been implicated in ROS production (Dias et al., 2013), of which mitochondria has a close relationship with αSyn and PD etiology. A significant mitochondrial accumulation of αSyn is observed in substantia nigra pars compacta and striatum of PD patient, compared to healthy age-matched controls (Devi et al., 2008b). Neurons are highly active cells containing large number of mitochondria to provide ATP by oxidative phosphorylation. Impaired components of the electron transporter chain may cause leakage of electrons to oxygen, resulting in a production of superoxide anion, which is a

precursor of most other ROS (Turrens, 2003). The protein αSyn has an inhibitory effect on complex I activity. Reduced complex I activity by αSyn was observed in cell culture (Devi et al., 2008a; Loeb et al., 2010) and transgenic animals (Liu et al., 2009a). These observations are consistent with the decrease in complex I activity observed in PD brain samples (Devi et al., 2008a; Parker et al., 2008).

Apart from direct inhibition of complex I, oxidative phosphorylation may be impaired as a consequence of mitochondrial dysfunction induced by αSyn (Protter et al., 2012). αSyn could induce mitochondria dysfunction by perturbing mitochondrial fission-fusion cycle (Kamp et al., 2010; Nakamura et al., 2011), inhibiting of autophagy and mitophagy (Winslow et al., 2010), blocking endoplasmic reticulum-Golgi traffic (Porte et al., 2006). As these cellular processes are essential to maintain homeostasis and functionality of mitochondria, perturbing the processes could result in mitochondrial dysfunction.

Interestingly, in addition to being a causative agent of mitochondrial dysfunction, αSyn can be affected by mitochondria. Inclusion or aggregation of αSyn was induced by mitochondria-disrupting drugs, rotenone and MPTP, in mouse and cell models (Fornai et al., 2005; Lee et al., 2002). The interplay between mitochondrial dysfunction, ROS and αSyn misfolding is complicated and it is unclear which one may be the cause or consequence. αSyn could be a cause by impairing the mitochondrial respiratory chain, which results in increased ROS production. Alternatively, αSyn may become oxidised and aggregated by increased ROS as a result of mitochondrial dysfunction (Nakamura, 2013).

1.5 Random insertional transgenesis of hES cells using plasmid vectors

hES cells are pluripotent cell lines isolated from the ICM of blastocysts (Thomson et al., 1998). Their capacity to differentiate *in vitro* into various cell types in the body holds great promise to regenerative medicine, and represents an experimental resource to study developmental biology and disease modelling. The application potential of hESC lines has been accelerated by their amenableness to genetic modification without losing pluripotency. For instance, transgenic hESC reporter lines can be used to identify hESC derivatives during differentiation, allowing purification of the target cells or understanding the functions of the gene of interest during hESC differentiation.

Among several genetic modification approaches, random integration of transgenes into the genome of hES cells is one of the most commonly used methods, especially, for

overexpression of genes. This strategy is based on a natural cellular process that employs endogenous DNA-modifying machinery to incorporate exogenous DNA into the chromosomal DNA of the host cells (Wurtele et al., 2003). As it is not site-targeted, DNA insertion can occur more than once at various chromosomal sites, which could result in multiple copy number of the transgenes to integrate per cell. This advantage enables scientists to generate clonal lines that differ in transgene expression level, which are useful generating an allelic series to study the effect of the gene at different doses.

The disadvantages of random insertional transgenesis include: (i) DNA integration into a chromosomal site that is less accessible by transcription factors, which can lead to silencing or reduced expression of the transgene, (ii) random DNA integration may interrupt the expression of endogenous genes or cause structural changes, which could affect the stability of the genome (Wurtele et al., 2003). As these effects may influence cell phenotype, screening and analysis of multiple clonal lines during hESC propagation and differentiation should be rigorously performed.

There are two platforms for gene delivery, viral transduction and transfection of plasmid DNA. Viral delivery of genes is normally highly efficient. If retroviruses are used then DNA is not integrated into the genome, which can cause problems with the longevity of the effect. Lentiviruses integrate into the genome, ensuring longevity of the effect, but then can cause other effects due to integration of parts of the viral genome. Methods exist to try and ensure that viral genome is not left in the host genome. The plasmid platform gives lower transfection efficiency and survival rate (Cao et al., 2010); however the method allows rapid transfection with a relatively simple and straightforward preparation process. Indeed, transfection efficiency and survival rate of hES cells is mainly dependent on transfection method. A comparison of gene delivery via electroporation, nucleofection and chemical transfection reagent revealed that nucleofection provided the highest transfection efficiency (5.8-6.1%) with modest survival rate (Cao et al., 2010). The electroporation and Lipofectamine transfection methods gave relatively low transfection efficiency (1.9-2.1% and 1.3-1.5%, respectively). Of these, electroporation gave the poorest cell survival. Low survival rate during nucleofection or electroporation is due to dissociated hES cells in single-cell suspension. Treatment with an inhibitor of Rho-associated kinase (ROCK) inhibitor, such as Y-27632, significantly improved the survival rate of dissociated hES cells (Watanabe et al., 2007). Alternatively, electroporation in clumps can also increase hESC

viability; however, this will result in multi-cell non-clonal lines (Zwaka and Thomson, 2003).

One of the most important parts of transgenesis is plasmid design. Besides a transgene of interest, two major components of an expression plasmid include a promoter to drive transgene expression, and a selectable marker. A selectable marker allows selection of stably transfected clones whereas the promoter determines the level and pattern of transgene expression. Liew et al. demonstrated that the choice of promoter and expression cassette are critical factors for establishing stable hESC lines (Liew et al., 2007). The authors compared four different promoters in driving eGFP expression in hES cells, and found that pUbiC, pR26, pCAGG are more superior to the pCMV for generation of stable transfectants. Additionally, long-term culture of these eGFP-expressing hESC clones lead to gene silencing, which could be prevented by combining a promoter with another regulatory element, more specifically in this study, pCAGG with PyF101 Polyoma Enhancer. The pCAGG promoter is commonly used for stable, constitutive expression during both ES cell propagation and differentiation. The functional stability of pCAGG has been demonstrated in driving eGFP expression in transgenic mice produced by germ transmission of transgenic eGFP mouse embryonic stem (mES) cells (Hadjantonakis et al., 1998). Some transgenic mES cell line clones stably maintained ubiquitous fluorescence expression during ES cell culture, *in vitro* differentiation, and *in vivo* when the mES cells were used to make chimeric mice. The pCAGG promoter also has been applied successfully in hES cells. Ectopic expression of SOX17 or SOX7 in hES cells followed by *in vitro* differentiation allowed establishment of stable endoderm progenitors that can be maintained stably in culture (Seguin et al., 2008).

1.6 Neural differentiation of hES cells

Neural differentiation of hES cells employs activation and inhibition of defined developmentally-relevant signalling pathways to dictate the fate of cells. Generally, directed hESC differentiation into specific neuronal subtypes has two stages: 1. Neural induction of the pluripotent stem cells and 2. Directed neuronal subtype specification.

1.6.1 Neural induction

Traditional protocols for neural induction include embryoid body (EB) formation and co-culture with stromal cell lines. These methods benefit from enabling simple and low-cost

differentiation; however, the results can be variable. The EB-based protocol often produces heterogeneous cell populations, and the differentiation is difficult to control due to the 3-dimentional structure of the aggregates. With the co-culture methods, the interaction between stromal cells and ES cells is poorly defined and are difficult to control and manipulate.

Recent advances in protocols for neural induction are based on an adherent, monolayer culture protocol known as "dual-SMAD inhibition" (Chambers et al., 2009). With this protocol, hES cells are differentiated while growing as a monolayer on a feeder-free basement matrix (Figure 1.4A). Neural induction is achieved by the synergistic action of two inhibitors of SMAD signalling, a bone morphogenetic protein (BMP) inhibitor and an Activin/Nodal inhibitor. The protocol used recombinant human Noggin to inhibit BMP signalling and the chemical antagonist, SB431542, to inhibit Activin/Nodal signalling and achieved >80% of neural induction efficiency after 11 days of differentiation (Chambers at al., 2009). The resulting neuroepithelial cells default to a forebrain identity, expressing PAX6, OTX2 and FOXG1 (Figure 1.4), and are patternable to neuronal subtypes, such as dopaminergic neurons and motor neurons (Chambers et al., 2009).

SB431542 is an antagonist of type I receptors of Nodal/Activin/TGFβ signalling (Inman et al., 2002), which play a role in maintaining pluripotency of hES cells (James et al., 2005). Noggin is a BMP inhibitor, blocking BMP signalling by direct interacts with BMPs at the receptor binding sites (Groppe et al., 2002). In Xenopus, Noggin is secreted from Spemann's organizer, and induces neural tissue from dorsal ectoderm (Lamb et al., 1993). Chambers et al. observed a synergistic effect of these two inhibitors on hESC neural induction. Combined treatment yielded great neural induction efficiency with 80% PAX6+ cells compared to <10% when Noggin or SB431542 were used alone. The results suggested that Noggin and SB431542 worked synergistically on multiple stages of differentiation including destabilizing the pluripotency network and suppression of alternative embryonic lineages induced by BMP and nodal/activin/TGFβ signalling.

The dual-SMAD inhibition protocol in monolayer format enables cells to be exposed to nutrients and exogenous factors in the medium evenly. As a result, neural differentiation of hES cells is effective, robust, and with a high degree of homogeneity. Using chemically defined medium and exogenous factors makes the differentiation controllable. A recent

modified protocol employed a chemical BMP receptor antagonist, LDN-193189, in place of Noggin; thus lower the cost of differentiation (Chambers et al., 2012).

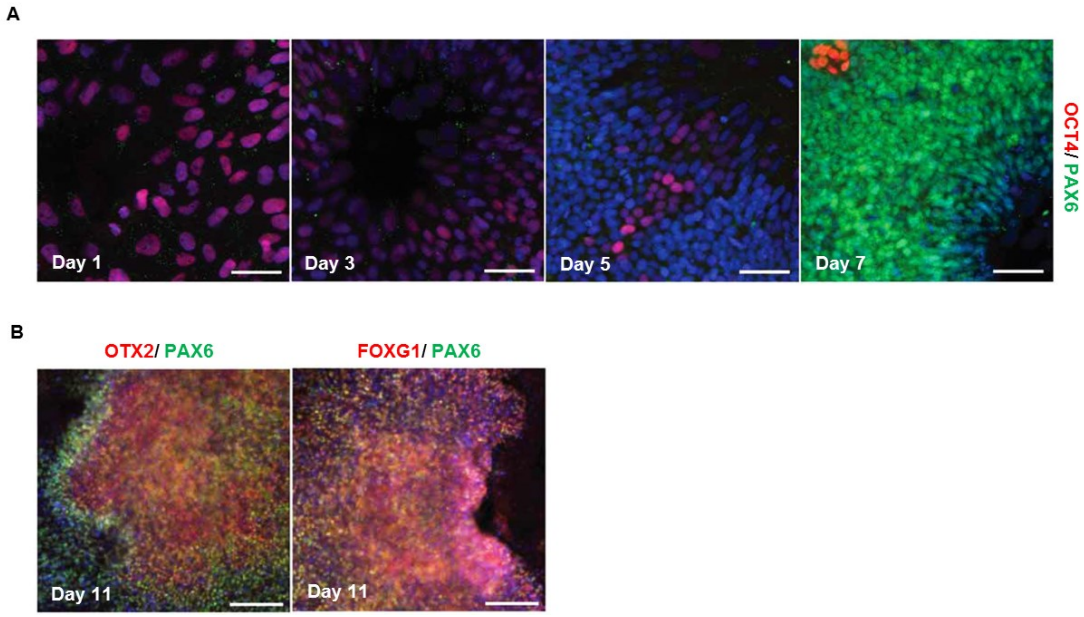

Figure 1.4 Neural induction of hES cells by dual-SMAD inhibition. (Adapted from Chambers et al., 2009).

A) **Immunustain for OCT4 and PAX6 of neuralised hES cells at Day 1, Day 3, Day 5 and Day 7 of neural induction.** The hES cells were neuralised by dual-SMAD inhibition. By Day 7 of differentiation, the protocol yields PAX6+ neuroepithelial cells.

B) **Day 11-neural induced cells immunostained for PAX6, OTX2 and FOXG1.** At Day 11 of differentiation, the neuroepithelial cells express PAX6, OTX2 and FOXG1, transcription factors characteristic of anterior CNS.

Scale bars are equivalent to 50 μm.

1.6.2 Directed differentiation towards cortical neurons

Shi et al. reported a protocol of directed differentiation of human pluripotent stem cells towards cortical projection neurons under a feeder-free, adherent culture condition (Shi et al., 2012). The protocol consisted of: 1. cortical neural induction, and 2. genesis and terminal differentiation of cortical projection neurons.

Cortical neural induction

Employing dual-SMAD inhibition and retinoid signalling, neural induction produced a population of neuroepithelial cells with anterior CNS character as indicated by the expression of PAX6, FOXG1 and OTX1/2 (Figure 1.5A-B). Three known populations of cortical stem and progenitor cells were identified in the rosettes, the ventricular zone epithelial cells or radial glia cells, the basal progenitor cells and the outer radial glia (oRG) cells. Of these, the radial glia cells, characterized by radial processes and PAX6+, OTX+ and Ki67+, account for the majority of the population. The authors also showed that retinoid signalling, vitamin A and it derivatives added as a component of B27, was essential for efficient cortical neural induction. With retinoic acid, almost all of the cells are PAX6+ after 15 days of differentiation, compared to 25% when retinoic acid was not applied.

Genesis and terminal differentiation of cortical projection neurons

Similar to cortical genesis *in vivo*, it took almost three months following neural induction to generate all classes of cortical projection neurons using this protocol. Immunostaining for transcription factors specific to different cortical layers revealed that neurogenesis occurred in a temporal order, in which deep layer neurons were generated before those in upper layers. The early born neurons were Tbr1+ (layer VI), which appeared within the first week of FGF2 withdrawal. And several weeks later (between days 65 and 80), the neurons layers II-III-IV, which express Satb2, were produced (Figure 1.5).

The neurons developed maturity overtime in culture. As early as day 28 of differentiation, the neurons were electrophysiological excitable with a single firing of action potential in response to step current. And by day 65, firing of a train of action potentials was detected in many neurons. Additionally, the neurons acquired functional excitatory glutamatergic synapse as early as day 50.

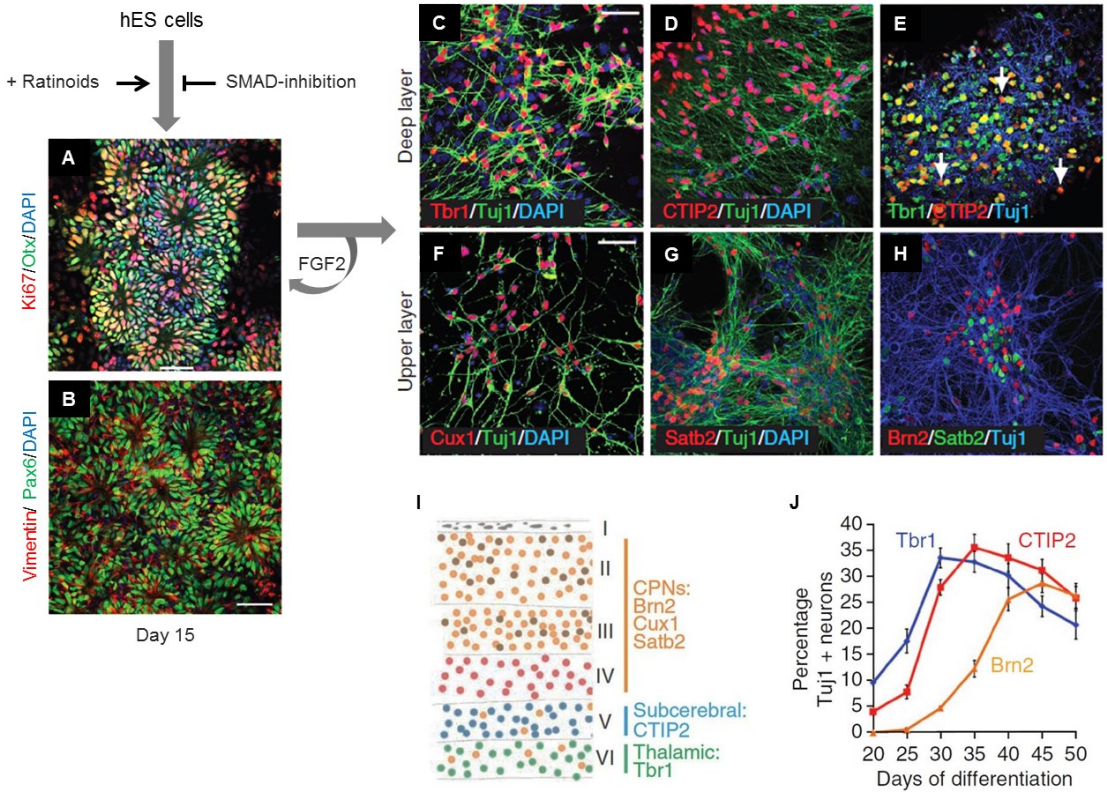

Figure 1.5 Directed differentiation of hES cells into cortical neurons. (Adapted from Shi et al., 2012).

A) - B) Neural induction of hES cells via dual-SMAD inhibition in the presence of retinoids results in neural rosettes comprising of neural stem and progenitor cells with cortical identity. FGF2 allows cells to propagate and remain in this stage whereas withdrawal leads to further differentiation and genesis classes of cortical neurons.

C) - E) Deeper-layer neurons are identified by expression of Tbr1 and/or CTIP2. White arrows indicate CTIP2+, Tbr1- neurons, which are corresponding to corticospinal motor neurons of layer 5.

F) -H) Upper-layer neurons are identified by expression of Cux1, Satb2 and Brn2.

I) Diagram shows classes of cortical projection neurons in adult mouse brain, with transcription factors indicated.

J) Time-course quantitative analysis of subsets of cortical neurons derived from hES cells showed that deeper-layer neurons (Tbr1+ or CTIP2+) were produced before those in upper-layers.

Scale bars are equivalent to 50 µm.

Chapter 2

Materials and Methods

2.1 Materials

2.1.1 Cell lines

Shef4 hESC line

The Shef4 hESC line was kindly provided by Dr. David Hay (University of Edinburgh), upon MRC Steering Committee approval (ref. no. SCSC11-60). The line was established at the Centre for Stem Cell Biology at the University of Sheffield under a license from the Human Fertilisation and Embryology Authority (HFEA), and has been validated to show the standard hESC characteristics including a normal karyotype (Aflatoonian et al., 2010).

Human iPS cell lines

Two human iPS cell lines, NAS2 and AST18, were established using Yamanaka retroviruses and fully characterised within the lab (Devine et al., 2011).

SNL feeder cells

The SNL cell line is available from European Collection of Cell Cultures, ECACC. It is a derivative of STO feeders with a G418-restance transgene to constitutive express LIF (McMahon and Bradley, 1990).

2.1.2 Plasmid DNA

The cDNA3.1 plasmid containing WT-human *SNCA* was provided as a generous gift from Professor John Hardy, UCL Institute of Neurology, UK. FCT-IVpBS and PGK-Puro-pCAG-stuffer, sources of IRES-Venus and pCAG backbone, respectively, were kindly provided by William Hamilton, a former PhD student in the Kunath lab. pCAG-GFP was kindly provided by Agnieszka Paca, a former PhD student in the Kunath lab.

2.1.3 Media for molecular cloning

LB broth

An amount of 25 g of Difco™ LB Broth powder (BD, 244620) was dissolved in deionised water and sterilised by autoclaving. The medium was stored at 4°C to use within 4 weeks. Prior to use, 100 µg/ ml ampicillin was freshly added.

LB agar (500 ml)

To produce 15% LB agar, unsterilized LB broth was added with 15% Difco™ LB agar and sterilised by autoclaving. When the medium was cooled down to 50°C, 100 µg / ml ampicillin was added and mixed thoroughly. The medium was poured into ½ volume of 10-cm polystyrene Petri dishes and allowed to solidify at room temperature for at least one hour. The agar plates were stored at 4°C to use within 4 weeks.

2.1.4 Media used for tissue culture

HESC medium

KnockOut™ DMEM/ F-12 (Gibco, Cat. no. 12660-012) supplemented with 20% KSR 1X non-essential amino acids (Gibco, Cat. no. 1140-035), 2 mM L-glutamine (Invitrogen, Cat. no. 25030-024), 50 mM 2-mercaptoethanol (BDH, Cat. no. 44143-31), 100 U/ml penicillin, 100 µg/ml streptomycin (Invitrogen, Cat. no. 15140-122) and 20 µg/ml FGF2 (Peprotech, Cat. No. 100-18B).

mTeSR™1 medium

The two components of the medium including mTeSR™1 Basal Medium (400 mL) (Catalog no. 05851) and mTeSR™1 5X Supplement (100 mL) (Catalog #05852) was mixed, and then dispensed into 50 ml tubes. The aliquots were stored in -20 °C and used within 4 weeks after preparation.

SNL medium

GMEM (Sigma, Cat. no. G5154) supplemented with 10% FCS (Invitrogen, Cat. no.10270), 2 mM L-glutamine (Invitrogen, Cat. no. 25030-024), 100 U/ml penicillin and 100 µg/ml streptomycin (Invitrogen, Cat. no. 15140-122).

N2B27 (200ml)

N2B27 was prepared by mixing: 98 ml DMEM/F12 (Gibco, Cat. no. 20331-020), 98 ml Neurobasal medium (Gibco, Cat. no. 21103-049), 1ml N2 supplement, 2 ml B27 with retinoic acid (Gibco, Cat. no. 17504-044). In addition, 2 mM L-glutamine, 0.1 mM β-mercaptoethanol (BDH, Cat. no. 44143-31), 100 U/ml penicillin and 100 µg/ml streptomycin (Invitrogen, Cat. no. 15140-122) were added.

3N medium

3N medium is N2B27 supplemented with 100 µM non-essential amino acids (Gibco, Cat. no. 1140-035).

DAP213

The hES cell freezing medium was prepared by mixing: 5.37 ml hES medium, 1.43 ml DMSO, 1.0 ml acetamide and 2.2 ml propylene glycol. The solution was aliquoted in 1.5 ml Eppendorf tubes and stored at -80 °C to be used within 1 month after preparation.

2.2 Methods

2.2.1 Molecular cloning

Polymerase chain reaction and purification of PCR products

Amplification of IRES-Venus or *SNCA* fragments were performed in 200 µl tubes using PCR machine (MJ Research, PTC-200 Peltier Thermal Cycler). A 50 µl PCR reaction includes 1x PCR *Pfx* amplification buffer, 1 mM $MgSO_4$, 1 unit Platinum® *Pfx* polymerase (all from Invitrogen, Cat. no. 11708-013), 1 mM of each dNTPs, 1 pmol/µl of forward primer, 1 pmol/µl of reverse primer, 1 ng template DNA and RNase/DNase free water.

All primers are available in Table 2.1. Resulting PCR was analysed for product size by electrophoresis using 0.8% agarose gel (Invitrogen, Cat. no. 16500-100) in 1XTAE buffer at 80 volts for 1 hour using 1 kb DNA ladder (Invitrogen, Cat. no. 15615-016) as DNA marker. After PCR product size had been verified, PCR product was purified using DNA Clean & Concentrator™-5 Kit (Zymo Research, Cat. no. D4003) resulting in 20 µl of eluted DNA, which would be enzymatic digested in later steps.

DNA digestion

A total volume of 25 µl digestion reaction is consisted of 600 ng backbone plasmid vector or 20 µl of purified PCR product, 1X bovine serum albumin, 1X digestion buffer and 50 U digestion enzyme (all from New England Biolabs® Inc). The reaction was incubated at 37°C for 1.5 hour. Only for the digested DNA vector, 0.5 µl of CIP (New England Biolabs® Inc, Cat. no. M0290S) was added into the digestion reaction followed by incubation at 37°C for 20 minutes. Subsequently, the reaction was heat-inactivated at 65°C for 20 min. Along with 1 kb DNA ladder (Invitrogen, Cat. no. 15615-016), digested DNA sample was electrophoresed in 0.8% agarose gel in 1XTAE at 80 volts for 1 hour.

DNA isolation from agarose gel

Enzymatic digested DNA was purified from agarose gel using Zymoclean™ Gel DNA Recovery Kit (Zymo Research, Cat. no. D4001) following manufacturer's protocol. In the final step, 20 µl of DNAse-free water was added to the column matrix to elute DNA. DNA concentration was measured using NanoDrop 2000 Spectrophotometer (Thermo Scientific) before use.

DNA ligation

Purified, digested DNA was ligated in a final volume of 20 µl using 2 U of T4 DNA ligase and 1x ligation buffer (all from Roche, Cat. no. 10481220001). The amount of vector DNA and DNA insert was used at 1:3 or 1:6 molar ratio of vector to insert. The ligation reaction was performed at 16°C overnight.

Table 2.1 Primer sequences for PCR or qPCR.

Primer	Sequences 5'-3'	fragment or gene	UPL no.
NVEN-R	TTATCTAGCGGCCGCTTACTTGTACAGCTCGTCCATGC	IRES-Venus	-
NVEN-F	TATTCGCGGCCGCAGTACTCCCTCTCAAAAGCGG		-
XVEN-F	AATTCCTCGAGAGTACTCCCTCTCAAAAGCGGGCATGAC		-
XSNCA-F	AATTCCTCGAGCCGCCACCATGGATGTATTCATGAAAGGACTTTCAAAGG	SNCA	-
XSNCA-R	TTATCGAGCGGCCGCTCATTAGGCTTCAGGTTCGTAGTCTTG		-
hSNCA-68L	GAGGGAGTGGTGCATGGT	SNCA	68
hSNCA-68R	TGCTGTCACACCCGTCAC		
NCAM-F	GCGTTGGAGAGTCCAAATTC	NCAM	51
NCAM-R	GGGAGAACCAGGAGATGTCTTT		
MAPT-F	ACCACAGCCACCTTCTCCT	MAPT	55
MAPT-R	CAGCCATCCTGGTTCAAAGT		

Transformation of plasmids into competent *E. coli*

Plasmid DNA was transformed into TOP10 chemically competent cells (Invitrogen, Cat. no. c4040-10) or home-made *E. coli* DH5α competent cells (see below) by the heat-shock method. Firstly, plasmid DNA and a vial of competent cells were thawed on ice. Once thawed, 1.0 to 1.3 ng of plasmid DNA was gently mixed with the competent cells in the vial, and then incubated on ice for 5 minutes. To heat-shock, cells were incubated in a 42°C water-bath for 45 seconds prior to placing on ice immediately for 5 minutes. To recover bacterial cells, a volume of 250 µl of pre-warmed (37°C) SOC medium (Invitrogen™, Cat. no. 15544-034) was added into the vial followed by incubation at 37°C with constantly shaking for 45 minutes. A volumes of 20 µl and 100 µl of cell suspension were spread onto two LB agar plates containing 100 µg/ml ampicillin. In an effort to recover all transformants, the rest of cell suspension was centrifuged, and then, following supernatant removal, cells were plated on another antibiotic-containing agar plate. Plates were then incubated at 37°C for 13-15 hours and colonies were picked and expanded for plasmid extraction.

Minipreps of *E.coli* cultures

Plasmid DNA was extracted using QIAprep®-Spin Miniprep kit (Qiagen, Cat no. 27104) following the manufacturer's protocol. Briefly, bacterial cell pellet was re-suspended with 250 µl of buffer P1 in a 1.5 ml Eppendorf tube. Then, cells were lysed with 250 µl of buffer P2 followed by inverting the tube to mix thoroughly. Next, 350 µl of buffer N3 was added to each tube, and mixed well. To separate DNA from cell debris, the lysate was centrifuged at 13,000 rpm (Eppendorf, Centrifuge 5415 C) for 10 minutes, and the supernatant was gently transferred into a clean QIAprep spin column. To isolate DNA from the supernatant, the column was centrifuged at 13,000 rpm for 10 min, and the resulting filtrate was discarded. To wash DNA, 750 µl of buffer PE was applied into the column followed by centrifugation at 13,000 rpm for 1 minute. After filtrate has been discarded, the column was centrifuged again to remove residual washing buffer. Then the column was transferred into a new, clean Eppendorf tube, and 20-50 µl of buffer EB was subsequently applied to the column. DNA was eluted by centrifugation at 13,000 rpm for 1 min. DNA concentration was measured using NanoDrop 2000 Spectrophotometer (Thermo Scientific), and samples were stored at -20°C.

Maxipreps of *E.coli* cultures

DNA extraction was performed using QIAGEN plasmid Maxi Kit based on the manufacturer's protocol (Qiagen, Cat. no. 12662). In a 50-ml Corning tube, bacterial pellets were re-suspended with 10 ml of buffer P1. To lyse cells, 10 ml of buffer P2 was added into each tube followed by vigorously inverting 4-6 times. Next, the mix was incubated at room temperature for 5 minutes, and then 10 ml of buffer P3 was applied. The tube was vigorously inverted for 4-6 times, and then incubated on ice for 20 minutes until lysed blue colour was gone and the suspension became colourless. To separate DNA from cell debris, cell lysate was centrifuged at 20,000 g for 30 minutes at 4°C, and resulting supernatant was transferred into a new tube. The supernatant was centrifuged again for 15 minutes to remove residual cell debris. During centrifugation, QIAGEN-tip was prepared by applying 10 ml of buffer QBT, and then the column was allowed to empty by gravity flow. Next, supernatant was applied in the QIAGEN-tip and allowed to enter the resin by gravity flow. Then, the QIAGEN-tip was washed twice by gravity flow with 30 ml Buffer QC. To elute DNA, the QIAGEN-tip was placed in a clean 50-ml corning tube, in which and 15 ml of buffer QF was subsequently added. Eluted DNA was precipitated with 10.5 ml of isopropanol followed by centrifugation at 15,000 g for 30 minutes at 4°C. After supernatant removal, the DNA pellet was washed with 5 ml 70% ethanol followed by centrifugation at 15,000 g for 10 minutes. Supernatant was discarded and the tube was re-centrifuged to remove residual ethanol. Finally, the DNA pellet was air-dried for 10-15 minutes at room temperature. Finally, DNA was dissolved with 500 µl of EB buffer and stored at -80°C.

Desalting DNA for nucleofection of Shef4 hES cells

Linearised plasmid DNA was desalted using Millipore centrifugal filter units (UFC503024 24PK, Millipore). DNase-free water was added into an Eppendorf tube containing DNA to top up the volume to 500 µl, and then desalting was performed following manufacturer's protocol. DNA concentration was measured using the NanoDrop 2000 Spectrophotometer (Thermo Scientific), and DNA was used for transfection immediately or stored at -20°C.

Preparation of chemically-competent *E. coli* DH5α cells

LB agar plate was streaked with *E. coli* DH5α and incubated at 37°C overnight. To grow starter culture, a single colony was inoculated in 3 ml LB medium and incubated at 37°C with shaking overnight. Next day, 1 ml of starter culture was added into a flask containing 200 ml of LB medium following by incubation at 18°C until OD_{600} of the culture had

reached 0.3. Cells were harvested by centrifugation at 3,000g for 10 minutes at 4°C. Following supernatant removal, pellet was re-suspended in 10 ml of ice-cold CCMB80 buffer (pH7.4) (10 mM KOAc at pH 7.0, 80 mM $CaCl_2$, 20 mM $MnCl_2$, and 10 mM $MgCl_2$, 10% glycerol) and incubated on ice for 20 minutes. Then cells were collected again by centrifugation at 3,000 g at 4°C for 10 minutes. The resulting pellet was re-suspended with 10 ml of ice-cold CCMB80 buffer and incubated on ice for 10 minutes. To aliquot competent cells, cells were dispensed in Eppendorf tubes at 50 µl per tube and were further incubated on iced for 20 minutes. Finally, cells were snapped frozen on a mixture of dry ice and ethanol prior to storing at -80°C to use within 2-3 months.

2.2.2 Cell culture

Preparation of irradiated SNLs for hESC culture

SNLs were cultured on 100-ml dishes coated with 0.1% gelatin (Sigma, Cat. no. G1890) in SNL medium at 37°C in a humidified incubator in the presence of 5% CO_2. Cells were fed daily until confluent or nearly confluent. Then cells were trypsinised (Invitrogen, Cat. no. 15090-046) and harvested to a 15-ml universal tube and collected by centrifugation at 1,300 rpm (Eppendorf 5702) for 3 minutes. Following supernatant removal, cells were washed with PBS (Sigma, Cat. no. D8537), spun again, and then the resulting pellet was subsequently re-suspended in PBS. Finally, cells were irradiated at 80 Gray, and then aliquoted at 4×10^6 cells per vial in 0.5 ml of freezing medium before storing at -80°C. A frozen vial of aliquoted-irradiated SNLs were hand-thawed and immediately transferred into a universal tube containing 9.5 ml of SNL medium (see section 2.1.4). Cells were centrifuged at 1,300 rpm (Eppendorf 5702) for 3 minutes, and then supernatant was aspirated. Resulting cell pellet was re-suspended in SNL medium and plated on a 100-ml dish coated with 0.1% gelatine in SNL medium. Cells were incubated at 37°C in a humidified with 5% CO_2 incubator overnight and will be used within 1-2 days after plating. Prior to plating hES cells, SNL medium was replaced with hESC medium (see section 2.1.4) and cells were incubated at 37°C in a humidified with 5% CO_2 incubator for at least 1 hour.

Matrigel coated plates

Growth-factor reduced Matrigel (BD, Cat. no. 356234) was thawed and aliquoted following manufacturer's instructions. To prepare a Matrigel-coated plate, all procedures were performed in cold conditions to slow down Matrigel polymerisation. An aliquot of frozen Matrigel was thawed at 4°C, and then diluted at 1:36 in cold KnockOut™ DMEM/F-12

(Gibco, Cat. no.12660-012). Diluted Matrigel was dispensed into a pre-chilled multi-well plate and incubated at 4°C overnight or until use. Generally, the plates were used within 1 week from the date of preparation. To use Matrigel coated plates, excess liquid Matrigel was aspirated and mTeSR1 was added into the wells. The plate was warmed in the incubator for 10-15 minutes before used for plating cells.

hES cell and iPS cell Culture

hES cells were cultured on Matrigel-coated 6-well plates (BD, Cat. no. 356234) in mTeSR1 medium (Stemcell™ Technologies, Cat. no.05850). Cells were fed daily by replacing spent medium with 1.5-2 ml of fresh medium per well. Cell passaging was performed approximately every 4 days, when cells have reached a confluency of 70%-80% or colonies started to grow too large. To passage cells, spent medium was removed, and then cells were rinsed once with KnockOut™ DMEM/F-12 (Gibco, Cat. no.12660-012). Cells were treated with dispase for 3-5 minutes at 37°C in a humidified incubator at 5% CO_2. After dispase removal, cells were rinsed with KnockOut™ DMEM/F-12 once prior to adding 2 ml of mTeSR1 medium into the well. Colonies were scored using 10-ml plastic pipette, and then the entire surface was scraped using a cell scraper (Costar, Cat. no.3010). Cells were repeatedly pipetted to adjust clump size, and then were plated on a new pre-warmed Matrigel-coated 6-well plate in mTeSR1 medium at 1:2 ratio to 1:4 ratio depending on the confluency of a passaged plate. The was moved back and forth in order to have a good repartition of cells, and were cultured at 37°C in a humidified incubator at 5% CO_2.

Freezing and thawing of hES cells and iPS cells

Cells were frozen using DAP213 medium. Firstly, hES cells were treated with 10 µM ROCK inhibitor (Ascent, Cat. no.Y27632) for 1 hour in the incubator. Then, spent medium was removed and cells were rinsed once with KnockOut™ DMEM/F-12. To detach cells, cells were treated with Accutase™ (Gibco, Cat. no. A11105-01) for 10-15 minutes in the incubator. When colony detachment started to appear, Accutase™ was aspirated and mTeSR1 (Stemcell Technologies™, Cat. no. 05850) was added into the well. Cells were scraped using a cell scraper and subsequently transferred into a universal tube. Then cells were collected by centrifugation at 1,300 rpm (Eppendorf 5702) for 3 minutes. After supernatant removal, cell pellets were re-suspended with 250 µl of DAP213 medium.

Cells were quickly transferred into a cryovial and immediately snap frozen in liquid nitrogen. Cells were immediately stored in liquid nitrogen for long-term storage.

At 1 hour prior to thawing hES cells, SNLs was prepared by replacing SNL media in SNL culture with mTeSR1 medium supplemented with 10 μM ROCK inhibitor (Y27632, Ascent). To thaw cells, a cryovial of frozen hES cells was taken from liquid nitrogen and place on dry ice immediately. Warm mTeSR1 medium (800 μl) was added to each vial to promptly dilute and thaw the DAP213-frozen cells by hand. As soon as completely thawed, cells were transferred into 10 ml of warm mTeSR1 in a universal tube. Cells were collected by centrifugation at 1,300 rpm for 3 minutes. Following supernatant removal, the cell pellet was gently resuspended in warm mTeSR1 containing 10 μM ROCK inhibitor (Y27632, Ascent), and then transferred to a previously prepared SNL plate. Cells were incubated at 37°C in a humidified incubator at 5% CO_2 and fed daily with mTeSR1 until ready to passage.

2.2.3 Nucleofection of hES cells

Nucleofection was performed using the Neon and reagent kit (Invitrogen, Cat. no. MPK5000) as follows.

1. **Preparation of Matrigel-coated plate**
    1) Matrigel (BD) was removed from each well of previously prepared Matrigel-coated 6-well plate.
    2) A volume of 1.5 ml of MEF-conditioned medium (R&D systems, Cat. no. AR005) supplemented with LIF and 10 μM ROCK inhibitor (Y27632, Ascent) was added in to the wells.
    3) The plate was incubated at 37°C in a humidified incubator at 5% CO_2.
2. **Preparation of Shef4 hES cells**
    1) Spent medium was removed from each well of a total 6 wells of a 6-well plate of hESC culture.
    2) Cells were rinsed with 2 ml of KnockOut™ DMEM/F-12 (Gibco, Cat. no. 12660-012).
    3) Then 800 μl of trypsin was added into each well. The plate was incubated in the incubator for 2-3 minutes. Then cells were observed for sings of detachment under a microscope.
    4) When the edges of colonies start to detach, trysin was removed. Cells were rinsed gently with 2 ml of K/O DMEM.
    5) Following K/O DMEM removal, the volume of 2 ml of K/O DMEM supplemented with ROCK inhibitor (Y27632, Ascent) was added into each well of hESC culture.

6) The entire surface of cells culture was scraped using a cell scraper, and then cell suspension was transferred into a universal tube.
7) Cell suspension (10 µl) was applied onto hematocytometer for cell count to calculate the volume to obtain 1.2×10^6 cells (for $0.2x10^6$ cells/well subsequent plating).
8) Cells were collected by centrifugation at 1,300 rpm for 3 minutes, and then supernatant was discarded.
9) Cell pellet was re-suspended with 59.4 µl buffer R, and then was mixed with 6.6 µl of 500 ng of linearized plasmid DNA.

3. Transfection of hES cells

Transfection was performed with Neon™ Transfection System following manufacturer's protocol. A volume of 10 µl of cells-DNA mix was electroporated for each reaction at 1050 V for 2 pulses with duration of 30 msec. Following electroporation, cells were plated on previously prepared Matrigel-coated 6-well plates containing warm mTeSR1medium supplemented with 10 µM ROCK inhibitor (Y27632, Ascent) (BD). The plate was placed in the incubator, in which it was moved back and forth to allow even dispersion of cells. Next day, cells were observed for fluorescence expression under a microscope, and then were fed daily with mTeSR1 medium after 48 hours transfection.

4. Clonal expansion and drug selection of transgenic Shef4 hES cells

When colonies are formed, consisting of 50-100 cells, drug selection started by feeding cells daily with mTeSR1 medium supplemented with 1 µg/ ml puromycin for at least 2 weeks. To isolate clones, colonies were manually picked and transferred into a 12-well plate, and then into a 6-well plate to expand. To bank hESC clones, cells were frozen in DAP213 medium and stored in liquid nitrogen.

2.2.4 Transfection of hES cells using Lipofectamine® LTX

Transfection was performed when hES cells were on MatriGel in mTeSR1 medium following a protocol developed by Ludovic Vallier (University of Cambridge, UK) as follows.

Day 1: A well of a confluent 6-well plate of hES cells was splited into 6 to 18 wells (depending on how confluent the cells are. Resulting plated cells should have very low density). Cells were fed with mTeSR1 medium without antibiotics.

Day 2: Cells were fed with mTeSR1 without antibiotics.

Day 3: The spent mTeSR1 medium was replaced with OPTIMEM medium (Invitrogen, 519 085-026). The hESC colonies were transfected based on an Invitrogen protocol as follows.

1) In an Eppendorf tube, the amount of 4 µg DNA was diluted in 500 µl of OPTIMEM medium.
2) A volume of 4 µl of Plus reagent was added in the tube from step 1.
3) The mix was incubated at room temperature for 5 minutes.
4) Then12 µl of Lipofectamine® LTX (Invitrogen, A12621) was added into the tube from step 3.
5) The mix was mixed thoroughly, and then was incubated at room temperature for 30 minutes.
6) A volume of 500 µl of the DNA-Lipofectamine mix was added drop by drop into a well containing cells. The plate was moved back and forth in order to have a good distribution of the transfection mix.
7) The plate was placed back in the incubator to allow incubation for 18-20 hours.

Day 4: The OPTIMEM medium was replaced with mTeSR1 (without antibiotics).

Day 5: Drug selection was performed by replacing spent medium with mTeSR1 supplemented with 1µg/ml Puromycin (Sigma, P8833).

Day6-Day 19: Cells were fed daily with mTeSR1 supplemented with 1µg/ml Puromycin.

Day 20: Colonies were picked into 24-well plates coated with Matrigel (BD). Cells were fed daily with mTeSR1 supplemented with 1μg/ml Puromycin. When colonies grow large, each of them is transferred into a 12-well plate, and then into a 6-well plate to expand. To bank hESC clones, cells were frozen in DAP213 medium and stored in liquid nitrogen.

2.2.5 RNA isolation from hES cells

RNA was isolated using Trizol® reagent (Life Technologies, Cat. no.15596026) and further purified using Zymo-Spin™ Kit (Zymo Research, Cat. no. R1011) as follows.

1. **Harvesting hES cells**
   1) When hES cells are on feeder-free conditions in a 6-well plate, spent medium was removed, and then hES cells were rinsed with K/O DMEM.
   2) The volume of 1.0 ml of QIAzol® Reagent was added into the well. The plate was agitated gently to allow cells to lyse for 1-2 minutes.
   3) Cell lysate was transferred into an RNase-free Eppendorf tube. The lysate was subjected to RNA isolation or snap frozen on the mixture of dry ice and ethanol before storing in -80°C for later RNA extraction.
2. **RNA isolation and purification**
   1) Frozen cell lysate was thawed at room temperature.
   2) Then 200 μl of chloroform was added into the tube in step 1. The tube was securely capped, and then was vortexed vigorously for 30 seconds. The lysate was incubated at room temperature for 2-3 minutes.
   3) The lysate was centrifuged at 12,000 g for 15 minutes at 4°C.
   4) A volume of 200 μl of the upper, aqueous layer was transferred into a new DNase/RNase-free Eppendorf tube.
   5) Then 200 μl of chloroform was added into the tube in step 5
   6) The tube was centrifuged at 12, 000 g at 4°C for 20 minutes
   7) Then 120 μl of the upper phase was transferred into a new tube.
   8) A volume of 360 μl of RAD buffer was added in to the tube, and then it was mixed thoroughly.
   9) The mix in step 8 was transferred into a Zymo-Spin™ Column in a collection tube.
   10) The collection tube was centrifuged at 12,000g for 2 minutes. And then the flow-through was discarded.
   11) A volume of 400 μl RNA prep Buffer was added into the column.

12) The column was centrifuged at 12,000 g for 1 minute. Then the flow-through was discarded.
13) A volume of 800 µl of RNA wash buffer was added into the column.
14) The column was centrifuged at 12,000 g for 30 minutes. Then the flow-through was discarded.
15) The column was subjected to Steps 13) and 14).
16) The Zymo-Spin™ Column was centrifuged at 12, 000 g for 2 minute to ensure the complete removal of wash buffer.
17) The Zymo-Spin™ Column was carefully removed from the tube, and then placed into a new DNase/RNase-free tube.
18) A volume of 10 µl DNase/RNase-free water was added directly into the centre of the column matrix. Incubation was allowed at room temperature for 1 minute.
19) The column was centrifuged at 10,000 g for 30 seconds to elute RNA from the matrix.
20) RNA samples were measured for concentration and purity, and then store at -80°C.

2.2.6 Neural induction of hES cells

Neural induction was performed based on a previously published monolayer protocol (Chambers et al., 2009) with slight modifications (Figure 4.1). hES cells were dissociated into single cells with Accutase (Gibco, Cat. no. A11105-01) and plated on a Matrigel-coated 6-well plate in mTeSR1 medium. Cells were fed daily until they reached 90% confluency or above. Neural induction started at day 0, when mTeSR1 was replaced with hESC medium lacking FGF2, supplemented with 10 µM SB431542 (Tocris) and 100 nM LDN-193189 (Stemgent, Cat. no. 04-0019). Cells were fed daily with this medium until day 4. From day 5 to day 11, SB431542 was withdrawn and cells were fed every other day with a mixture of hESC medium and N2B27, which was gradually added into culture medium from 25%, 50%, 75% and 100% at day 5, day 7, day 9 and day 11, respectively.

2.2.7 Directed differentiation towards cortical neurons

To generate cortical neurons, human pluripotent stem cells were processed based on a protocol described previously (Shi et al., 2012). Briefly, cells were plated as single cells on a Matrigel-coated 6-well plate in mTeSR1 medium and allow to grow until nearly confluent. Neural induction started at day 0, when cells were fed daily for 11 days with 3N medium (in 2.1.2) supplemented with 10 μM SB431542 (Tocris) and 100 nM LDN-193189 (Stemgent). To expand neural progenitors and stem cells, at day12, cells were dissociated into small clumps with dispase, and then plated on laminin/poly-L-ornithine-coated plates (see section 2.2.7) in 3N medium supplemented with 100 nM LDN-193189 and 20μg/ml FGF2 (Peprotech). Cells at this stage were expanded for 7-10 days prior to gentle dissociation into small clumps with Accutase, and subsequently plated on laminin/poly-L-ornithine-coated plate in N3 medium supplemented with human 10 ng/ml brain-derived neurotrophic factor (BDNF) (Peprotech, INC, Cat. no. 450-02) and 10 ng/ml human GDNF (Peprotech, INC, Cat. no. 450-10) to support neuronal growth. Half of the spent medium was replaced with new medium daily for 2 weeks. For the neuronal maturation step, cells were gently dissociated with Accutase and plated at 1×10^4 cells on a glass 22mm coverslip coated with laminin/poly-L-ornithine in a 6-well plate (see section 2.2.7) in 3N medium supplemented with 10 ng/ml BDNF and 10 ng/ml GDNF. From the first day of plating, cells were fed every 3 days by replacing half of the spent medium with new medium.

2.2.8 Preparation of laminin/poly-L-ornithine-coated glass coverslips

Glass coverslips (22 mm, VWR international, Cat no. 631-0158) were cleaned by soaking in 70% nitric acid for 30 minutes and washed several times with water (Sigma, Cat no. W1503). Then, coverslips were sterilised by autoclaving before placing in each well of 6-well culture plates. Coverslip were coated with 15 μg/ml poly-L-ornithine (Sigma, Cat. no. P4957) at room temperature overnight. After removal of poly-L-ornithine and washing with water for 3 times, the coverslips were air dried, and then subsequently coated with 10 μg/ml laminin (Sigma L2020-1MG) for 4 hours or overnight at 37°C. To prepare the plate for seeding of neural cells, laminin was aspirated and plating medium was added into the well. The plate was warmed in the incubator for 5-10 minute before use.

2.2.9 Immunocytochemistry

Immunostaining was performed on cells growing on a glass coverslips or in multi-well plates. Spent medium was removed gently and cells were immediately fixed with 4% PFA for 15 minutes. Then, cells were washed 3 times with PBS with 10-minutes incubation for each wash. Cells were permeabilized and blocked with 2% goat serum/0.1% Triton-X100 in PBS for 30 minutes prior to overnight incubation at 4°C with a primary antibody. Following primary antibody removal, cells were washed 3 times with PBS. Secondary antibody conjugated with a fluorescent dye was applied and incubated at room temperature for 1 hour in the dark. Following secondary antibody removal, cells were washed 3 times with PBS. Finally a coverslip was mounted on a clean glass slide using mounting medium (Vectashield, Cat. no. H-100). For long-term storage, nail polish was applied to seal the edge of coverslip with a glass slide. Stained cells were subjected to imaging immediately or stored at 4°C in dark conditions. The a-synuclein antibody used was developed against amino acids 15-123 of rat a-synuclein, raised in mouse, and had been successfully tested in humans (BD Transduction laboratories, 1 in 500).

2.2.10 Chromosome Counting

After 45-48 hour of cell splitting, cell division was arrested with colchicine (Gibco, Cat no.15210-040). Cell were trypsinised and dissociated to single cells. Cells were then treated with a hypotonic solution, 0.075 M KCl, for 10-15 minutes at room temperature. After KCl removal, cells were fixed with a mixture of methanol and acetic acid in 3:1 ratio, and subsequently washed twice. Cell pellets were re-suspended in fixative and dropped on glass slide. Cells were allowed to air dry, and then stained in Giemsa dye. Finally, cells were mounted on glass slides with xylene and examined for chromosome number under a microscope with 100X objective. G-banding was kindly analysed by the transgenic service of SCRM (The University of Edinburgh, UK).

2.2.11 MTS assay for measuring proliferation rate of hES cells

Cell proliferation was measured in 96-well plates using CellTiter 96® AQ_{ueous} One Solution Reagent (Promega, Cat. no. G3582). hES cells were dissociated into single cells with Accutase, and then plated on Matrigel-coated 96-well plates in mTeSR1 at a density of 5×10^4 cells/well. To investigate cell proliferation over 8 days, a total number of 8 plates of a set of hESC lines were prepared, of which each plate contained triplicates of each cell line to be analysed. At the day of assay, 20 µl of the MTS reagent was added into each well, which

contained 100 µl spent medium. Cells were incubated at 37°C in the incubator for 1 hour. The soluble formazan product was determined by measuring absorbance at 490 nm using a 96-well plate reader (FLUOstar OPTIMA). The data was subtracted from background using a reading from control wells, which are wells without cells and contain 100 µl mTeSR1 and 20 µl MTS. The assay was performed daily for 8 days.

2.2.12 Western blotting

Following removal of spent medium, cells were washed once with KnockOut™ DMEM/F-12 (Gibco, Cat. no. 12660-012). Cells were then lysed at 4°C with occasional agitation for 30 minutes with lysis buffer (120 mM Tris, pH 6.8, 4% SDS, 20% glycerol and 100 mM DTT) supplemented with protease inhibitor cocktail (Roche, Cat No. 04693159001). Cell lysate was transferred into an Eppendorf tube and sonicated until homogenous. Each lysate was incubated at 100°C for 5 minutes, and then placed on ice. Protein concentration was measured using the Bradford reagent (Sigma, Cat. no. B6916). Protein samples were adjusted to equal concentration and subjected to SDS-PAGE immediately or stored at -80°C until use.

Protein samples were diluted in 4X LDS sample buffer (Life Technologies, Cat. no. NP0007) supplemented with β-mercaptoethanol. Samples were boiled at 100°C for 5 min. Along with Seeblue® Plus2 pre-stained protein marker (Invitrogen, Cat. No. LC5925), protein samples were loaded onto NuPAGE® 4-12% Bis-Tris gel (Life Technologies, Cat. no. NP0322BOX). Electrophoresis was performed in NuPAGE® MES SDS running buffer gel (Life Technologies, Cat. no. NP0002) at 180 V for 1 hour. Then, protein was transferred onto Hybond ECL membrane (Amersham, Cat no. RPN203D), and blocked with 3% skimmed milk in 0.01% Tween 20, with agitation for 1 hour. After a brief rinse with washing buffer, membrane was incubated with a primary antibody against αSyn (BD Transduction, Cat. no. 610787) or β-actin (Sigma, Cat. no. A1978), which was diluted in blocking buffer. The membrane was washed three times prior to incubating with anti-mouse IgG HRP-conjugated secondary antibody (Promega, Cat No. W402B) for 1 h at room temperature. Following three washes, detection was performed using SuperSignal® West Femto Kit (Thermo Scientific, Cat no. 34094) and a film processor (Konica medical Film processor, SRX-101A).

2.2.13 ROS assay

Production of cytosolic ROS was determined by live-imaging with dihydroethidium (dHEt) (Sigma, Cat. no. D7008). This is a blue fluorescent dye, which becomes oxidised by superoxide in cytosol and then binds DNA to produce red fluorescence. Measuring the rate of increase of nuclear red fluorescence gives a direct measure of dHEt oxidisation, which is indicative of ROS production within cells. The assay was performed on neurons growing on a 22-cm glass cover slip coated with laminin/poly-L-ornithine (see section 2.2.7). To load cells with dHEt, a cover slip was securely assembled within a chamber (ref). Cells were washed gently once with HBSS (Gibco, Cat. no. 14025), and then dHEt (5 μM) was applied into the chamber. Cells were imaged immediately to avoid intracellular accumulation of oxidized products. Imaging was performed with 10 second intervals using a fluorescent inverted microscope integrated with CCD camera (Hamamatsu, Orca ER). Excitation light was generated from a Xenon arc lamp with beams passing through filters centred at 380 nm and 530 nm, and emitted fluorescence light was reflected through a 488 nm and 605 nm longpass filters. Obtained data were collected and analysed using software from Andor (Belfast, UK), by which ratio of emitted fluorescence, red:blue, was determined.

In the experiments where more mature neurons were assayed, a fluorescent inverted microscope (Ziess) integrated with CCD camera (AxioCam MRM) and Axio Observer software with the same settings applied. Acquired data was analysed using ImageJ. In case that data filtering was applied, data was sorted based on average emitted blue fluorescence (designated as initial blue) of the first 3 frames of imaging. Data were classified into two groups; one with initial blue less than 30 and the other with initial blue equal to or more than 30.

2.2.14 RT-qPCR for total αSyn

Total RNA was reverse transcribed in a final volume of 50 μl using Superscript III (Invitrogen, Cat. no. 18080-093). Firstly, 35.5 μl of a mixture containing 0.5 -1.5 μg of total RNA, 2 μl of 200 ng/μl of random primer and 2.5 μl of 10 mM dNTPs was heated to 65°C for 5 minutes, and then incubated on ice for 5 minutes. Next, the mixture was added to 14.5 μl of reverse transcription mix containing 10 μl of 5x first strand buffer, 2.5 μl of 0.1 M DTT, 1 μl of RNase inhibitor and 1 μl of Superscript III Reverse Transcriptase. Reverse transcription was performed using a PCR machine (MJ Research, PTC-200 Peltier Thermal Cycler) with parameters as follows; 25°C for 5 minutes, 50°C for 60 minutes, and 70°C for 15 minutes. cDNA samples were used immediately or stored at 4°C.

A 10-µl qPCR reaction was set up with the Universal Probe Library (UPL) system (Roche), 1 pmol/µl of each primer and cDNA. PCR was performed using a LightCycler 480 (Roche) with PCR parameters as follows: (95°C for 5 min), [(95°C for 10 sec) + (61°C for 10 sec)] for 45 cycles. Data was analysed by comparing C(T) to standard curves generated by qPCR of serial diluted cDNAs or plasmid DNA. The quantitation was performed using the comparative C(T) method (Schmittgen and Livak, 2008) and normalised to 18S rRNA as internal control.

2.2.15 FACS Analysis

Prior to cell detaching, hES cells were treated with 10 µM ROCK inhibitor for 1 hour. Cells were dissociated with Accutase (Gibco, Cat. no. A11105-01) and washed in FACS Buffer. To obtain single cell suspension, cells were filtered through cell strainers. FACS analysis was performed using a FACSCalibur flow cytometer (Becton Dickinson) with an acquisition rate of 1,000-3,000 events per second for a total of 10,000 events per sample. Cells were excited with 488-nm laser, and green fluorescence was detected using 490 LP and 510/20 filters. Data were further analysed and presented using FlowJo software (Tree Star, Ashland). All samples were performed in duplicate.

Analysis of mES cells was similar to that of hES cells except that mES cells were detached and dissociated using trypsin/EDTA without prior treatment with ROCK inhibitor.

2.2.16 Cell death assay

This experiment was performed on differentiated neurons cultures on 22-mm glass coverslips (see section 2.2.7). To perform the assay, a coverslip was securely assembled with a metallic chamber, and cells were washed once with HBSS (Gibco, Cat. no. 14025). Cells were incubated 5 µM Hoechst 33342 (Sigma Cat. no. B2261) and 5 µM propidium idodide (PI) (Sigma, Cat. no. P-4170) in HBSS for 15 minutes in dark conditions. Images were captured using a Ziess fluorescent microscope with a 20x objective. Two excitation/emission filter sets; 380/535 nm for Hoechst and 555/645 nm for PI, were applied to acquire images. Four to five microscopic images covering 500-1000 nuclei were applied in data analysis using Velocity software. Cell nuclei that are double stained for both Hoechst and PI were counted as dead cells, while those that are only positive for Hoechst were considered as live cell.

2.2.17 Statistics

The number of technical and biological repeats for each experiment is stated in each figure legend. Bar charts are shown with the mean and standard deviation. Statistical tests between 2 groups were done using the Student's t-test, with significance taken as $p<0.05$.

Chapter 3

Establishment of transgenic SNCA hESC lines

3.1 Plasmids for transgenesis

3.1.1 Plasmid design

My aim in designing the αSyn over-expression construct was to obtain a high level of αSyn production in neurons without compromising the viability of the hES cells or any of the progenitors produced during neuronal differentiation. Two major factors I have considered are promoter strength and its activity in hES cells and differentiated neurons. Regarding these criterion, the constitutive CAG promoter has been chosen. This promoter, first developed in 1991, has been optimised to efficiently drive ubiquitous and high expression of a transgene in the majority of cell types (Niwa et al., 1991). Furthermore, it also has been applied in mES cells, in which its activity still maintains when the cells are differentiated (Alexopoulou et al., 2008; Chambers et al., 2003; Hadjantonakis et al., 1998).

In order to rapidly identify hESC clones with differing levels of expression and to monitor transgene silencing a Venus reporter protein was linked to αSyn expression with an internal ribosome entry sequence (IRES).

I have constructed two plasmids for the purpose of making transgenic hESC lines. The pCAG-*SNCA*-IRES-Venus (pCAG-SIV) plasmid is designed to express human wild-type αSyn and a fluorescent reporter protein, Venus. The control plasmid, pCAG-IRES-Venus (pCAG-IV), has an identical structure without the SNCA coding sequence (Figure 3.1).

The pCAG-SIV construct contains the αSyn -encoding gene, *SNCA,* driven constitutively by the CAG promoter. Downstream of *SNCA* is an IRES linking the Venus-encoding gene, so that αSyn expression could be monitored in living cells by observing Venus fluorescence. The plasmid also has a puromycin-resistant gene, puromycin *N*-acetyl transferase, driven by a separate promoter (mPGK), which will allow drug-selection of cells harbouring the plasmid.

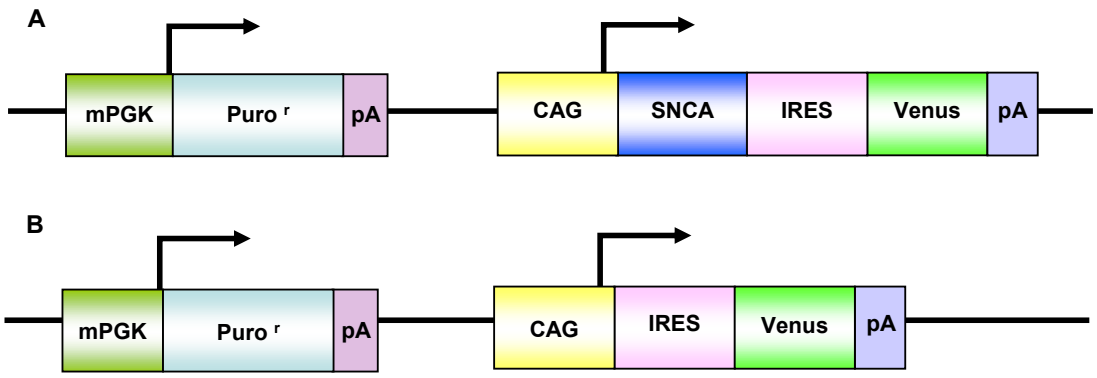

Figure 3.1 Schemes of pCAG-SNCA-IRES-Venus and pCAG-IRES-Venus vectors.

A) pCAG-SNCA-IRES-Venus. The plasmid contains 2 major elements: an αSyn (SNCA) and Venus expression cassette, and a drug-selectable cassette. The first element has a constitutive promoter pCAG to drive the expression of SNCA and Venus, by which the expression of SNCA was expected to be traced. The puromycin-resistant gene ($Puro^r$) serves as a selectable maker under the murine phosphoglycerate kinase (mPGK) promoter.

B) pCAG-IRES-Venus. This control plasmid contains the same elements as pCAG-SNCA-IRES-Venus with the exception of the *SNCA* coding sequence.

The control plasmid, pCAG-IV, contains the same elements as pCAG-SIV except that it does not contain *SNCA*.

3.1.2 Plasmid construction

Both expression plasmids were successfully constructed using the approaches shown in Figure 3.2 and Figure 3.3. DNA digests during plasmid engineering are shown in Figure 3.4. The final plasmids were analysed by restriction digestion (Figure 3.4F and 3.4G) and verified to be free of mutations by DNA sequencing (data not shown).

Restriction digestion analysis shows that 4 out of 5 clones (no. 1, no. 2, no. 3, and no. 4) of pCAG-SIV have expected sizes of the inserts (Figure 3.4F). These clones were subjected to DNA sequence analysis, and only clone no. 1 and clone no. 3 had the correct orientation of the IRES-Venus element. As there were no mutations within the IRES-Venus region and *SNCA* gene in both clones, either of them could be applied for transgenesis. In this work, I have used clone no. 1.

The control plasmid, pCAG-IV, was constructed by replacing the *SNCA* gene in pCAG-SNCA with a PCR-amplified IRES-Venus product. Plasmid DNA of 5 bacterial transformants were enzymatically analysed for the IRES-Venus insert. Only clone no. 1 and clone no.2 had an insert with a size corresponding to IRES-Venus fragment (Figure 3.4G), thus they were further analysed by DNA sequencing. Since mutations in Venus were detected in clone no. 2 (positions 535-538), but not in clone no. 1, the latter was applied for transgenesis.

3.2 Establishment of αSyn-overexpressing hESC lines

3.2.1 Determination of optimal puromycin concentration for selection of hESC clones

I have investigated the efficiency of puromycin in killing wild type Shef4 hES cells by treating them with various concentrations of the drug ranging from 0.125 µg/ ml to 2 µg/ ml. The cells were challenged with media containing puromycin for 12 days, and they were observed daily for the cell death.

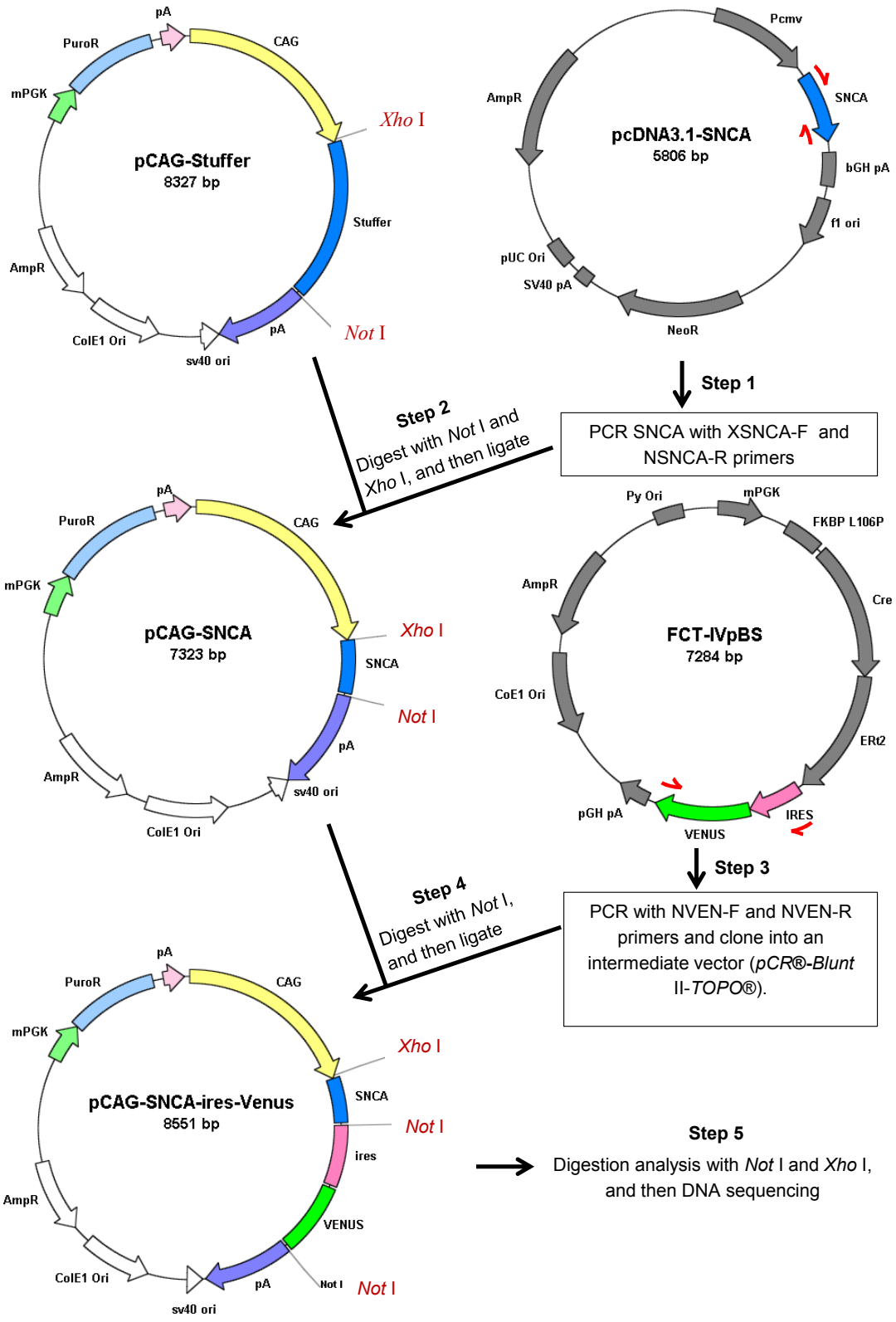
pA
PuroR
CAG
mPGK
pCAG-Stuffer
8327 bp
Xho I
Stuffer
AmpR
ColE1 Ori
pA
Not I
sv40 ori
Pcmv
AmpR
SNCA
pcDNA3.1-SNCA
5806 bp
bGH pA
f1 ori
pUC Ori
SV40 pA
NeoR
Step 1
PCR SNCA with XSNCA-F and NSNCA-R primers
Step 2
Digest with Not I and Xho I, and then ligate
pA
PuroR
CAG
mPGK
pCAG-SNCA
7323 bp
Xho I
SNCA
Not I
pA
AmpR
sv40 ori
ColE1 Ori
Py Ori
mPGK
FKBP L106P
AmpR
Cre
FCT-IVpBS
7284 bp
CoE1 Ori
ERt2
pGH pA
IRES
VENUS
Step 3
PCR with NVEN-F and NVEN-R primers and clone into an intermediate vector (pCR®-Blunt II-TOPO®).
Step 4
Digest with Not I, and then ligate
pA
PuroR
CAG
mPGK
pCAG-SNCA-ires-Venus
8551 bp
Xho I
SNCA
Not I
ires
AmpR
VENUS
ColE1 Ori
pA
Not I
Not I
sv40 ori
Step 5
Digestion analysis with Not I and Xho I, and then DNA sequencing

Figure 3.2 Scheme of plasmid construction of the αSyn expression vector, pCAG-SNCA-IRES-Venus. Step 1, the *SNCA* fragment was derived from pcDNA3.1-SNCA by PCR with a pair of primers containing additional enzymatic restriction sites; *Xho*I site for the forward primer (XSNCA-F) and *Not*I site for the reverse primer (NSNCA-R). Step 2, the PCR product was digested, purified, and then ligated in to between *Xho*I and *Not*I restriction sites of the pCAG-stuffer plasmid, yielding the plasmid pCAG-SNCA. Step 3, the IRES-Venus element with *Not*I sites at both ends was derived from the FCT-IVpBS plasmid by PCR with the primers NVEN-F and NVEN-R. The PCR product was then cloned into the intermediate vector, pCR®-Blunt II-TOPO®. Step 4, the IRES-Venus fragment was digested from the intermediate vector, and then ligated into of the pCAG-SNCA at the *Not*I site, downstream of the SNCA element. This process resulted in a final plasmid construct, pCAG-SNCA-IRES-Venus. The final plasmid was analysed for the correct orientation by enzymatic digestion and DNA sequencing.

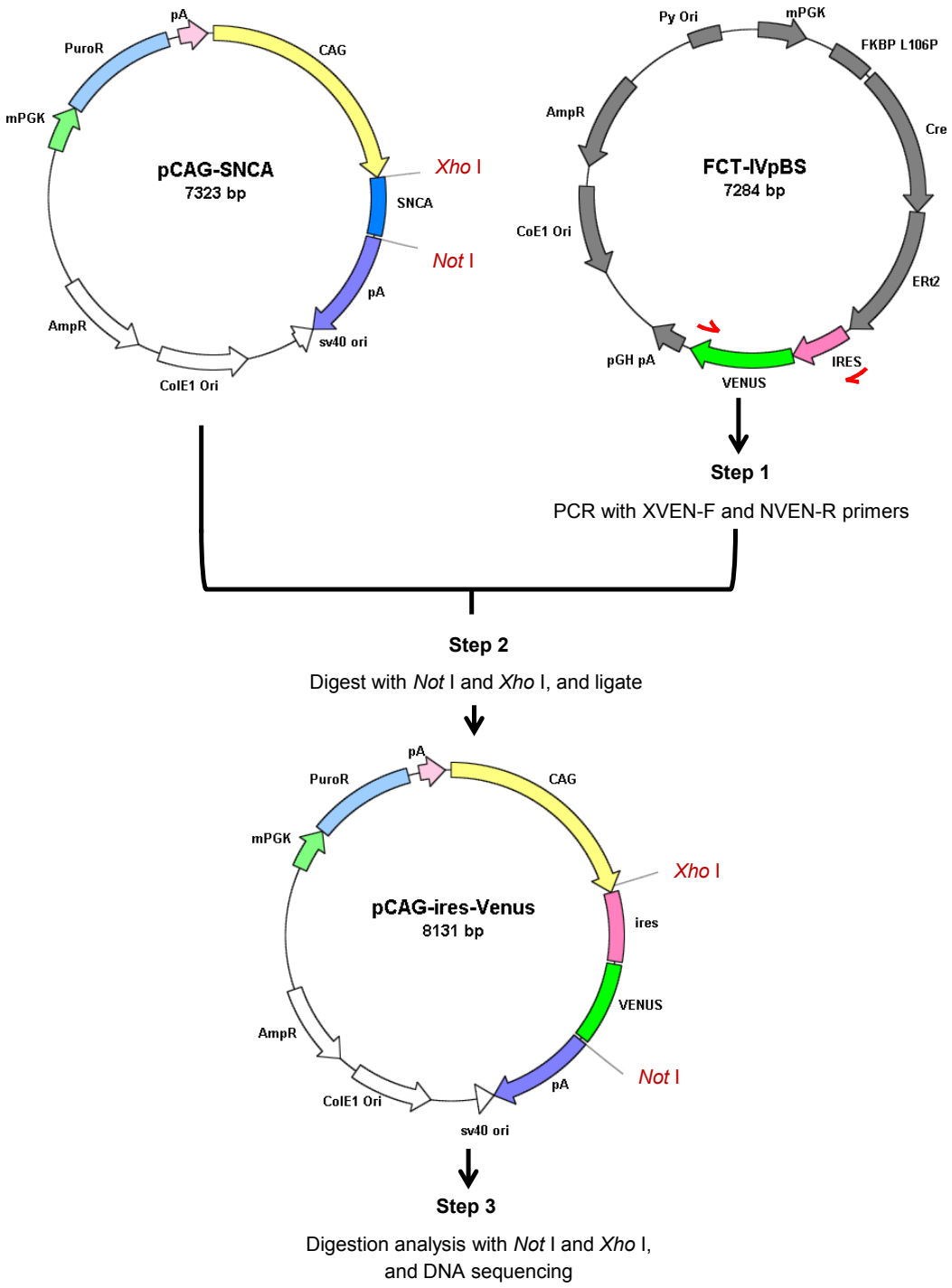

Figure 3.3 Scheme of plasmid construction of the Venus expression vector, pCAG-IRES-Venus. The *SNCA* fragment of pCAG-SNCA, which is an intermediate plasmid during construction of pCAG-SNCA-IRES-Venus, was replaced with the IRES-Venus fragment at the *Xho*I and *Not*I sites. The replacing element is derived from FCT-IVpB via PCR with indicated primers to create compatible restriction sites at both ends. The resulting plasmid has been analysed by enzymatic digestion and DNA sequencing.

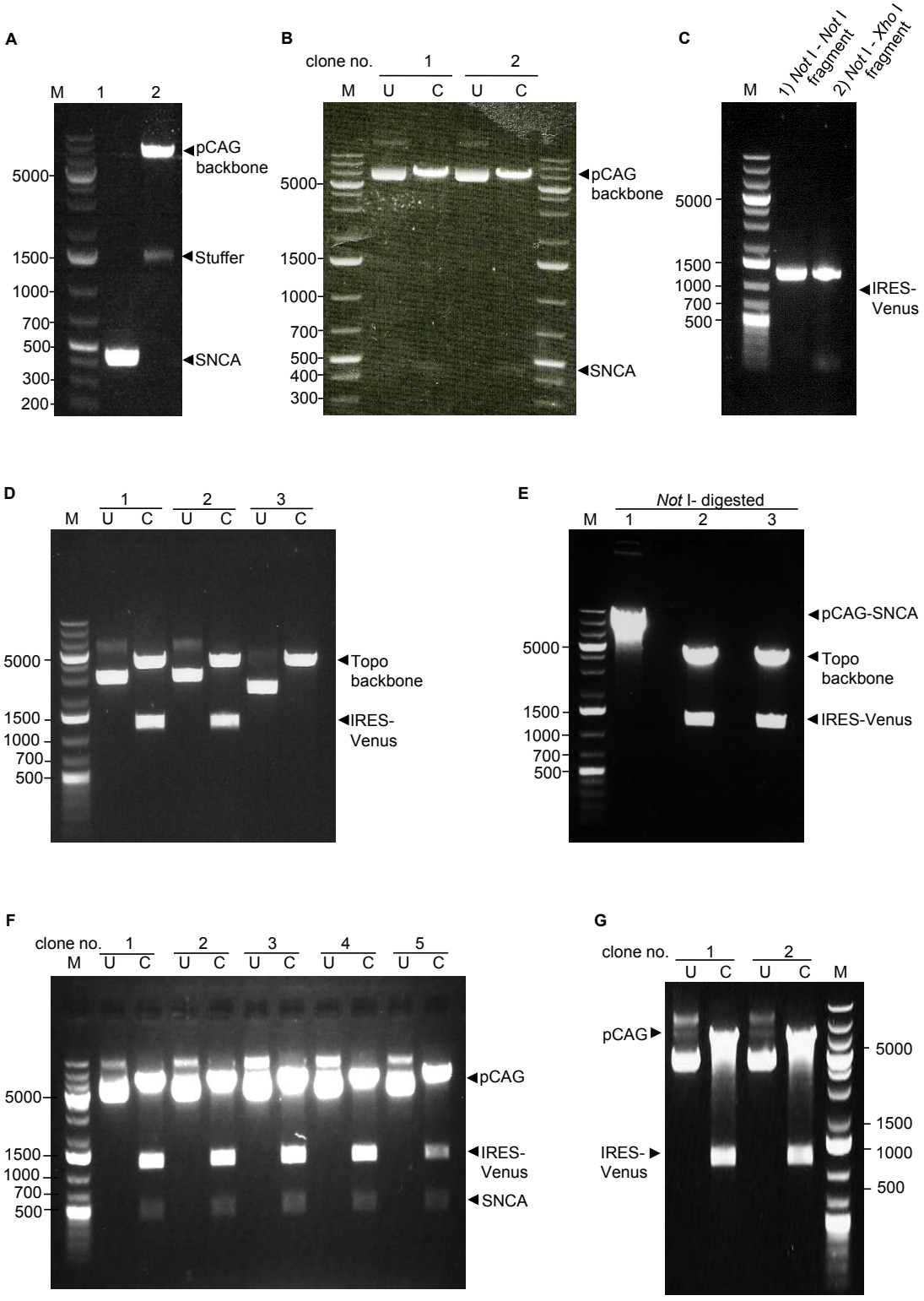
A
M
1
2
pCAG backbone
Stuffer
SNCA
5000
1500
1000
700
500
300
200
B
clone no.
1
2
M
U
C
U
C
pCAG backbone
SNCA
5000
1500
1000
700
500
400
300
C
M
1) Not I - Not I fragment
2) Not I - Xho I fragment
IRES-Venus
5000
1500
1000
700
500
D
1
2
3
M
U
C
U
C
U
C
Topo backbone
IRES-Venus
5000
1500
1000
700
500
E
Not I- digested
M
1
2
3
pCAG-SNCA
Topo backbone
IRES-Venus
5000
1500
1000
700
500
F
clone no.
1
2
3
4
5
M
U
C
U
C
U
C
U
C
U
C
pCAG
IRES-Venus
SNCA
5000
1500
1000
700
500
G
clone no.
1
2
U
C
U
C
M
pCAG
IRES-Venus
5000
1500
1000
500

Figure 3.4 Representative DNA gels of PCR products and digests.

A) PCR product of SNCA and host plasmid (step 1 & step 2, Figure 3.2). The *SNCA* fragment, amplified from pcDNA3.1-SNCA vector (lane 1), and pCAG-stuffer (lane 2) have been digested with *Not*I and *Xho*I. The bands of SNCA and pCAG backbone were excised, purified, and then ligated to make pCAG-SNCA. M: 1 Kb plus DNA ladder.

B) Digestion analysis of pCAG-SNCA shows expected size of an insert corresponding to SNCA fragment. Plasmid DNA of two bacterial transformants was digested with *Not*I and *Xho*I. The result shows an insert with size corresponding to SNCA fragment. DNA sequencing of the insert confirmed correct sequences of SNCA (data not shown). M: 1 Kb plus DNA ladder, U: undigested, C: cut/digested.

C) PCR product of IRES-Venus amplified from FCT IVpBS (step 3, Figure 3.2, and step 1, Figure 3.3).

1: To construct pCAG-SNCA-IRES-Venus, the fragment was amplified with a primer pair that contains *Not*I sites at each end, NVEN-F and NVEN-R.

2: To construct pCAG-IRES-Venus, the fragment was amplified by PCR with a forward primer with a *Xho*I site (XVEN-F) and reverse primer with a *Not*I site *(*NVEN-R). M: 1 Kb plus DNA ladder.

D) Restriction analysis of Topo-IRES-Venus (step 3, Figure 3.2). Digestion with *Not*I shows that bacterial transformants clone no. 1 and clone no. 2 harbour an insert with a size corresponding to IRES-Venus. Clone no. 3 appeared to lack an insert. M: 1 Kb plus DNA ladder, U: undigested, C: cut/digested.

E) Fragments of pCAG-SNCA and of IRES-Venus for making pCAG-SNCA-IRES-Venus (step 4, Figure 3.2). pCAG-SNCA and Topo-IRES-Venus have been digested with *Not*I. The bands of linearized pCAG-SNCA and IRES-Venus were purified, and then ligated before transforming into *E. coli* DH5α. M: 1 Kb plus DNA ladder, 1: pCAG-SNCA, 2 and 3: Topo-IRES-Venus clone no. 1 and clone no. 2.

F) Restriction analysis of pCAG-SNCA-IRES-Venus shows expected size of inserts (step 5, Figure 3.2). The IRES-Venus fragment from Topo-IRES-Venus clone no.1 was inserted into the *Not*I site of pCAG-SNCA. Double digestion with *Xho*I and *Not*I shows an insert with expected size corresponding to IRES-Venus in all transformants. However, DNA

sequencing showed only two clones, clone no.1 and clone no.3, had the correct orientation. M: 1 Kb plus DNA ladder, U: undigested, C: cut/digested.

G) Restriction analysis of pCAG-IRES-Venus shows an insert with a size corresponding to the fragment of IRES-Venus (step 3, Figure 3.3). Plasmid DNA of two bacterial clones was digested with *Xho*I and *Not*I. The results reveal an insert with expected size corresponding to IRES-Venus fragment in both clones. DNA sequencing revealed only clone no. 1 to be free of mutations. M: 1 Kb plus DNA ladder, U: undigested, C: cut/digested.

Note: For all experiments, the results were from a single experiment otherwise stated.

On day 1, the treatment resulted in dramatic cell death at all concentrations (Figure 3.5). The degree of killing efficiency correlated well with the concentrations as expected. At the lowest concentration of 0.125 µg/ ml, cells survived better than those treated with higher concentrations. On day 2, complete cell death was observed at the concentration of 0.5 µg/ ml or higher whereas surviving cells still remained at lower concentrations. On day 5, complete cell death was observed at the concentration of 0.25 µg/ ml. However, there was a group of cells surviving in the 0.125 µg/ ml condition.

From day 6 to day 12, the group of cells observed on day 5 at 0.125 µg/ml continued to proliferate and formed an obvious colony as shown in Figure 3.5. However, their growth rate was retarded compared to the control.

To summarise, puromycin at 0.25 µg/ml and higher concentrations were able to completely kill hES cells within the experimental period of time, whereas 0.125 µg/ml puromycin allowed a degree of colony formation. Generally, the lowest drug concentration that is able to completely kill non-transfected cells within 7 days is considered as an optimal concentration to apply in drug selection for generating stable cell lines. Based on this principle, puromycin at the concentration of 0.25 µg/ml is the optimal concentration. However, as drug resistance has been observed when the concentration was just slightly lower, it raised the concern of using this concentration for selection. Furthermore, during colony formation of hES cells, the accessibility of drug to cells may be reduced, which may increase cell survival. Regarding this concern, I decided to use 0.5 ug/ml puromycin, which is the second lowest concentration that efficiently killed cells in this experiment. Consistent with other work, this concentration also has been used in the HB9 hESC line (Moore et al., 2010)

3.2.2 Optimisation of Shef4 hES cells electroporation

Electroporation using the Neon System (Invitrogen, Carlsbad, CA, USA) has been shown to efficiently deliver exogenous DNA into hES cells to generate stable transfectant lines (Moore et al., 2010). Like other electroporation technologies, it is based on using an electrical current to induce pore formation in the plasma membrane to allow biological molecules to enter cells. The major advantage of the Neon System is it used gold-plated electrodes in a narrow electroporation chamber. This dramatically reduces and the number of cells needed for electroportation. However, optimisation of electroporation conditions for each individual cell line is essential to minimise cell death. Human ES cells are considered to

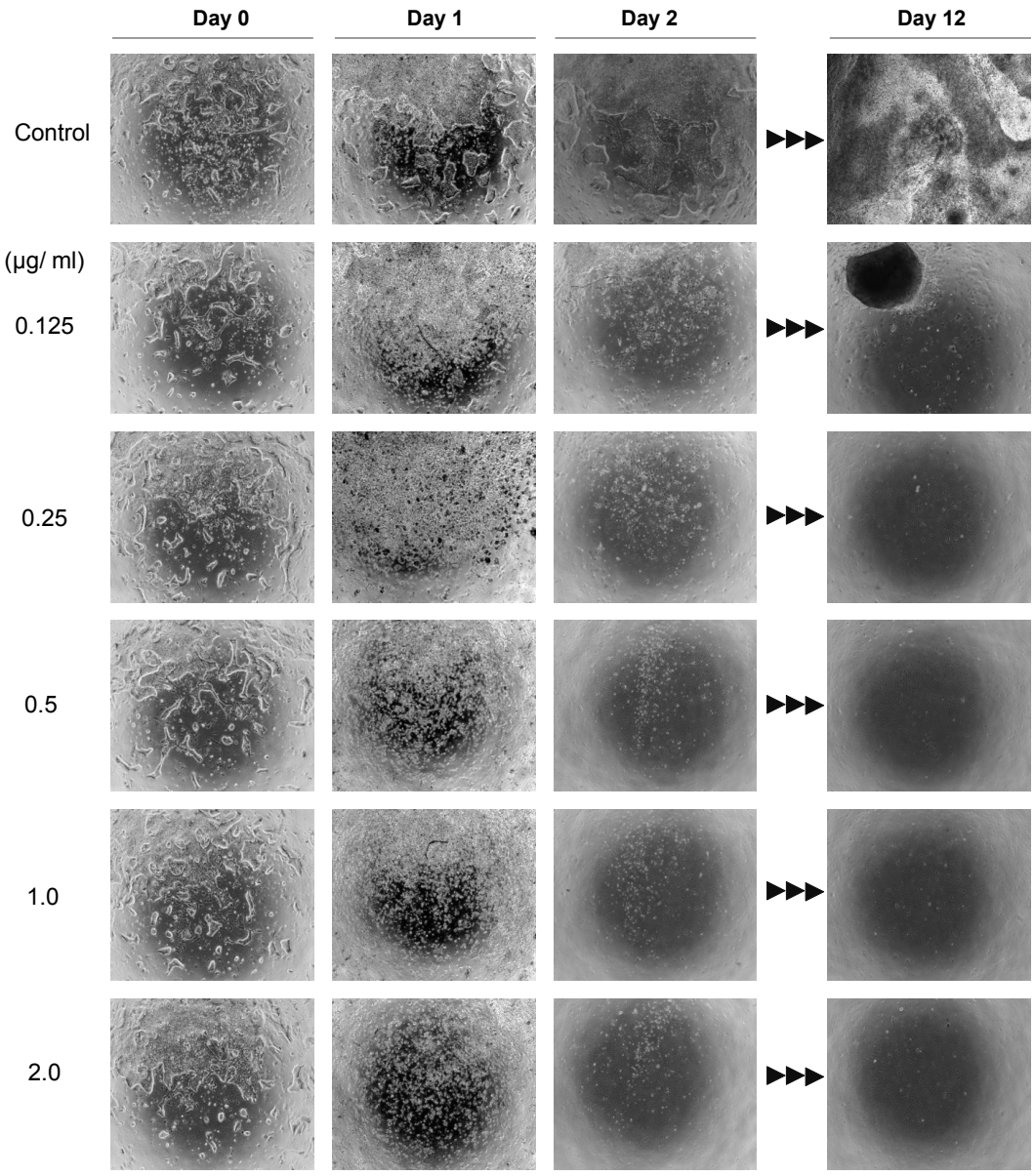

Figure 3.5 Puromycin kill curve. Wild-type Shef4 hES cells were treated with puromycin at different concentrations (0.125 – 2.0 µg/ml) for 12 days to find an optimal concentration for drug selection during the generation of stable transgenic hESC lines.

be the hard-to-transfect cells, in which low genomic integration frequency of introduced exogenous DNA have been reported. Therefore, to increase the chance of integration, efficient transfection is required. High cell viability and maximum transfection efficiency are the major aims of this optimisation.

Since electroporation efficiency is mainly dependent on the combination of three parameters; the electric field, pulse width, and pulse number, I have varied these parameters in four different electroporation conditions (Table 3.1). To investigate the transfection efficiency of each condition, Shef4 cells were electroporated with pCAG-GFP, kindly provided by Agnieszka Paca, a former PhD student in the Kunath lab. At 40 hours post-electroporation, cells were examined for numbers of total surviving cells using Trypan blue. Cells were also analysed for GFP expression by fluorescent microscopy and flow cytometry.

Total viable cell counts showed that electroporation reduces cell viability approximately 40% to 70% when compared to the controls (Table 3.2). The viability of cells appeared inversely correlated with the intensity of GFP and percentage of fluorescent cells. By fluorescent microscopy, condition D gave the highest proportion of cells with intense GFP, but also resulted in the lowest cell survival rate (Table 3.2 and Figure 3.6). Condition F gave a higher cell survival rate; however, it produced the lowest proportion of fluorescent cells. Consistent with the microscopic observations, FACS analysis showed that condition D gave the highest percentage of GFP-expressing cells (57%), and importantly the highest proportion with intense fluorescence (18%) (Figure3.7). These results indicate that among the tested conditions, condition D provided the highest efficiency of delivering plasmid DNA into hES cells with acceptable cell viability. Thus I have applied this condition to transfect Shef4 hES cells with the pCAG-SIV and pCAG-IV plasmids.

3.2.3 Electroporation of Shef4 hES cells with pCAG-SIV or pCAG-IV

The electroporation was performed using condition D optimised previously. Microscopic observation for the Venus fluorescent protein at 24 hours post- electroporation showed that cells electroporated with pCAG-SIV were negative for Venus fluorescence whereas those with pCAG-IV showed only rare fluorescent cells (Figure 3.8). However, the pCAG-GFP produced robust GFP fluorescence in transfected cells. According to this, the absence of Venus expression in Shef4 cells transfected with pCAG-SIV is unlikely to be due to the failure in DNA delivery.

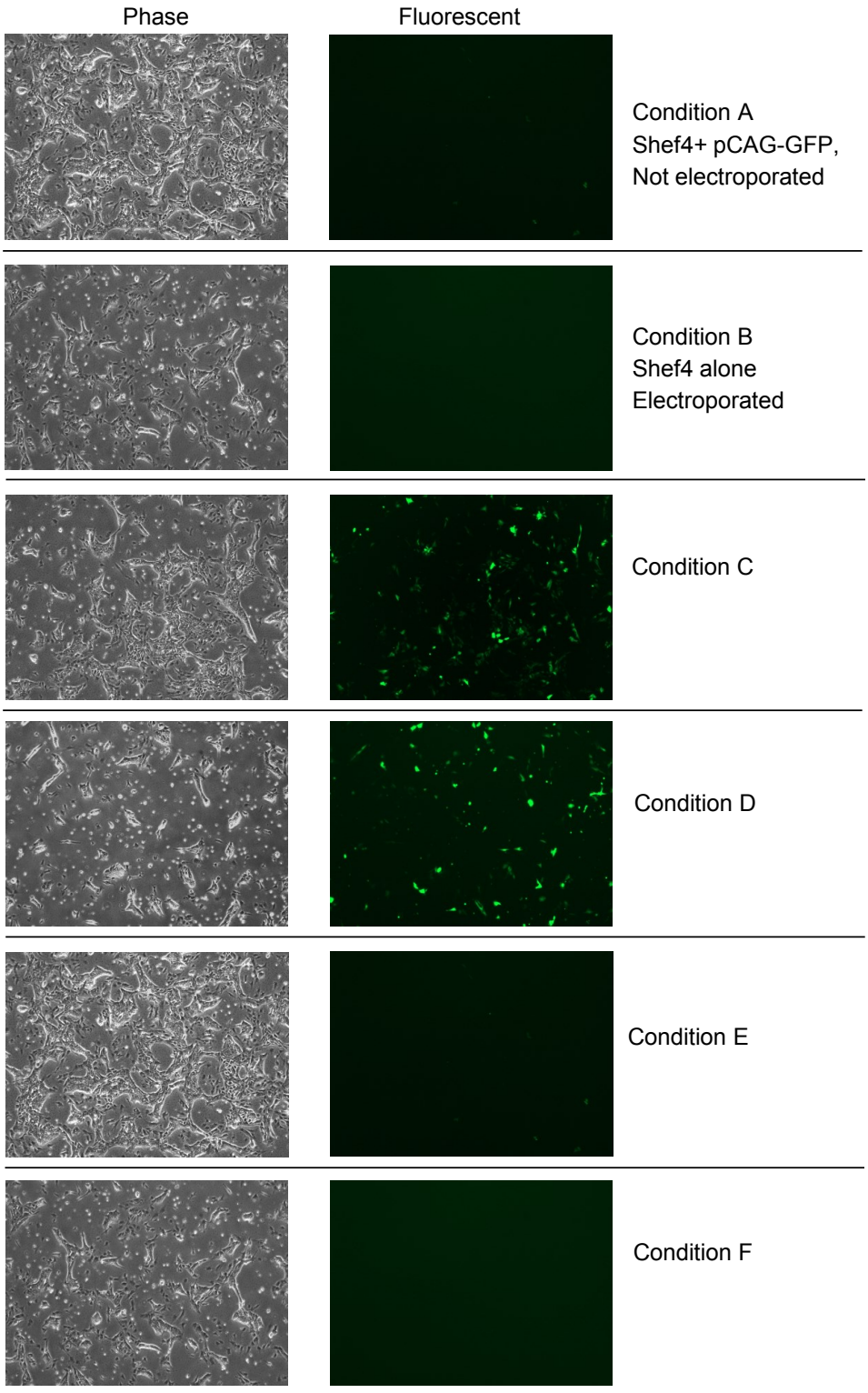

Figure 3.6 GFP fluorescence at 40 hours post-electroporation. To optimise the electroporation of plasmid DNA into Shef4 hES cells, cells were electroporated with pCAG-GFP in different electroporation conditions (A to F, see Table 3.1). Condition C and Condition D provided efficient plasmid delivery as indicated by the expression of GFP.

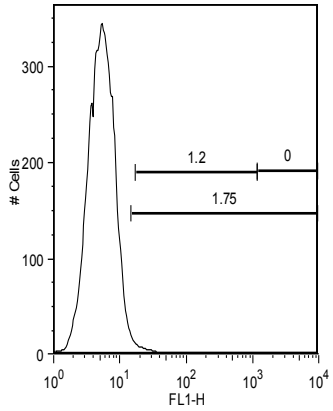

Condition B (negative control)
Shef4 electroporated without pCAG-GFP

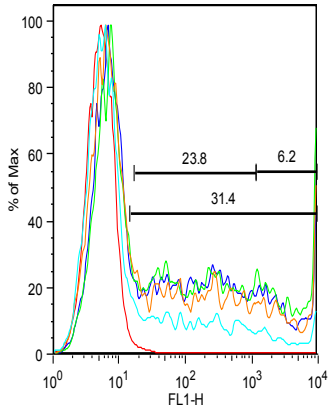

All conditions (merged)

	Control B	1.75
	Condition C	53.5
	Condition D	57.4
	Condition E	48.4
	Condition F	31.4

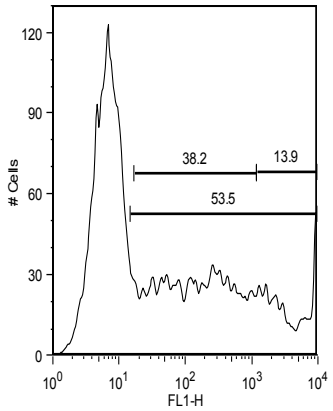

Condition C

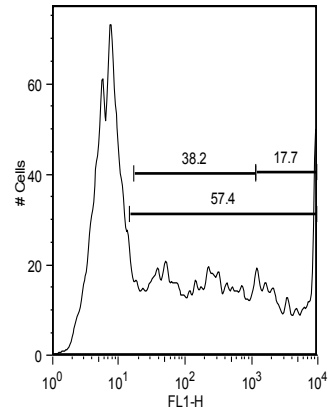

Condition D

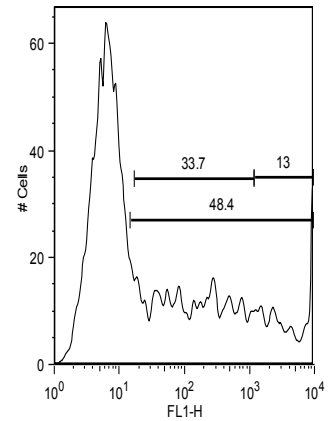

Condition E

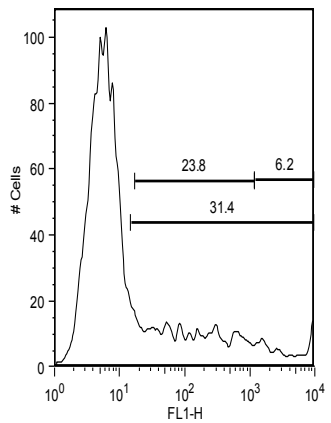

Condition F

Figure 3.7 FACS analysis of GFP-expressing Shef4 hES cells after electroporation of pCAG-GFP. Cells were analysed by FACS 40 hours after electroporation to determine DNA-delivery efficiency. Condition D gave the highest percentage of GFP-positive cells, with over 57% of the total population. This condition was selected for downstream experiments.

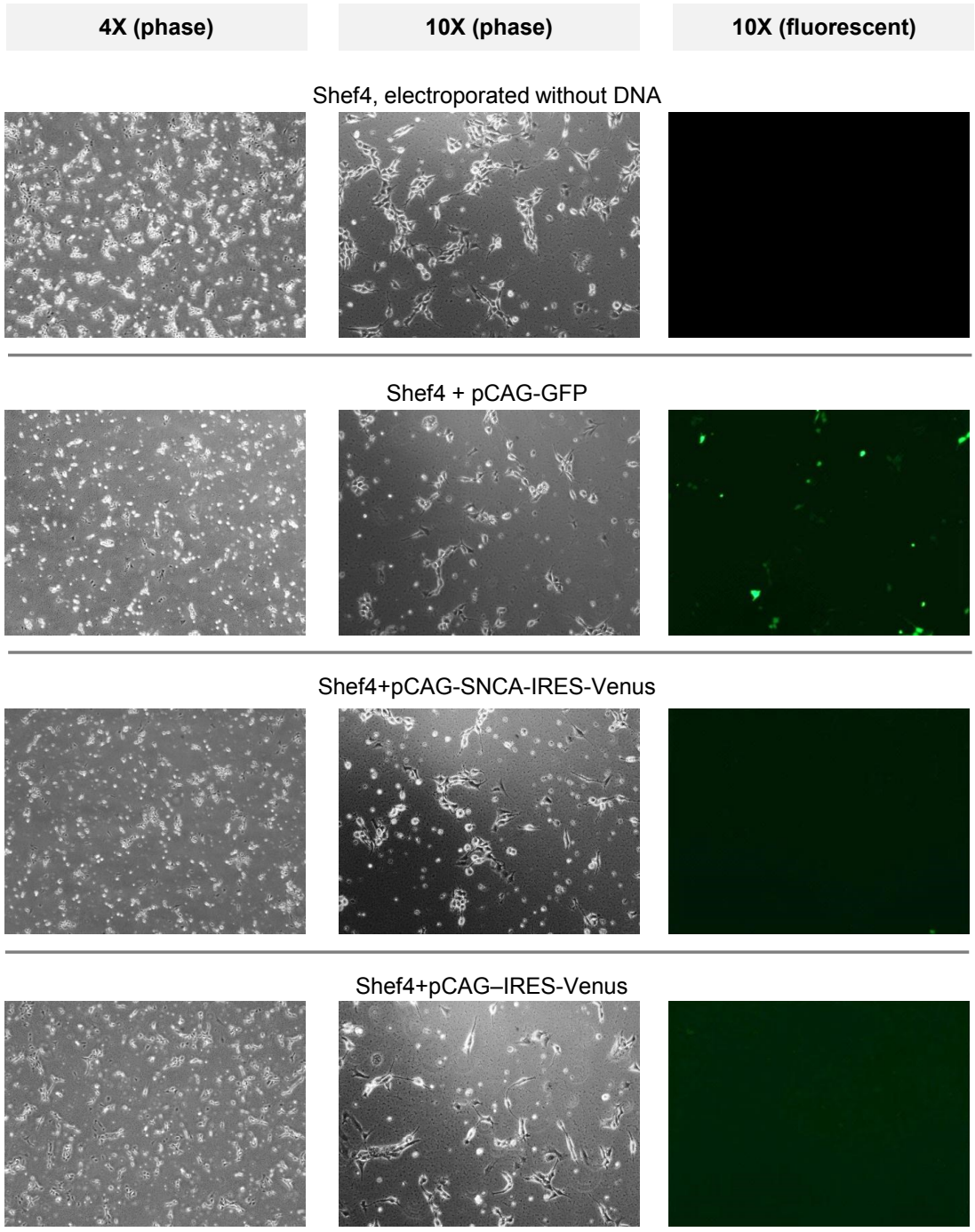

Figure 3.8 Shef4 cells 24 hours after electroporation with pCAG-SNCA-IRES-Venus or pCAG-IRES-Venus. GFP fluorescence in electroporated cells was investigated under by fluorescence microscopy. Cells electroporated with pCAG-SNCA-IRES-Venus exhibited no fluorescence. Rare cells electroporated with pCAG-IRES-Venus exhibited fluorescence (not shown). The cells delivered with pCAG-GFP showed robust GFP fluorescence.

Table 3.1 Optimisation of Shef4 hES cell electroporation conditions with pCAG-GFP.

Code of conditions	DNA	Voltage	Pulse width (ms)	Pulse
A	pCAG-GFP	-	-	-
B	-	1400	20	1
C	pCAG-GFP	1400	20	1
D	pCAG-GFP	1200	20	2
E	pCAG-GFP	1050	30	2
F	pCAG-GFP	950	30	2

Table 3.2 Cell viability and qualitative assessment of GFP fluorescence at 20 hours post-electroporation.

Conditions	Total viable cells	Observation under a microscope
A	1.48×10^5	few green cells
B	1.43×10^5	no green cells
C	8.4×10^4	variable fluorescent intensity within green cells
D	4.6×10^4	high proportion of intense green cells
E	7.2×10^4	number of green cells comparable to Condition D, but with weaker fluorescent signal
F	6.8×10^4	least number of green cells, weak fluorescent signal

I proceeded with puromycin selection, colony picking and expansion of these cells. In the meantime, I investigated Venus fluorescence under a fluorescent microscope regularly. In cells transfected with the plasmid control, pCAG-IV, Venus fluorescence was clearly seen in a majority of colonies (Table 3.3 and Figure 3.9A). However, there was no Venus signal in cells transfected with pCAG-SIV.

As it is possible that Venus expression was lower than that the fluorescent microscope can detect, I decided to use a more sensitive technique to examine the expression. I performed indirect immunostaining for Venus using an antibody against GFP (kindly provided by Mattias Malaguti from Sally Lowell's lab, MRC CRM) in conjunction with a fluorescent–conjugated secondary antibody. The GFP antibody was able to recognise Venus, as shown in the Shef4-IV clone no. 6 (Figure 3.9B). However, none of the clonal lines with pCAG-SIV were immuno-positive for this antibody (Figure 3.9B).

Consistent results were obtained for the two different methods of detection, indicating that cells transfected with pCAG-SIV must have produced very low level of Venus protein or in worst case, did not produce Venus at all. Failure to express Venus is unlikely to be due of a lack of activity of the CAG promoter, as the same promoter was able to drive Venus expression in pCAG-IV. Possible causes of the failure in Venus expression in Shef-SIV clones are listed as follows.

1. The IRES did not function or functions poorly in recruiting ribosomes for protein translation.

2. The IRES-Venus fragment was mutated or removed from the plasmid backbone before or during integration into the host genome.

3. The IRES function is normal, but there is selection for cells that produce very low Venus levels, which can occur when the transgenic protein is toxic to cells. In this case, only cells that have a tolerable level of αSyn can survive.

As different cell lines respond to toxic proteins differently, I have investigated how the transgene plasmids work in mES cells, which are easier to grow and expand more rapidly than hES cells.

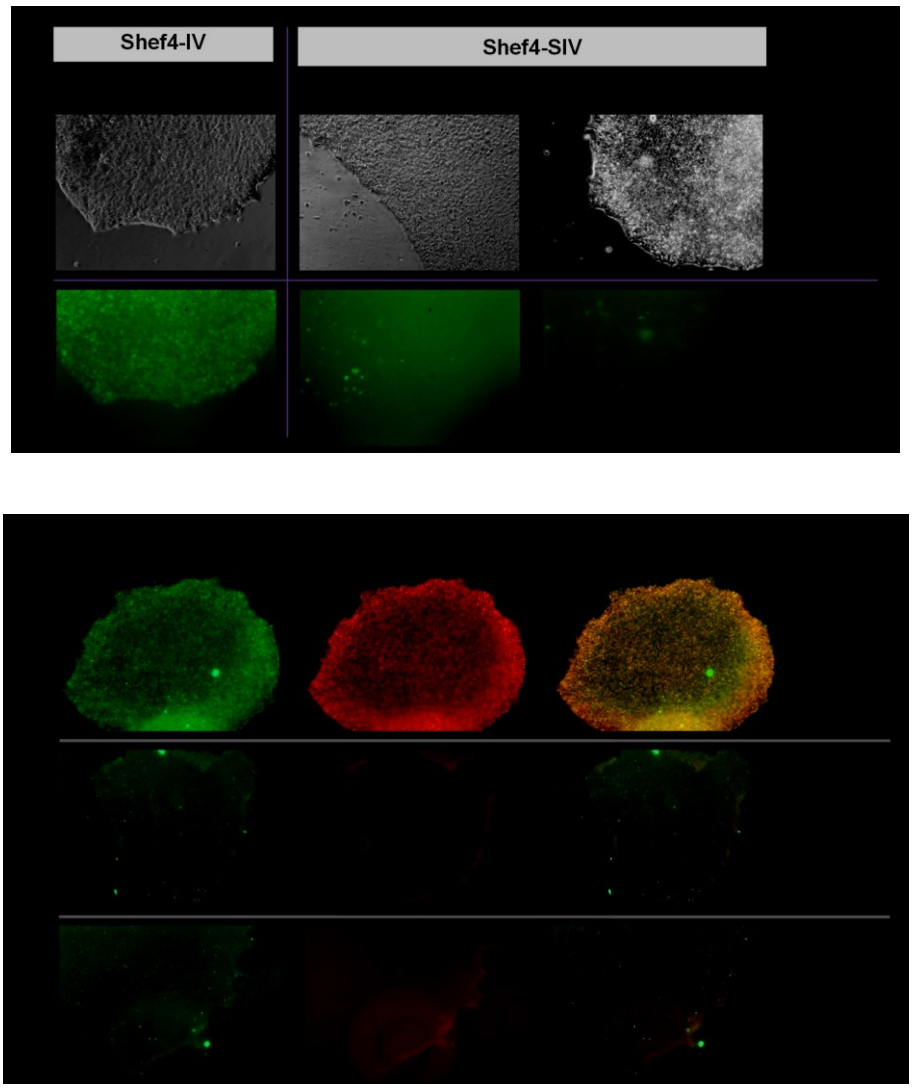

Figure 3.9 Venus expression in Shef4 hES cells transgenic for pCAG-SNCA-IRES-Venus (SIV) or pCAG-IRES-Venus (IV).

A) Venus expression in expanding clonal lines of transgenic Shef4. Representative images of Shef4-SIV and Shef4-IV clonal lines are shown. Venus has observed under a fluorescent microscope. Note that Shef4-IV clone no. 1 is positive for Venus, whereas two Shef4-SIV clones are negative.

B) Anti-GFP immunostaining of Shef4 transgenic clones. Representative images of Shef4-SIV and Shef4-IV clonal lines immunostained for Venus and observed under a fluorescent microscope are shown. Shef4-IV clone no. 6 is positive for the anti-GFP antibody, whereas two Shef4-SIV clones are negative. Shef4-IV, Shef4 with stable expression of pCAG-IRES-Venus; Shef4-SIV, Shef4 with stable expression of pCAG-SNCA-IRES-Venus.

Table 3.3 Number of Venus-ve and Venus+ve clonal lines for Shef4-SIV and Shef4-IV.

Line	Total clonal lines	Venus+ve	Venus-ve	%Venus+ve
Shef4-SIV	11	0	11	0
Shef4-IV	8	6	2	75

3.2.4 Transfection of mES cells with pCAG-SIV

The mES cell line, E14Tg2a, was transfected with pCAG-SIV using Lipofectamine™ 2000 (this experiment was performed by William Hamilton, a former PhD student in the Kunath lab). At 16 hours post-transfection, cells were examined for Venus expression under a fluorescent microscope. Unlike Shef4 hES cells, a large percentage of transfected mES cells exhibited robust Venus fluorescence as shown in Figure 3.10A. The same result was also observed for mES cells transfected with pCAG-IV (data not shown).

I further investigated Venus fluorescence in the transfected population using FACS. The analysis showed that pCAG-IV gave a higher percentage of fluorescent cells than pCAG-SIV; 54% versus 31%, respectively (Figure 3.10B). Moreover, transfection with pCAG-IV produced a population with intense fluorescence, as indicated by a narrow sharp peak at the bottom right of the graph, which is absent in those transfected with pCAG-SIV (Figure 3.10B).

The transfected mES cells underwent puromycin selection and the total numbers of drug-resistant colonies were counted for each construct. The pCAG-IV produced more colonies than pCAG-SIV; 488 versus 395, respectively (Table 3.4). Approximately 50% of the colonies with the pCAG-IV are fluorescent, whereas only 15% of the colonies with *SNCA* expressing plasmid are fluorescent (Table 3.4). A smaller number of Venus-positive colonies obtained from the pCAG-SIV construct are consistent with the FACS results (Figure 3.10B).

Regarding the plasmid components, pCAG-IV and pCAG-SIV are very similar except that the latter plasmid has *SNCA* (Figure 3.1). It was interesting that without *SNCA*, cells appeared to survive better; mES cells transfected with pCAG-IV gave more puromycin-resistant colonies compared to pCAG-SIV. However, this is considered under the assumption that these two plasmids have equivalent transfection efficiency. If this is indeed the case, the results might indicate that there is a selection mechanism against cells that have high levels of αSyn expression. High αSyn protein produced by the *SNCA* transgene might be toxic to cells, producing a smaller number of colonies and less colonies with Venus fluorescence (Table 3.4).

This hypothesis fits well with the FACS observations where pCAG-IV produced higher percentage of Venus fluorescent cells, as well as generated a population with intense Venus fluorescence, which was not observed in cells transfected with pCAG-SIV. The pCAG-SIV

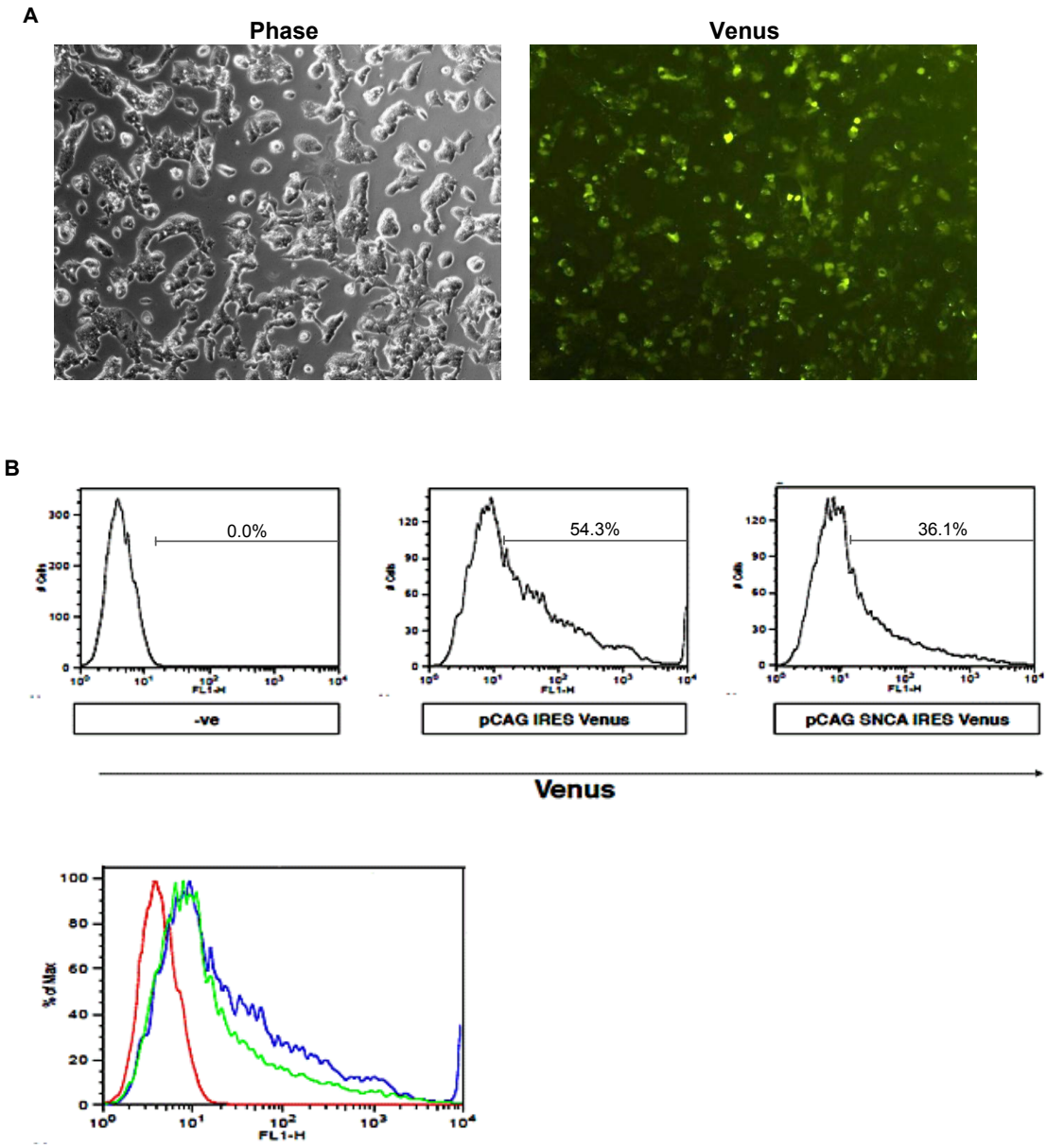

Figure 3.10 The pCAG-SNCA-IRES-Venus and pCAG-IRES-Venus constructs are able to drive the Venus expression in mouse ES cells. A) Fluorescence microscopy of pCAG-SNCA-IRES-Venus in mouse ES cells. Mouse ES cells were transfected with pCAG-SNCA-IRES-Venus, and observed under a fluorescent microscope at 16 hours post-transfection. B) FACS analysis for Venus in mES cells with either pCAG-SNCA-IRES-Venus or pCAG-IRES-Venus. Cells were analysed by FACS for Venus expression 16 hours after transfection. Both plasmids produced detectable fluorescent protein in mES cells. Note that the pCAG-IRES-Venus plasmid gave a higher percentage of Venus-positive cells, including an extremely fluorescent population (at ~10^4 FL1) that was absent in cells transfected with the αSyn-expressing plasmid.

Table 3.4 Number of Venus fluorescent colonies following transfection of mES cells with pCAG-SNCA-IRES-Venus (pCAG-SIV) and the control plasmid (pCAG-IV).

	pCAG-IV	pCAG-SIV
Total drug-resistant colonies	488	395
Venus expressing colonies	45%	15%

is a bicistronic expression vector, from which a single mRNA produces both αSyn and Venus. If selection against high αSyn expression had occurred, there would be a corresponding decrease in Venus expression.

However, low Venus expression from pCAG-SIV could also occur without any underlying selection mechanisms. The second gene downstream of an IRES in a bicistronic vector has been known to produce less protein compared to the coding sequence located immediately downstream of the promoter (Kim et al., 2004). Based on this, higher Venus expression from pCAG-IV could be because it does not have an upstream coding sequence as does pCAG-SIV.

3.2.5 Transfection of Shef4 hES cells using Lipofectamine® LTX

Transfection of pCAG-SIV and pCAG-IV constructs with Lipofectamine® LTX into mES cells gave many robust puromycin-resistant colonies (>300). However, electroporation of the same constructs in Shef4 hES cells gave less than 20 puromycin-resistant colonies. The difference in colony number could be from the nature of cells and/or DNA delivery approaches. To increase the number of Shef4 transgenic lines and potentially identify a pCAG-SIV clone that expresses Venus, I applied a similar transfection approach to Shef4 hES cells.

Shef4 hES cells were transfected with pCAG-SIV and pCAG-IV using Lipofectamine® LTX. At early as 16 hours post-transfection, both plasmids gave rise to a few Venus fluorescent cells within transfected colonies whereas many fluorescent cells were observed in cells transfected with pCAG-GFP (Figure 3.11). The few Venus fluorescent cells observed from transfection with pCAG-IV or pCAG-SIV disappeared when cells underwent puromycin selection and clonal expansion. FACS analysis for Venus expression confirmed the absence of fluorescent cells in these transgenic Shef4 cell lines (performed by Masumi Nagano, a visiting Postdoctoral researcher in the Kunath group) (Figure 3.12).

It is worth noting that using different DNA delivery approaches with the pCAG-SIV constructs never produced stable Venus fluorescent cells in Shef4 hES cells, which is strikingly different from that in mES cells. Whether mES cells are more capable to tolerate an increased αSyn load than hES cells, or the IRES element is preferentially active in mES cells compared to hES cells, remains unknown.

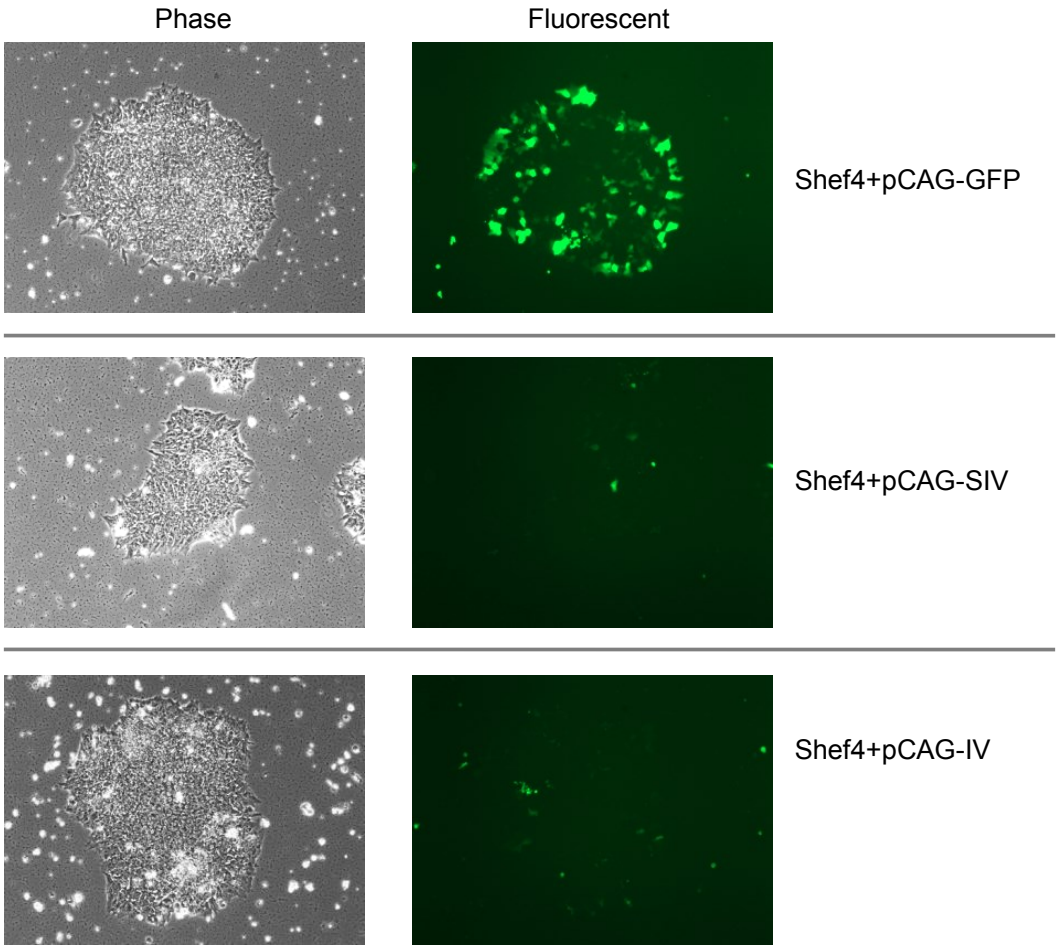

Figure 3.11 Using Lipofectamine® LTX to make additional Shef4 clonal lines. With a similar DNA delivery method to that of mES cells, Venus is not observed in very few Shef4 hES cells. Note that pCAG-GFP serves as a positive control for the transfection and images have been taken at 16 hours post-transfection.

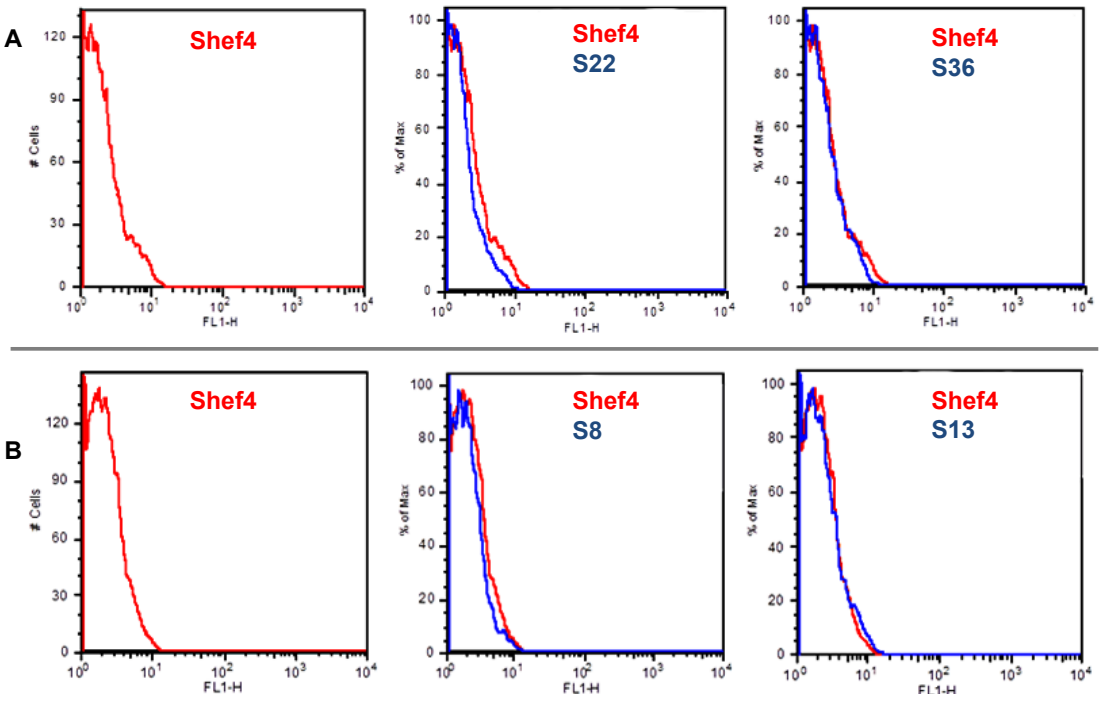

Figure 3.12 FACS analysis for Venus expression in clonal transgenic Shef4 lines. To further investigate the presence of Venus in clonal lines, cells at later passage are subjected to FACS analysis. A) and B) are representative FACS results obtained from two independent experiments. The transgenic lines are negative for Venus as shown by the comparable distribution of cell populations to that of wild-type Shef4, the negative control for Venus. Passage numbers of each clonal line are as follows; Shef4 p62 in A) and p56 in B), S22 p69+18, S36 p69+17, S8 p62+25, S13 p69+14. Note that the former numbers indicate the passage number of the parental line Shef4 when first used to generate the transgenic lines, and the latter numbers are the number of passages after the clones have been established.

.

I have derived more puromycin-resistant hESC colonies using the Lipofectamine™ method compared to that with electroporation using the Neon System (data not shown). This might be due to reduced toxicity of the Lipofectamine™ transfection method. I have picked robust colonies with good hESC morphology to expand into clonal lines. Table 3.5 summaries the total number of clonal pCAG-IV and pCAG-SIV transgenic Shef4 lines derived using each of these two methods.

3.2.6 RT-qPCR for total *SNCA*

The absence of Venus expression in Shef4-SIV lines does not necessarily mean that *SNCA* is not expressed. Venus fluorescence in mES cells transfected with pCAG-SIV indicated that the mRNA of *SNCA*-IRES-*Venus* must have been successfully produced. Failure to detect Venus fluorescence in the Shef4-SIV might be a problem specific to the IRES in hES cells. Regardless of the reason, it was reasonable to investigate the level of *SNCA* expression in these cells.

I investigated the level of total *SNCA* mRNA expression by reverse transcriptase-quantitative PCR (RT-qPCR). I extracted total RNA from expanding puromycin-resistant colonies of Shef4-IV and Shef4-SIV clonal hESC lines, and then performed RT-qPCR. As shown in Figure 3.13, most of the Shef4-SIV lines have an elevated level of *SNCA*; 17 out of 29 lines have more than 3-fold increased expression of *SNCA* to that of the wild-type Shef4 cells. The highest level of *SNCA* expression was observed in Shef4-SIV cell line no. 36 (S36, Figure 3.13). The RT-qPCR results were also consistent with immunostaining for αSyn (Figure 3.14). An increase in *SNCA* expression indicated that the *SNCA* transgene must have integrated in the genomic DNA of the Shef4-SIV cell lines. However, it is clear that Venus expression cannot be used to indicate *SNCA* transgene activity in these cell lines. Instead, the *SNCA* level must be examined by RT-qPCR and further confirmed by western blotting.

It is worth noting that even with high levels of α-synucelin, the transgenic hES cells still remained undifferentiated and maintained typical hESC morphology (Figure 3.9), normal chromosome counts (data not shown), and expression of the pluripotency factor OCT4 (Figure 3.14). However, there is still a concern that the increased level of *SNCA* will affect the differentiation potential of the transgenic hES cells. This was investigated in Chapter 4.

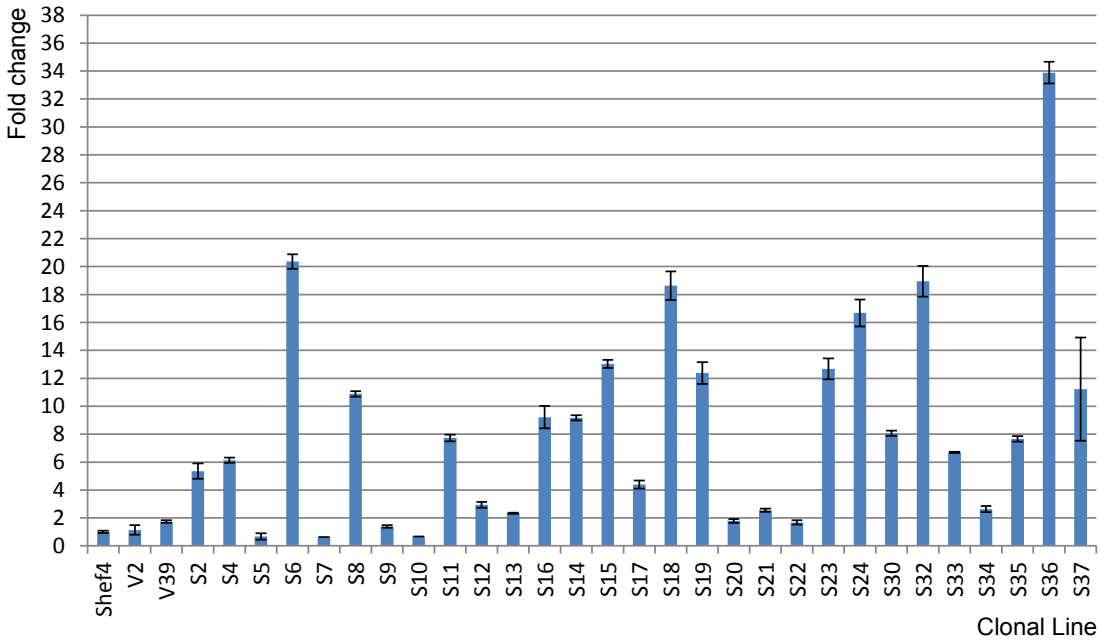

Figure 3.13 RT-qPCR for total *SNCA* in undifferentiated transgenic Shef4 hESC lines. The data has been normalized to 18S rRNA, and shown relative to the parental line, Shef4. V and S lines harbour pCAG-IV and pCAG-SIV, respectively. Each bar represents the mean and standard deviation of 3 technical replicates. These qPCRs were done at different time points and passage numbers, but a control sample was used each time and the data are normalised to this. The data are combined to show the range of values together.

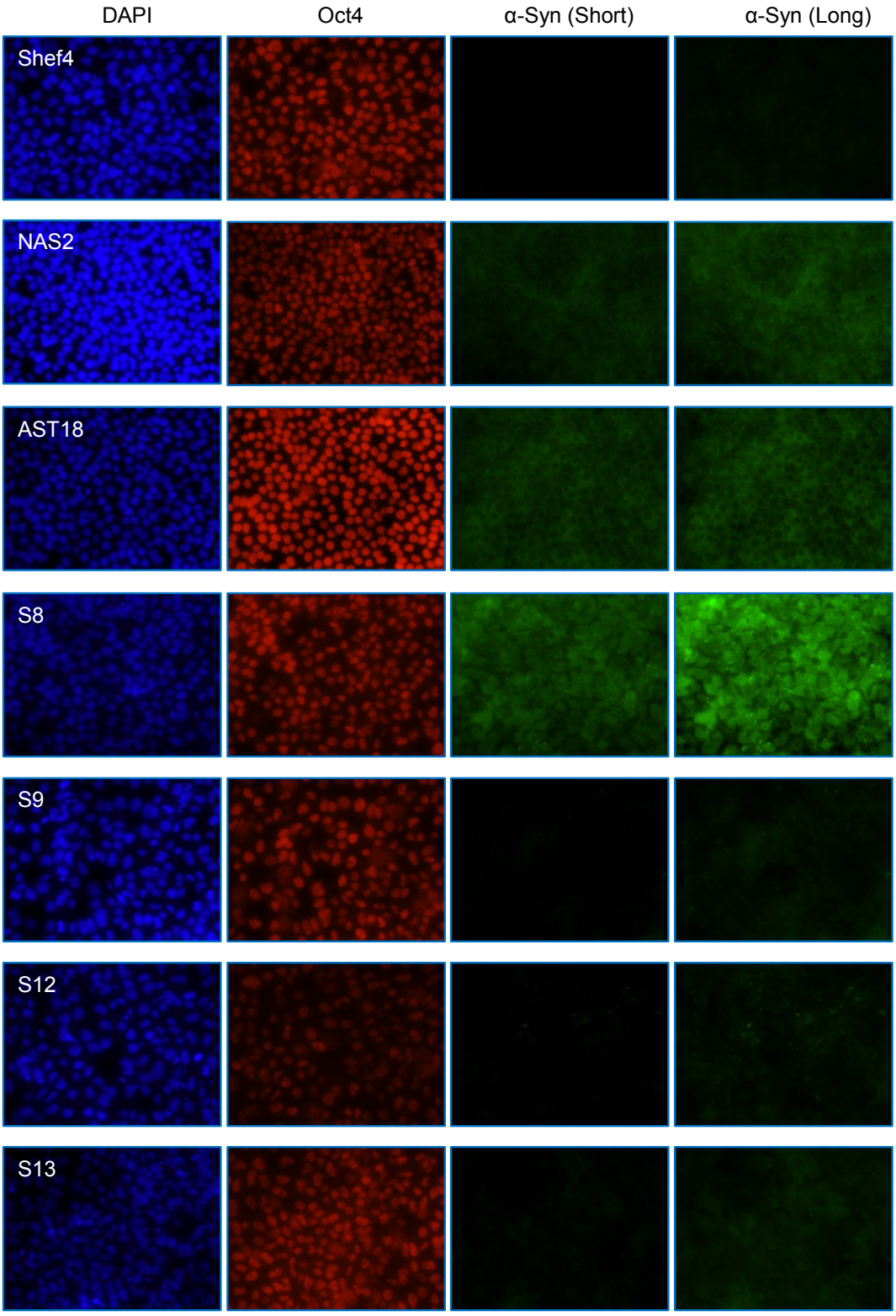
DAPI
Oct4
α-Syn (Short)
α-Syn (Long)
Shef4
NAS2
AST18
S8
S9
S12
S13

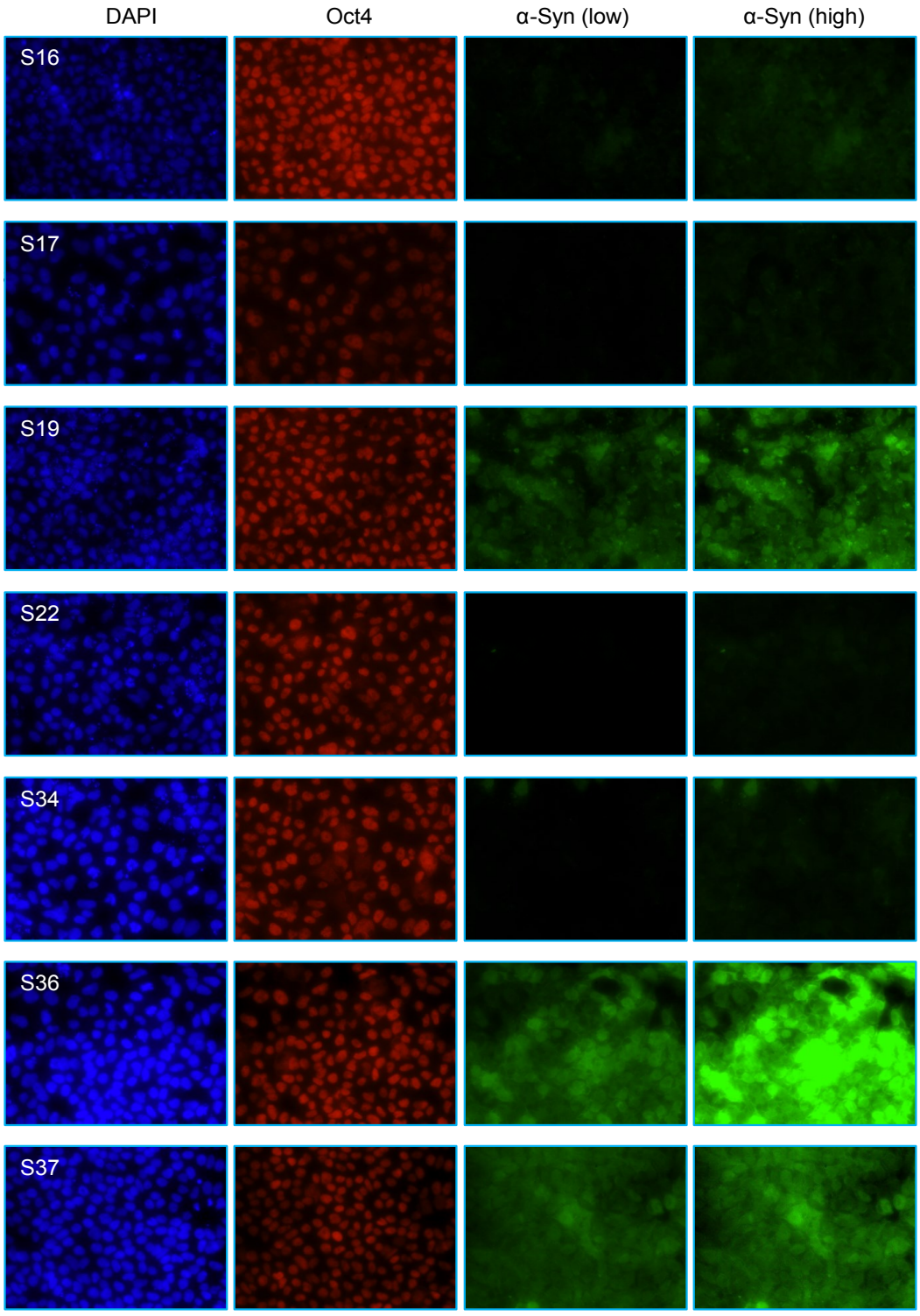

Figure 3.14 Immunostaining of undifferentiated ES cells and iPS cells for total α-Syn and Oct4. The immunostaining conditions were carefully controlled to ensure that all cells were treated the same throughout the staining process. For example, the same antibody batch and concentration, incubation time. To image αSyn, two fixed settings; short- and long exposure time, were applied for each cell line.

Table 3.5 Number of total clonal lines established in this study. The lines have been generated using two different DNA delivery strategies; electroporation and transfection using Lipofectamine® LTX.

Lines	Electroporation	Transfection	Total clonal lines
Shef4-SIV	9*	20	29
Shef4-IV	11	9	20

*Originally, 12 lines are picked, but later 3 lines failed to expand in culture.

3.2.7 Transgene silencing during passages

One of the common difficulties in generating stable transgene expressing hESC lines is the stability of the transgene expression. The stable transfection outcome varies between cell lines and the promoter of choice (Liew et al., 2007; Liu et al., 2009b). Many promoters showed robust transient expression but failed to retain the expression after drug selection and long-term culture. The pCAG promoter has been reported to drive stable transgene expression in undifferentiated mouse ES cells, and to maintain expression in all differentiated derivatives (Alexopoulou; Hadjantonakis et al., 1998). Similar to mES cells, stable transgenic hESC lines have been successfully generated using the CAG promoter (Liew et al., 2007; Seguin et al., 2008). Results from Draper and colleagues showed that although gene silencing was observed with the pCAG promoter, its incidence was less than observed for four other experimental promoters (Liew et al., 2007).

I have investigated the stability of the *SNCA* transgene in undifferentiated transgenic Shef4 hESC lines during continuous passaging by quantifying total *SNCA* mRNA levels in these cells at early and late passages. One out of 5 Shef4-SIV clonal lines had a dramatic reduction of total *SNCA* at later passages (Figure 3.15). Although the other four clonal lines still maintained high expression, their expression levels decreased slightly. These results indicate that some *SNCA* transgene silencing is occurring, but it is not widespread. Quantifying endogenous and exogenous *SNCA* expression separately should be able to more accurately monitor this. The potential for transgene silencing suggests that *SNCA* expression in the Shef4-SIV hESC lines should always be examined when conducting experiments with them. Chapter 4 will examine whether the transgene is silenced when the hES cells have undergone differentiation towards neurons.

3.2.8 MTS assay for cell proliferation

During clonal line expansion of transgenic Shef4 cells, I have noticed that some cell lines required cell passaging more often than others, raising the question whether αSyn can affect the proliferation rate of hES cells. Therefore, I investigated the correlation between cell proliferation rate and *SNCA* expression level in these cells. I divided the cell lines into two groups based on *SNCA* level assessed by RT-qPCR, namely low and high *SNCA* expression. I then employed a colorimetric assay, CellTiter96® AQ_{ueous} One Solution Cell Proliferation Assay (MTS assay), to measure cell proliferation. The assay utilises a compound called MTS tetrazolium, which is bioreduced, presumably by NADH or NADPH, in viable cells.

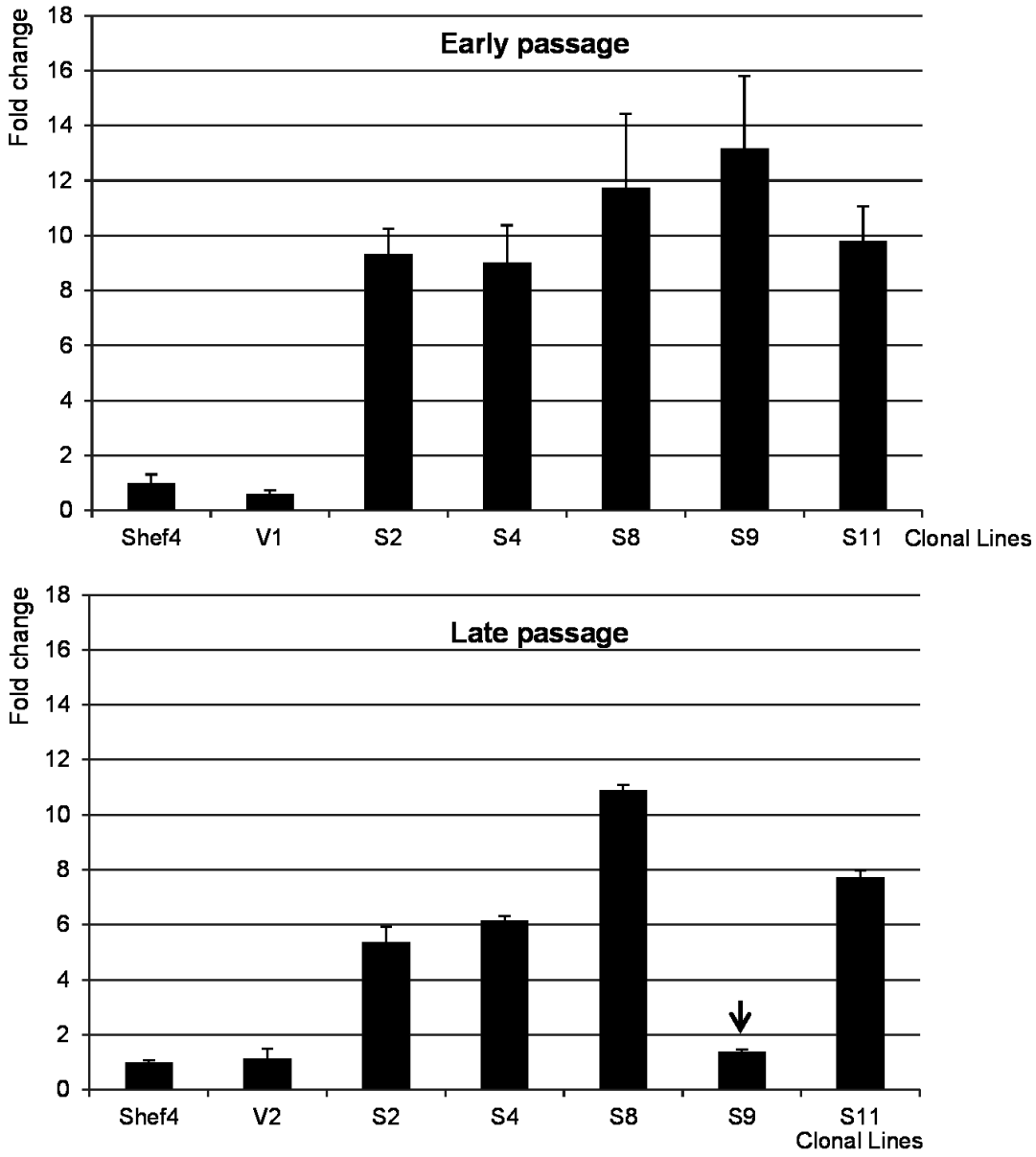

Figure 3.15 RT-qPCR for *SNCA* shows gene silencing in transgenic ES cells during passages. RT-qPCR has been carried out in early and late passages; passages 2 or 3 and passages 12 or 13 for early and late passages, respectively. Please note that S9 shows a reduction in *SNCA* expression in later passages. The data has been normalized to 18S rRNA, and shown in relative to the parental line, Shef4. Each bar represents the mean and standard deviation of 3 technical replicates. V: cell lines harbouring pCAG-IV, S: cell lines harbouring pCAG-SIV.

The process results in production of a soluble colour substance, known as formazan product, which specifically absorbs light at 490 nm. As the production of the formazan product is dependent on NADH or NADPH, which is produced by metabolic active cells, the amount of absorbance is proportional to the number of living cells in culture.

I initially validated the assay by investigating whether the absorbance and cell numbers are correlated. The analysis showed that there is a strong positive correlation between these two factors (R^2=0.98, P<0.05) when the cells are plated at a range between 3.8×10^4 cells/well to 20×10^4 cells/well (Figure 3.16). The results were obtained from two independent cell lines and performed in triplicate. I have chosen a cell density of 5×10^4 cells/well, the second lowest density that showed strong correlation with cell survival, for later experiments. This will prevent over-crowding of cells near the end of the experiment.

I assessed cell proliferation of the transgenic hESC lines using the conditions optimised above. The analysis revealed no statistically significant difference in the proliferation rates between two groups of cells as shown in Figure 3.17 and Figure 3.18A (Student's-t test, P > 0.05). Linear regression also indicated no significant correlation between *SNCA* expression levels and the proliferation rates of the cell lines (R^2 = 0.003, P = 0.884, Figure 3.18). It is also notable that there is no significant difference in cell survival between these groups of cells, as shown by the results of MTS assay at 24 hour post-plating (Figure 3.17). These results indicate that *SNCA* level does not affect hESC proliferation and survival of undifferentiated hES cells.

Variation of properties among the transgenic Shef4 hESC clonal lines is not correlated with *SNCA* levels, but might have been caused by two major factors – clonal variation and random integration of the transgene plasmids in the host genome. It is well known that hES cells are comprised of heterogeneous cell populations, in which sub-populations differ in functional properties (Stewart et al., 2006). Variation in clonal lines of hESC lines has also been reported (Heins et al., 2006). It must be acknowledged that these functional differences might have complications in response to an elevation of α-sunuclein. Although less likely, the clonal variation might be caused by random integration of transgenes into critical areas of the genome.

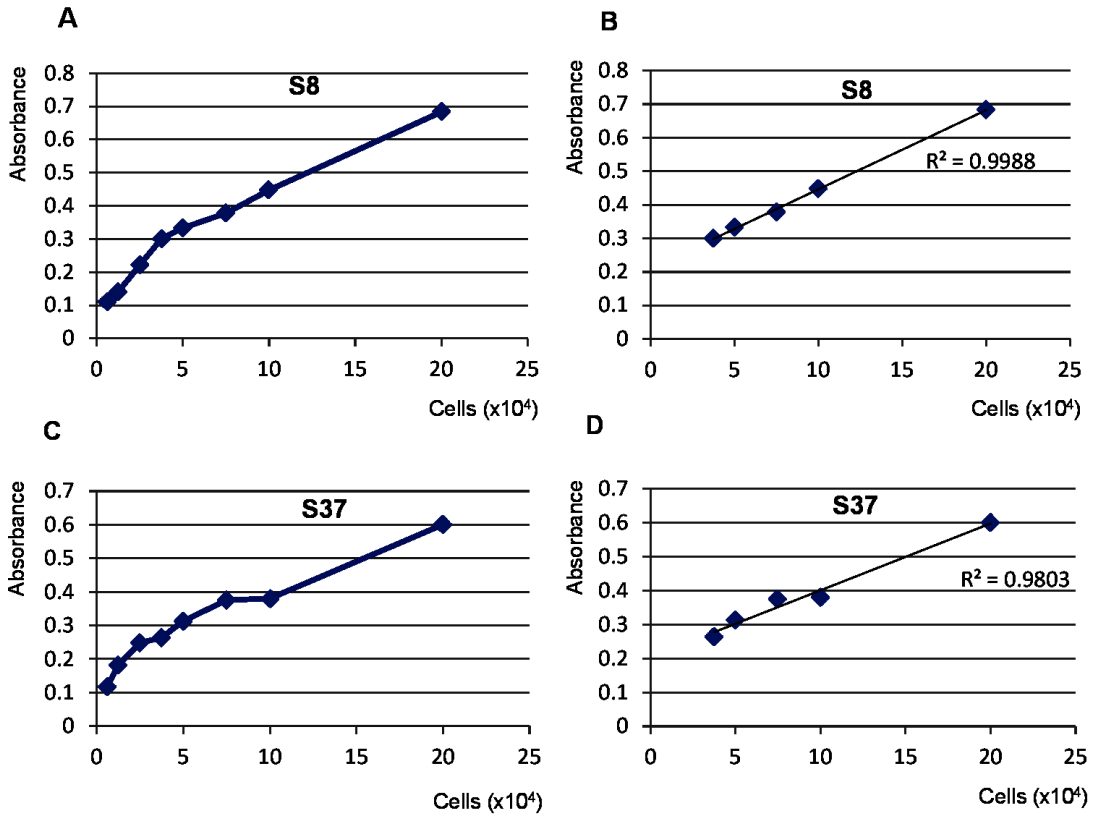

Figure 3.16 Determining suitable seeding density for cell proliferation assay using the CellTiter96® AQ_{ueous} One Solution reagent (MTS assay). Two transgenic Shef4 hESC lines (S8 and S37) were seeded as single cells at various densities in mTeRS1 medium in 96-well plates coated with GFR-Matrigel™. After 24 hours of incubation, the plates are collected for MTS assay, for which absorbance for each cell line was measured at 490 nm (A, C). Data at each cell density was obtained from triplicate samples. A strong linear relationship between cell number and absorbance was observed when cells were plated within a range of 3.38×10^4 cells/well to 20×10^4 cells/well, as indicated by the correlation coefficients displayed on the graphs (B, D).

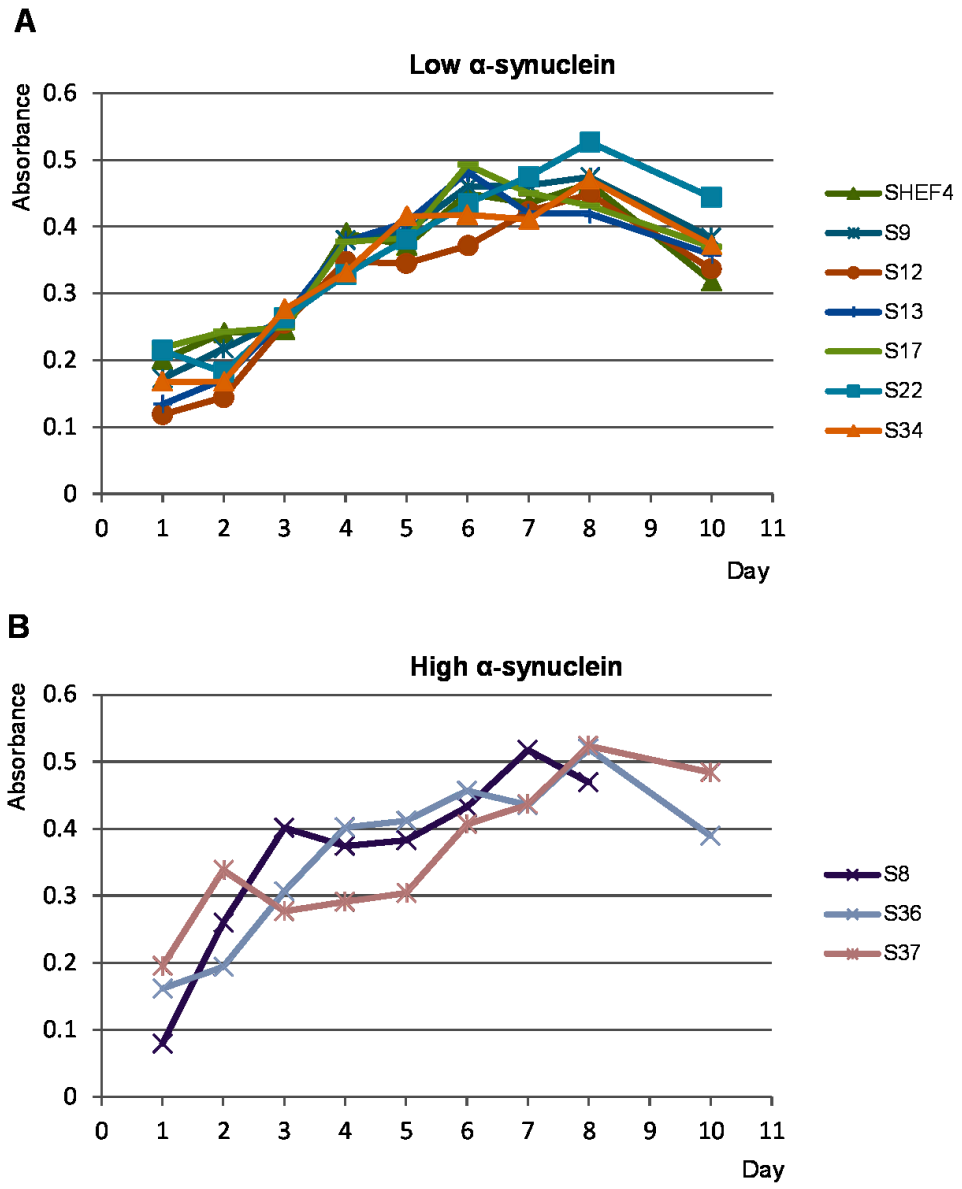

Figure 3.17 Cell proliferation of transgenic Shef4 hESC lines. The MTS assay was performed daily over a period of 10 days post seeding for six Low αSyn lines (A) and three High αSyn lines (B) seeded in three wells each. Proliferation curves have been constructed using the means of absorbance at 490 nm of triplicate samples (n=1). Note that the S8 data was only obtained for 8 days due to a shortage of cells.

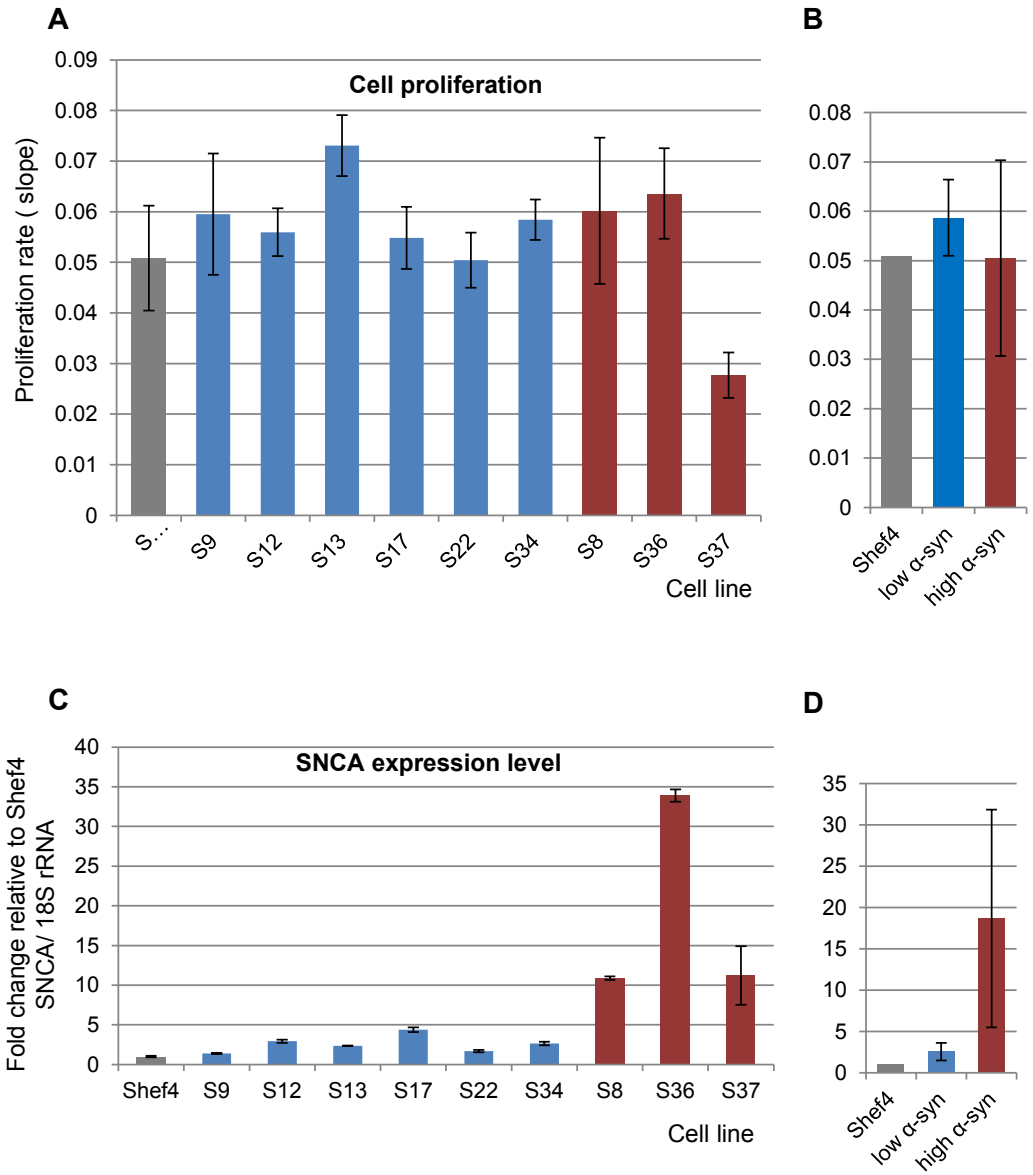

Figure 3.18 Effects of *SNCA* level on the proliferation rate of hESC lines. For each cell line, the proliferation is the slope of the linear trend line of the data obtained between Day 1 to Day 6 based on results shown in Figure 3.17. The colours of the bars indicate groups of cells regarding their SNCA expression level; grey: a parental line, blue: low *SNCA* expression, red: high *SNCA* expression. Statistical analysis shows no significant difference of the proliferation rates between the low α-syn and high α-syn groups (Student's-t test, $P > 0.05$). Linear regression also indicates no significant correlation between *SNCA* expression levels and proliferation rates of the cell lines ($R^2 = 0.003$, $P = 0.884$). A) and B) Rate of cell proliferation shown as of individual cell lines, and that shown as an average of each group, respectively. C) and D) *SNCA* expression level shown as of individual cell lines, and that shown as an average of each group, respectively.

Chapter 4

Characterisation of SNCA transgenic hESC lines

Introduction

In this chapter, I aimed to answer the following questions. 1) Is the level of *SNCA* transgene expression observed in hES cells maintained during differentiation into neural cells? 2) Does *SNCA* over-expression in undifferentiated hES cells affect their differentiation potential towards the neural lineage? 3) Does elevated αSyn increase reactive oxygen species (ROS) production and cell death in neurons?

Firstly, I have shown that in many hESC clones, the *SNCA* transgene is stably expressed in differentiated neural cells. When transgenic Shef4 hES cells are differentiated down the neural lineage, the resulting cells exhibited an elevation of total *SNCA* expression when compared to the control lines. The results indicated that the pCAGS-*SNCA* transgene can successfully drive expression in neural cell types.

Then, I investigated the correlation between *SNCA* expression in transgenic Shef4 hES cells and their neural differentiation potential, which was assessed by the expression of pan-neural genes, *NCAM* and *MAPT*. I have shown that there is no significant correlation between *SNCA* expression and the expression of either neuronal marker. From these results, I concluded that *SNCA* over-expression in transgenic Shef4 hES cells is unlikely to affect their differentiation potential towards the neural lineage.

4.1

In the final part of this chapter, I differentiated transgenic Shef4 hESC lines into cortical neurons. I compared the rate of ROS production in neurons with high αSyn and control neurons with normal levels of αSyn expression. I found that young neurons with *SNCA* over-expression exhibited a higher rate of ROS production when compared to the control neurons. However, when I investigated this effect in more mature neurons, the difference in ROS production was not observed. The issues related to these observations are discussed.*SNCA* transgene is stably expressed in neural cells differentiated from hES cells; however, transgene silencing occurred in some clonal lines.

One of the major concerns with using transgenic hESC lines to investigate a specialised cell type is the stability of transgene expression during differentiation. As transgenes can be

silenced during any step of the differentiation, it is essential to check for maintenance of expression.

To investigate whether *SNCA* transgene expression is maintained during neural induction and specification, I differentiated transgenic Shef4 hESC lines and parental Shef4 hES cells towards the neural lineage using a monolayer dual-Smad inhibition protocol (Chambers et al., 2009) (Figure 4.1A). The protocol combines inhibitors of BMP and Activin/Nodal signalling to induce neural differentiation of hES cells. The majority of neural cells produced by this protocol have forebrain identity and express the characteristic markers PAX6, OTX2 and FOXG1 (Chambers et al., 2009). In this study, I used LDN-193189, a chemical BMP receptor antagonist, to replace Noggin as it exhibited higher efficacy to induce neural differentiation with lower cost.

I first showed that neural induction using this protocol was efficient and robust. Transgenic S9 and parental Shef4 hES cells were differentiated towards the neural lineage as shown by expression of a neurectoderm cell fate determinant PAX6 and a neuronal marker TuJ1 after 14 days of neural induction (Figure 4.1B). Consistent with the immunocytochemistry results, RT-qPCR revealed a significant increase in the expression of neuronal genes *NCAM* and *MAPT* (Figure 4.1C). And as expected, *SNCA* expression also increased when hES cells were differentiated down the neural lineage for 11 days, compared to the undifferentiated state. Both the parental Shef4 hES cells and the transgenic S9 line exhibited a modest increase of *SNCA* expression between 2-4 fold (Figure 4.1C). Although S9 is a transgenic hESC line, it has a normal level of *SNCA* expression compared to undifferentiated parental Shef4 (Figure 3.13), and is therefore not considered an over-expression cell line. One might be able to assume that the elevation of *SNCA* expression in S9 cells at day 11 is only driven by endogenous *SNCA*, not the *SNCA* transgene (Figure 4.1C).

Then, I assessed total αSyn expression in 22 transgenic hESC lines by western blotting. By comparing the αSyn expression of the transgenic lines to that of the control lines, I identified cell lines that stably over-express αSyn when differentiated toward the neural lineage (Figure 4.2).

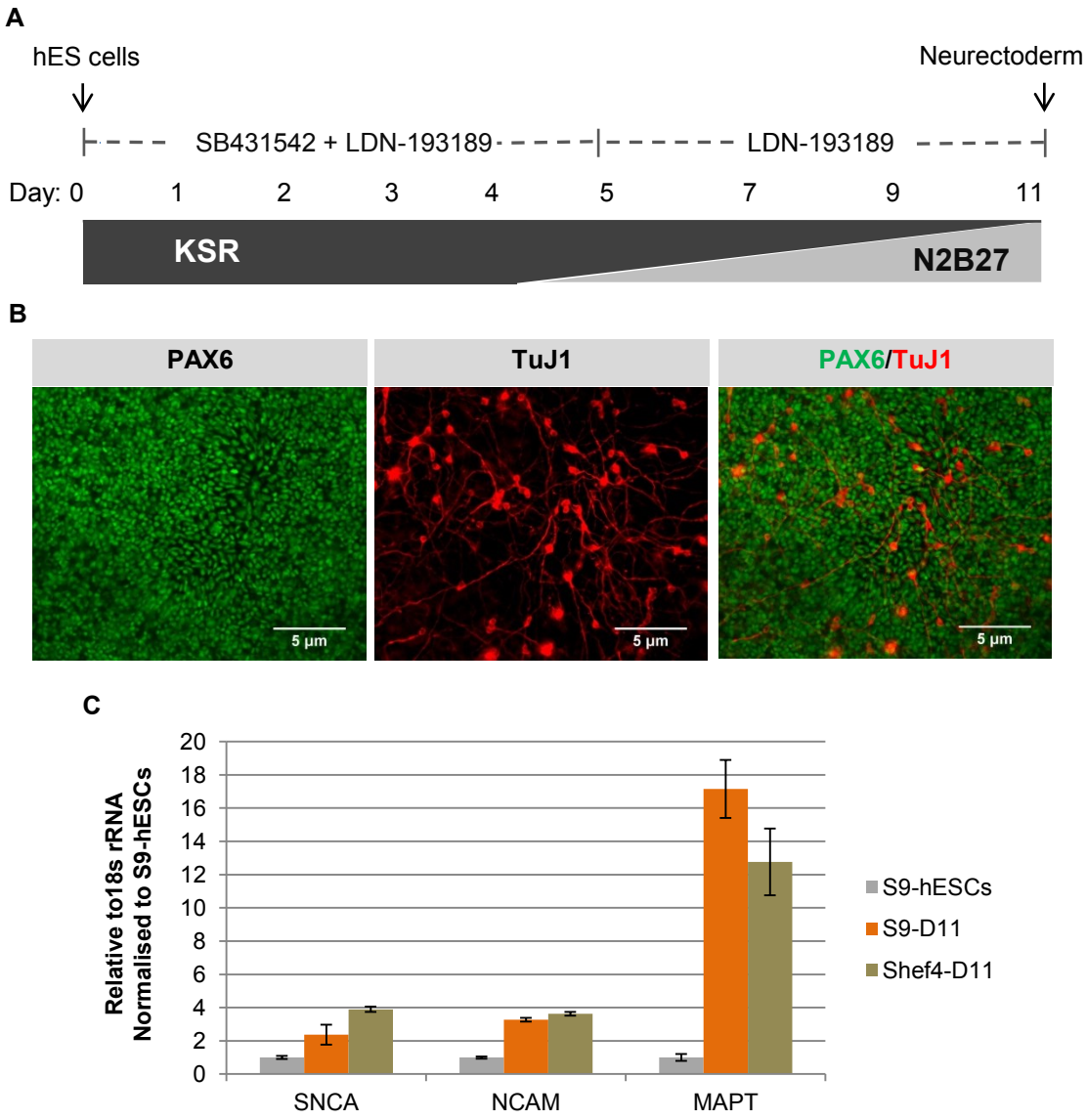

Figure 4.1 Neural induction of transgenic Shef4 hESC lines. A) Schematic of dual-SMAD inhibition protocol used to differentiate transgenic hESC lines towards neurectoderm. Human ES cells were fed daily with KSR medium supplemented with SB431542 and LDN-193189, inhibitors of TGF-β type I receptors and BMP receptors, respectively. From day 5 of differentiation, SB431542 was withdrawn and the KSR medium was gradually replaced by N2B27 medium. B) Immunocytochemistry for PAX6 and TuJ1 of neuralised transgenic Shef4 hESC line, S9. At day 14 of neural induction, the majority of cells expressed PAX6 and a number of TuJ1-positive neurons were also observed. C) RT-qPCR for total *SNCA*, *NCAM* and *MAPT* at day 11 of neural induction. All three genes increased expression during neural induction and significant differences were not observed between the transgenic (S9) and parental (Shef4) lines.

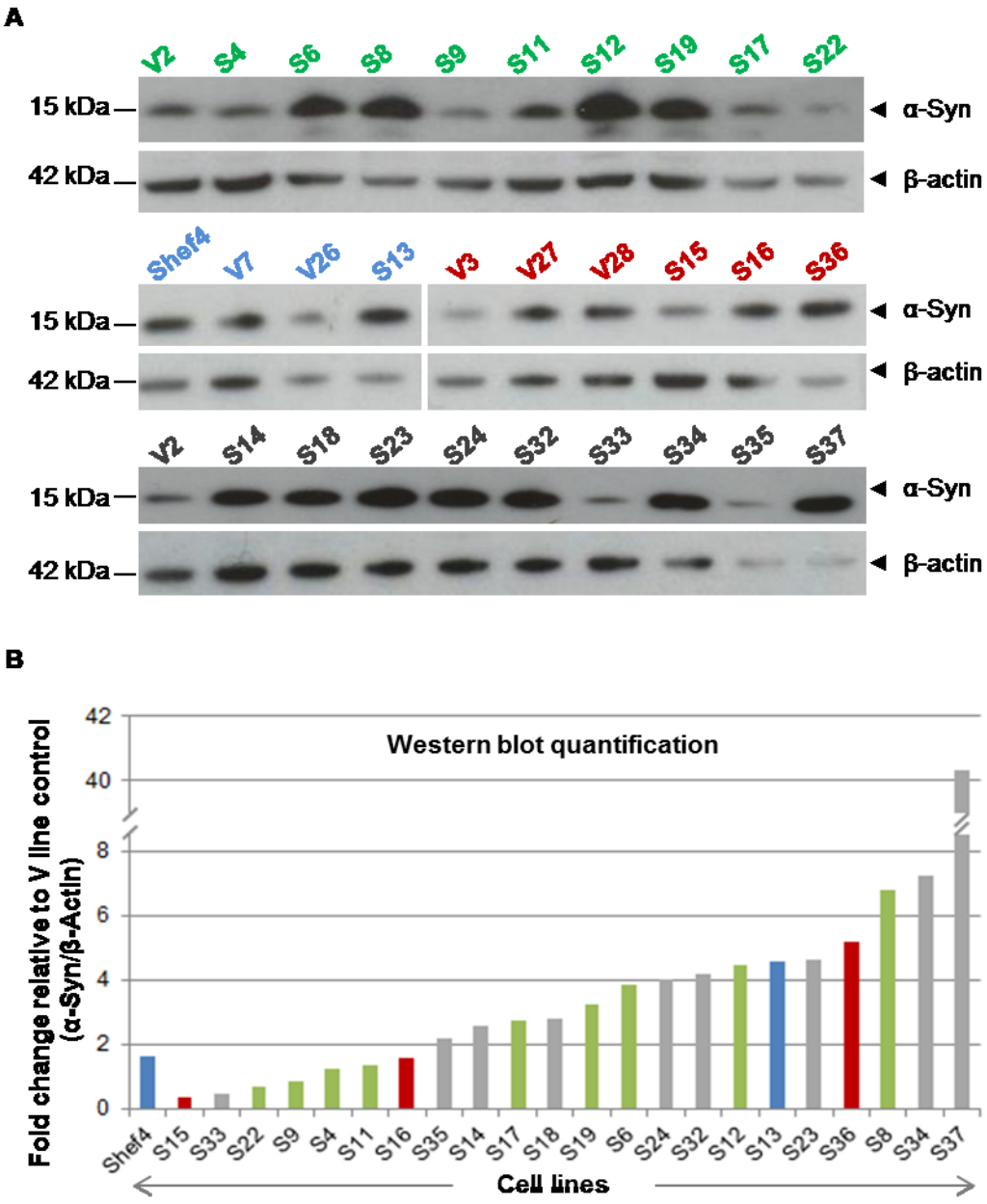

Figure 4.2 Quantification of αSyn protein levels in neural cells derived from transgenic Shef4 hESC lines. A) Western blot for total αSyn of neural cells (day 11). Transgenic Shef4 hESC lines underwent neural induction for 11 days, when total cell lysates were harvested and processed. Neural induction was performed in 4 different batches and each western blot has samples labelled in different colours. Each batch had Shef4–IV cell lines (V lines) to serve as internal controls. B) ImageJ quantification of αSyn western blots. αSyn is presented relative to internal control line (s) (V lines) in each batch of differentiation (n=1). The colours of the bars correspond to the western blots in A).

Although these measures do not discriminate between endogenous and transgenic αSyn, the normal level of expression in 6 control transgenic hESC lines (V2, V3, V7, V26, V27, and V28) suggests any observed over-expression is due to the *SNCA* transgene (Figure 4.2).

One might argue that the αSyn over-expression in these transgenic lines could be due to better neural differentiation, since αSyn increases with neuronal maturity. To address this issue, I examined the expression of neuronal markers, *NCAM* and *MAPT*, and found that most lines differentiated to a similar extent (Figure 4.5). Thus *SNCA* over-expression in these cell lines is most likely to be contributed by the exogenous *SNCA* transgene rather than more neurons being generated.

Gene silencing during neural differentiation seems to have occurred in some transgenic Shef4 hESC lines. Although regression analysis revealed a correlation between *SNCA* mRNA of undifferentiated hES cells (D0) and that of Day11-neural cells (R^2=0.5987 P <0.0001, Figure 4.3). There are some transgenic Shef4 hESC lines, for example, S33, S35 and S6, that exhibited high *SNCA* expression in the undifferentiated state, which then dropped to a near normal level at day 11 of differentiation; thus suggesting gene silencing during neural induction of these lines.

In addition, I investigated the correlation between *SNCA* mRNA and αSyn protein at Day 11 of neural differentiation. Surprisingly, I did not observe a significant correlation between mRNA and protein expression at this stage of neural differentiation (R^2=0.1379 P=0.117, Figure 4.4). Considering that αSyn could be toxic to neural cells at this stage, those that have extremely high αSyn protein might die, while surviving cells may adopt mechanism to reduce protein levels without affecting *SNCA* mRNA expression. Therefore, to investigate *SNCA* expression in these transgenic hESC lines, it is essential to determine the protein level instead of solely relying on mRNA expression.

4.2 Over-expression of αSyn in transgenic hESC lines does not perturb their ability to propagate and differentiate into neural lineages.

A report by Schneider and colleagues (Schneider et al., 2007) showed that over-expression of αSyn in expanded populations of neural progenitors derived from human fetal cortex impaired gliogenesis of these cells. This raised a concern that constitutive over-expression of the protein in transgenic hESC lines might affect their ability to differentiate into neurons.

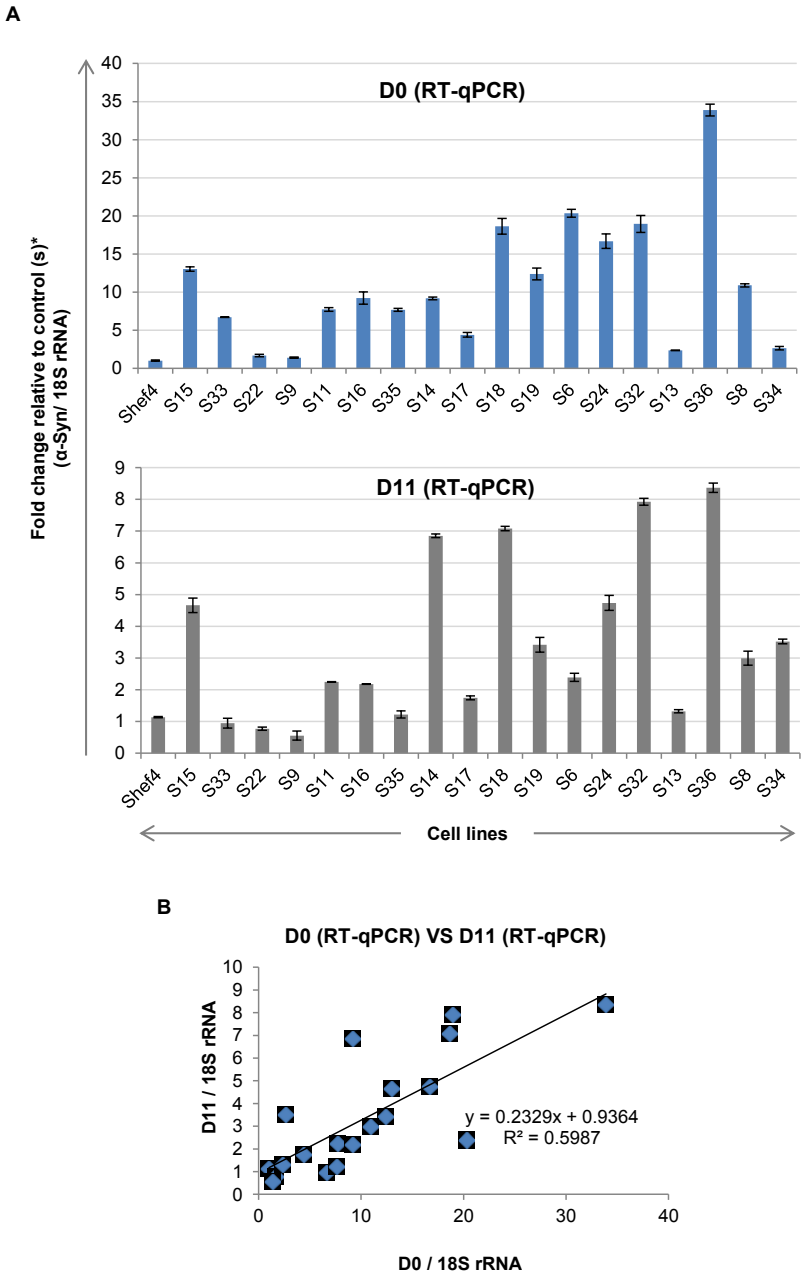

Figure 4.3 *SNCA* mRNA of undifferentiated transgenic hESC lines is positively correlated with *SNCA* expression in neural cells. A) Histogram shows RT-qPCR for *SNCA* expression in undifferentiated transgenic Shef4 cell lines (D0) and that of D11-neural differentiated cells. Please note that the Day 0 and Day 11 RT-qPCR sets were performed independently; *SNCA* expression of D0 cells was relative to Shef4 hESC line whereas that of D11 cells was relative to transgenic V hESC lines. Each bar represents the mean and standard deviation of 3 technical replicates. B) Regression analysis of D0 and D11 *SNCA* expression revealed a significant positive correlation between *SNCA* mRNA of these two time points (P<0.0001).

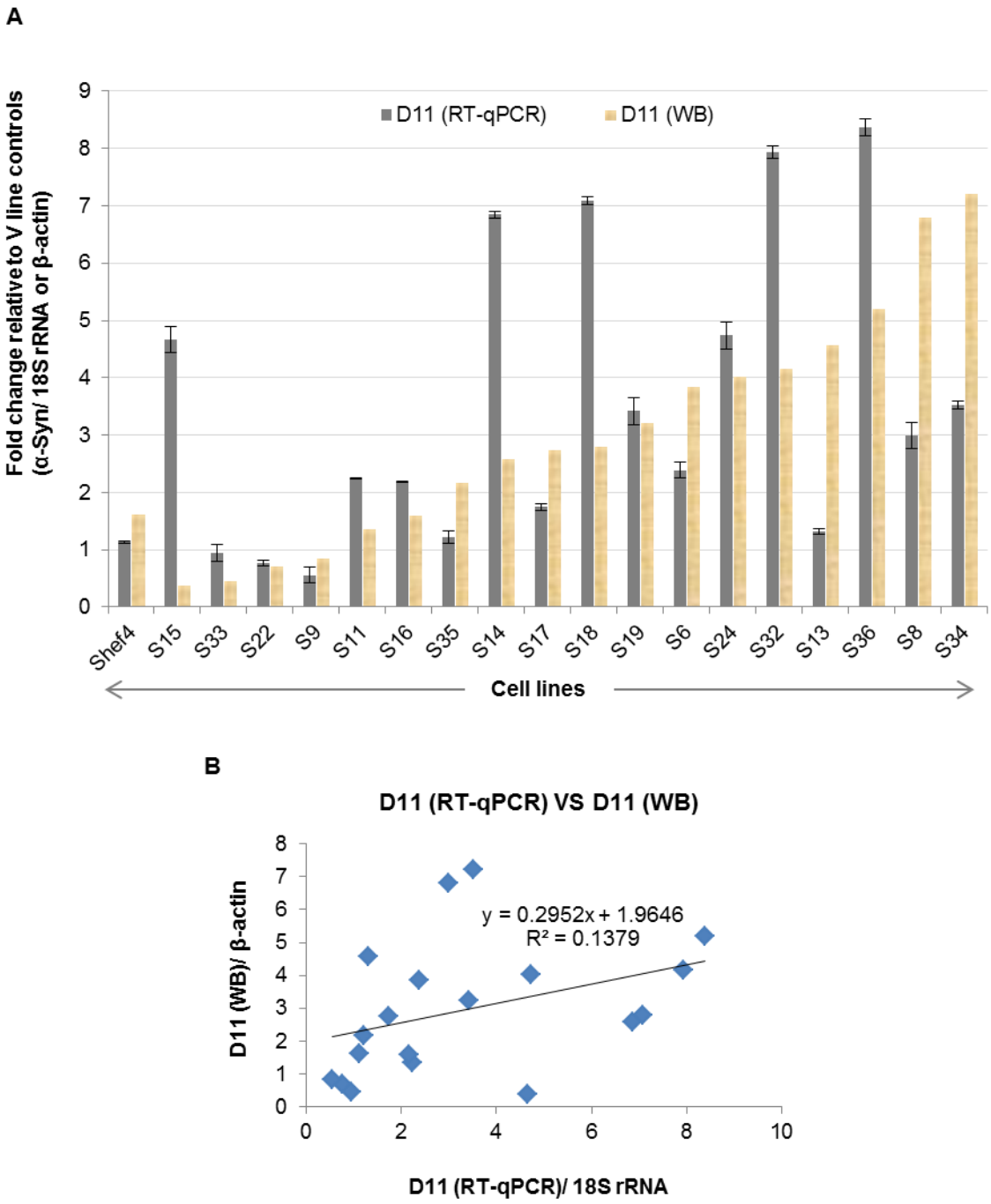

Figure 4.4 *SNCA* mRNA levels are not always predictive of αSyn protein levels at day 11 of neural differentiation. A) Histogram shows RT-qPCR for *SNCA* mRNA and αSyn protein, which is analysed by western blot, at day 11 of neural differentiation. B) Regression analysis of the αSyn expression revealed a lack of correlation between *SNCA* mRNA and αSyn protein of the neural cells (P=0.117 at 95% confidence).

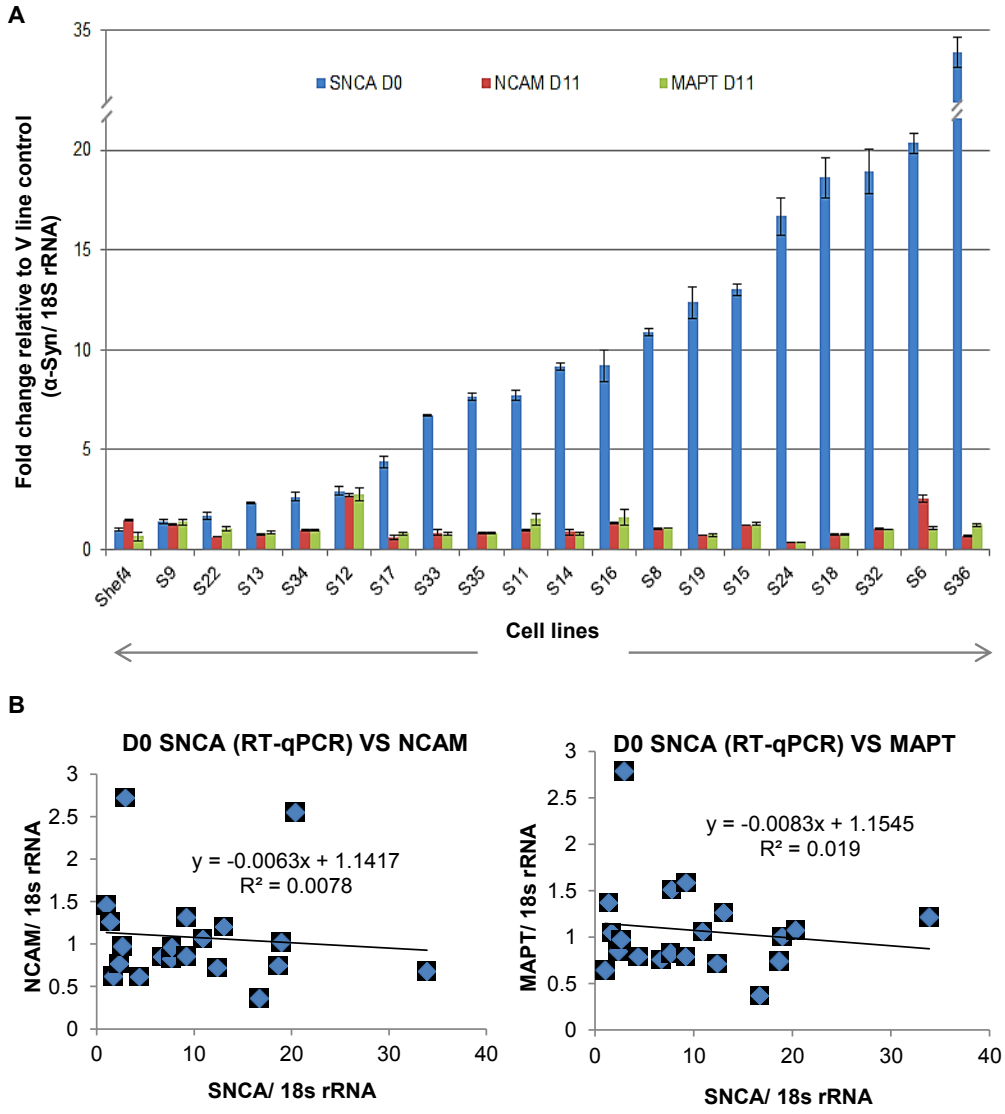

Figure 4.5 *SNCA* expression level in undifferentiated transgenic hESC lines does not affect their neural differentiation potential. A) Histogram shows RT-qPCR for *SNCA* of undifferentiated transgenic Shef4 cell lines, and *NCAM* and *MAPT* at day 11 of neural differentiation. Each bar represents the mean and standard deviation of 3 technical replicates. B) Regression analysis of the expression levels of *SNCA*, *NCAM* and *MAPT* (shown in A) revealed no statistically significant correlation between *SNCA* and each of the neural markers at 95% confidence (P=0.761 and P=0.461 for *NCAM* and *MAPT*, respectively).

Thus I investigated the correlation between (i) *SNCA* expression in undifferentiated transgenic hESC lines and (ii) their differentiation potential towards the neural lineage. I found that there is a lack of correlation between the level of expression of *SNCA* and that of neuronal markers ($R^2 = 0.008$, $P = 0.761$, for *NCAM* , and $R^2 = 0.019$, $P = 0.461$for *MAPT*, Figure 4.5). These results suggested that these transgenic hESC lines retain their potential to differentiate towards the neural lineage despite the over-expression of αSyn and are suitable to generate neurons for further study.

The result is also useful for selecting a pair of cell lines to do experiments. When whole-cell lysate is used in western blotting to assess the total αSyn level of differentiated cells derived from each cell line, a comparable number of neurons generated by each individual is an essential factor to control. From the differentiation results (Figure 4.5), the transgenic hESC lines S12, S6, and S24 were excluded from further studies as their neural differentiation potential is significantly different from the others.

4.3 Young neurons with αSyn over-expression exhibit increased ROS production while cell death is unchanged.

Several studies have reported that aberrant αSyn elevates ROS production (Cremades et al., 2012; Protter et al., 2012). To investigate whether this phenotype occurs in the current models, I have differentiated a pair of transgenic hESC clonal lines, S37 and S9, into cortical neurons and assessed ROS production. The S37 clone was chosen as it has high expression of αSyn in undifferentiated hES cells (Figure 4.2), and still maintained this high expression level when differentiated into neurons (Figure 4.6). The S9 clone was chosen as I had performed all of the previous experiments using this clone as the control. At 34 days of differentiation, the neurons were assessed for cytosolic ROS production using a dihydroethidium (dHEt) fluorescence-based real-time assay. This dye exhibits blue fluorescence in the cytosol, but upon oxidisation to ethidium it becomes localised to the nucleus and emits red fluorescence upon binding DNA. The increase in nuclear red fluorescence over time gives the rate of ROS production in cells. The αSyn over-expressing S37 neurons showed a higher rate of ROS production compared to the S9 control neurons at day 34 (Figure 4.7A). The same result was also observed at day 38 of differentiation (Figure 4.7B). It is important to note that in both S9 and S37 neurons, ROS production increased with differentiation time (Figure 4.7C).

The neurons at this stage were also assessed for percentage cell death using Hoechst 33342 and propidium iodide (PI) double-staining. The red fluorescent dye, PI, can only enter and

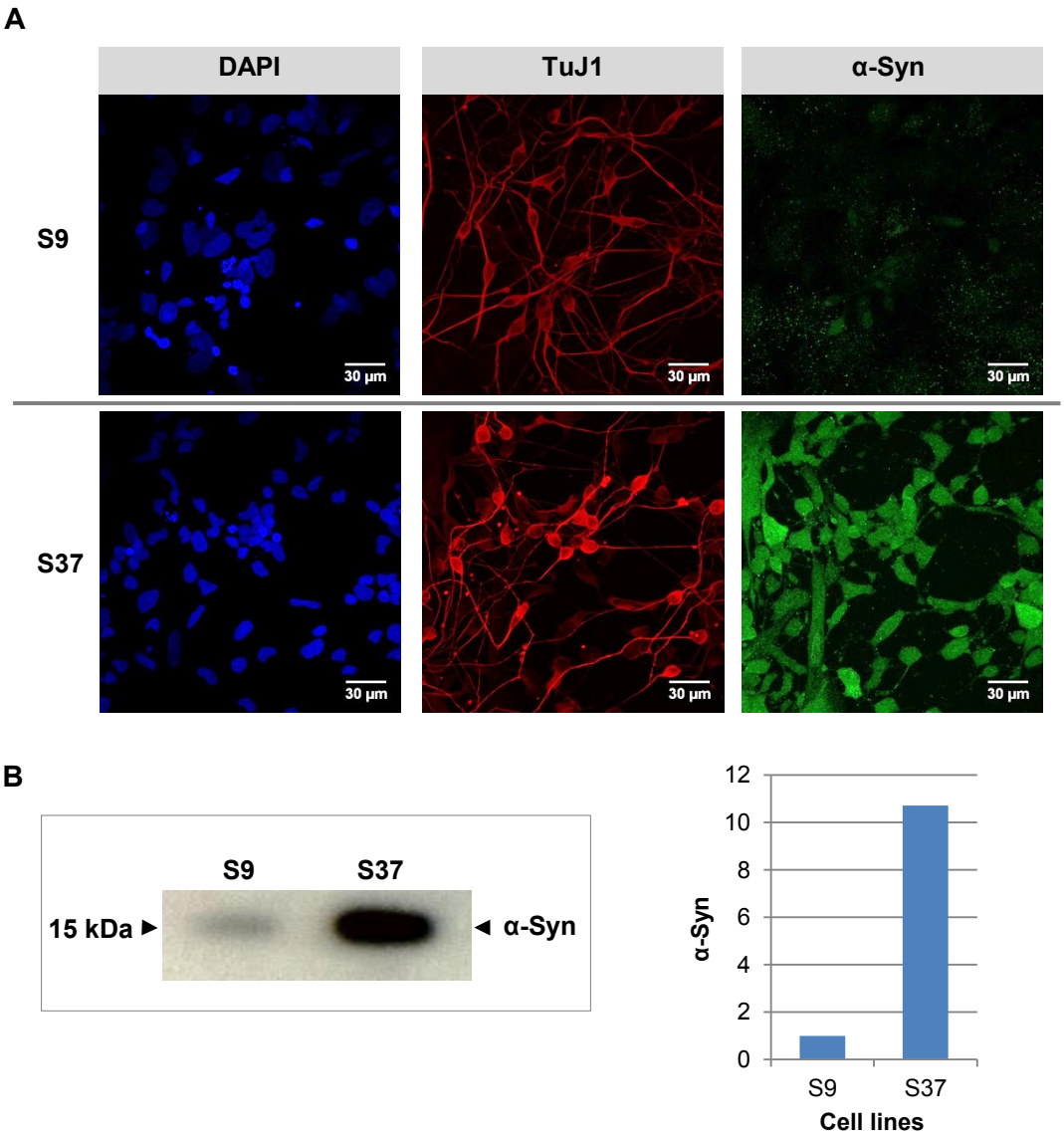

Figure 4.6 Neurons derived from transgenic hES cells over-expressing *SNCA* have elevated αSyn protein. A) Immunocytochemistry for αSyn in differentiated neuronal cells (day 34) showed higher immunofluorescence intensity in neurons derived from transgenic Shef4 clonal line no. 37 (S37), compared to those from the transgenic Shef4 clonal line no. 9 (S9, control). B) Western blot and ImageJ quantification of total αSyn in differentiated cells shown in A) revealed an elevation of αSyn in S37 neurons compared to the control neurons (S9) (n=1). An equal amount of total cell lysate was loaded for each sample and αSyn expression in S9 cells was set at 1 for quantification. This was not normalised to a house-keeping gene.

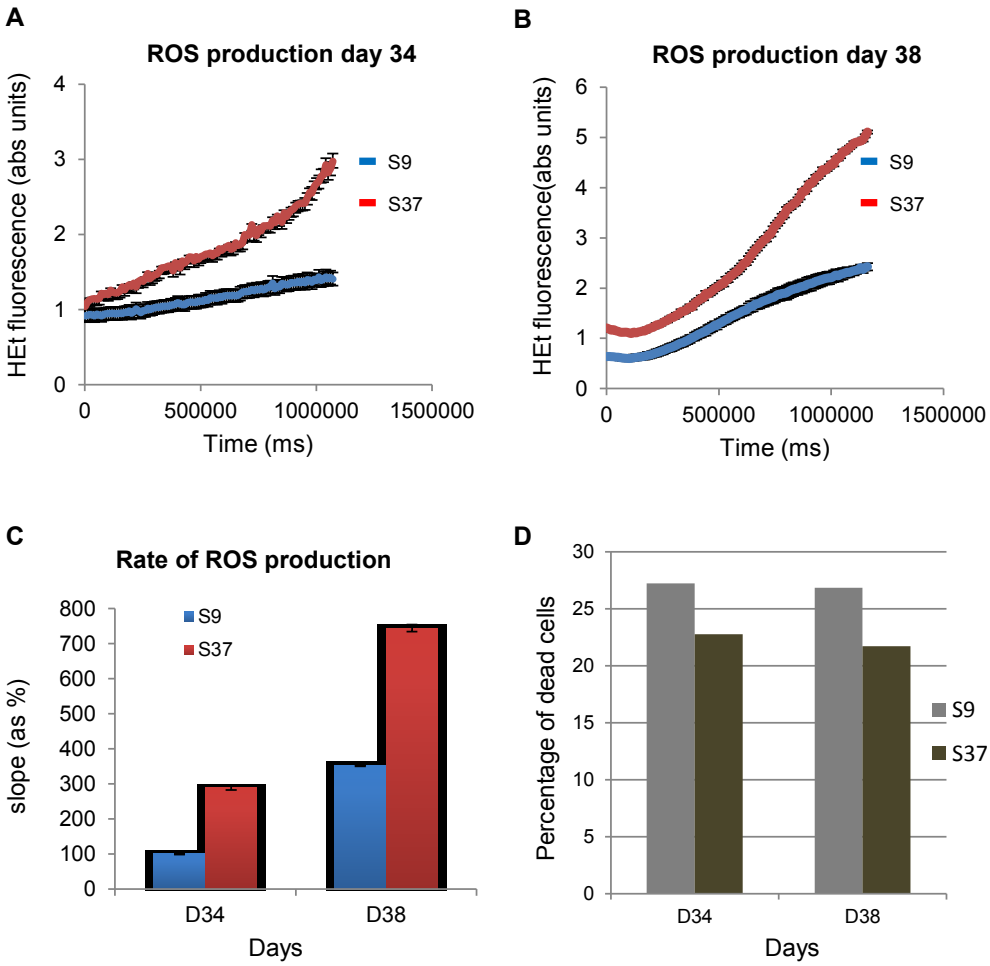

Figure 4.7 Neurons over-expressing αSyn exhibited increased production of cytosolic ROS, but not increased cell death. A) – B) Graphs show cytosolic ROS production, as presented by HEt intensity, in neurons derived from a pair of transgenic Shef4 cell lines; S9 (control) and S37 (SNCA-over-expressing) (n=1). Days of differentiation of neurons are indicated. Each point and error bars represent the mean and standard deviation of 20 neuronal nuclei. C) Rate of ROS production calculated from the slopes of graphs shown in A) – B). Neurons with αSyn over-expression exhibited a higher rate of ROS production than the control neurons at all time-points. D) Histogram shows percentage of dead cells in each neuronal culture assayed using propidium iodide (PI) and Hoechst 33342. No significant differences in cell death were observed between the two neuronal cultures (n=1).

mark dead cells, whereas a blue fluorescent dye, Hoechst 33342, which can enter both living and dead cells, thus marking the total cell population. The ratio of PI over Hoechst 33342 gives the percentage of dead cells. The double-stained cells were imaged using a camera-integrated microscope and analysed for percentage of cell death by counts of several fields ($n \geq 100$ nuclei). Surprisingly, despite the difference in rate of ROS production, there was no difference in percentage of dead cells between the S9 and S37 neurons using this assay (Figure 4.7D).

4.4 No difference in ROS production in more mature neurons

In previous experiments, the ROS production assay was performed in young neurons (day 34-38), which are not an affected population in PD, a late-onset disease. Thus in this experiment, I investigated ROS production in more mature neurons with the hypothesis that an increase in ROS production might be more severe in those over-expressing αSyn. I compared neurons derived from S37, which consistently over-express αSyn, with those from the parental line Shef4.

Along with these two cell lines, I also differentiated other cell lines including S22, S36 and a pair of iPS cell lines, AST18 and NAS2, to determine whether increased αSyn affected neural differentiation potential towards cortical neural lineage. S22 and S36 are transgenic Shef4 hESC lines; a control and a cell line over-expressing *SNCA*, respectively. AST18 and NAS2 are derived from a PD patient with *SNCA* triplication and a healthy first-degree relative, respectively. These two cell lines have been well characterised to ensure pluripotency and normal karyotype (Devine et al., 2011). The S9 clone was no longer used as was behaving differently due to it having a higher passage number.

4.4.1 No significant difference in differentiation potential towards the cortical lineage in pluripotent cell lines expressing different level of αSyn

At day 12 of cortical differentiation, cells were immunostained for PAX6, OTX1/2 and Vementin to determine the cortical identity (Figure 4.8). All cell lines were positive for these makers, which are proteins characteristic of cortical stem and progenitor cells (Shi et al., 2012), indicating similar differentiation potential of these cell lines towards the cortical neural lineage (Figure 4.8). Moreover, the results suggested that over-expression of αSyn is unlikely to cause a major effect on neural induction towards the cortical lineage, further confirming the results from the day 11 neural differentiation (Figure 4.5).

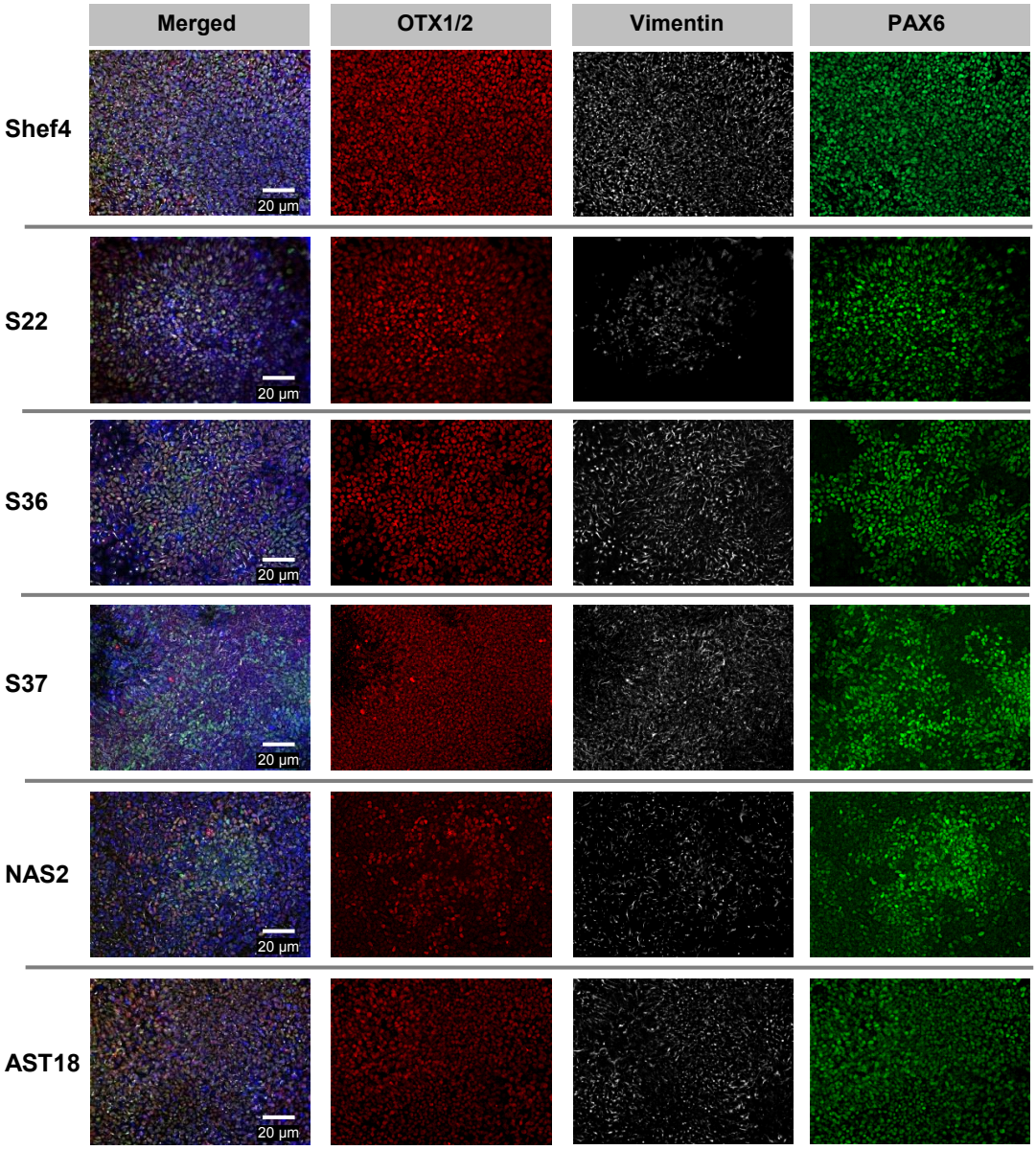

Figure 4.8 Neural progenitors derived from transgenic Shef4 cell lines and iPS cells express markers of cortical identity. Transgenic Shef4 hESC lines and iPS cells from a healthy control (NAS2) and *SNCA* triplication patient (AST18) were differentiated into neural progenitors using the dual-Smad inhibition method. At day 12 of differentiation, cells were fixed and immunostained for PAX6, Vimentin and OTX1/2, protein markers that represent cortical character (n=1). All cell lines were able to produce cortical progenitors as shown by robust immunostaining for these markers.

4.4.2 Selective neuronal loss in neurons derived from transgenic hESC lines over-expressing αSyn, and survival of glia-like cells with high αSyn expression

I then differentiated these neural cells to produce neurons. At day 72 of differentiation, neurons were investigated for αSyn expression (Figure 4.9A and Figure 4.9B). Western blot analysis of total αSyn protein revealed loss of αSyn over-expressing in the S36 cells, while other cell lines exhibited the expected results; AST18 neurons, which has *SNCA* triplication, had approximately twice αSyn level of that of the control iPS cell line, NAS2, and S37 neurons had the highest αSyn level with approximately 3.5-4 fold of that of the controls including a parental line Shef4 and transgenic line S22. Unlike S37, S36 has a comparable αSyn level to that of the controls.

The loss of αSyn over-expression during differentiation of S36 hES cells into neurons suggested the possibility of selective death of neurons with high αSyn expression. To investigate αSyn expression within S36 differentiated population, neurons were fluorescently immunostained for α- synuclein. Results revealed that S36 neurons have barely detectable αSyn (Figure 4.10). However, intense αSyn expression was seen in TuJ1-negative cells. These cells have large-flatten morphology similar to glia.

When considered carefully, this phenomenon seems to have occurred in S37 cultures as well (Figure 4.10). Even though its differentiated population is enriched with cells that have intense αSyn expression, the majority of them are TuJ1-negative (Figure 4.10). It is most likely that the elevated αSyn level observed previously by western blotting is mainly contributed by these glia-like cells, not neurons.

4.4.3 Heterogeneity in αSyn expression within neuronal population of control cell lines

The fluorescent immunostaining for αSyn also revealed heterogeneous expression of αSyn within the neuronal population of control cell lines, which include a parental Shef4, transgenic S22 and a control iPS cell line, NAS2 (Figure 4.10). For each of these cell lines, αSyn expression varies dramatically within the neuronal population; some neurons had barely detected αSyn whist other showed intense expression (Figure 4.11). Unlike S36 and S37, glia-like cells do not show intense expression of αSyn (Figure 4.12).

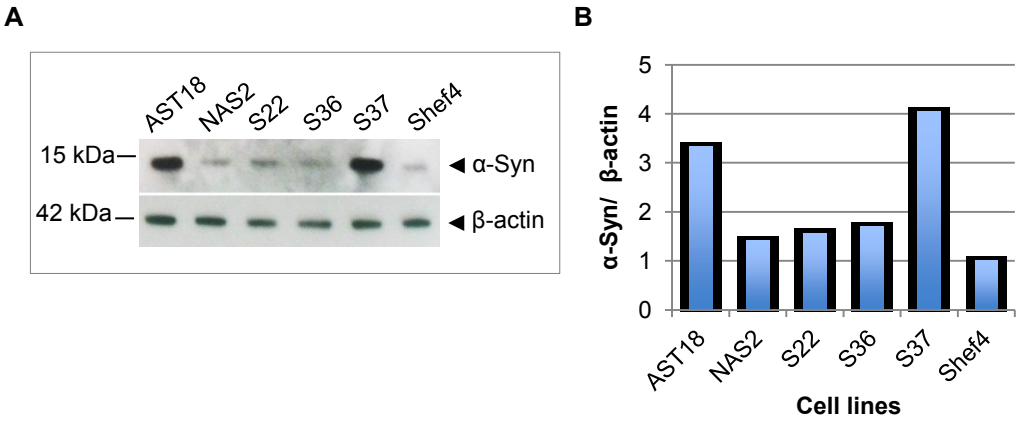

Figure 4.9 Loss of αSyn over-expression characteristic of day 72 cortical neurons derived from S36 transgenic Shef4 cell line. A) Western blotting for total αSyn in day 72 culture lysates derived from transgenic hES cells and iPS cells. β-actin western blotting served as a loading control. B) ImageJ quantification of αSyn shown in A). α-Syn is shown relative to Shef4. Note that αSyn in S36 neurons reduced to normal levels whereas the expression remained high in S37 and AST18 neurons (n=1).

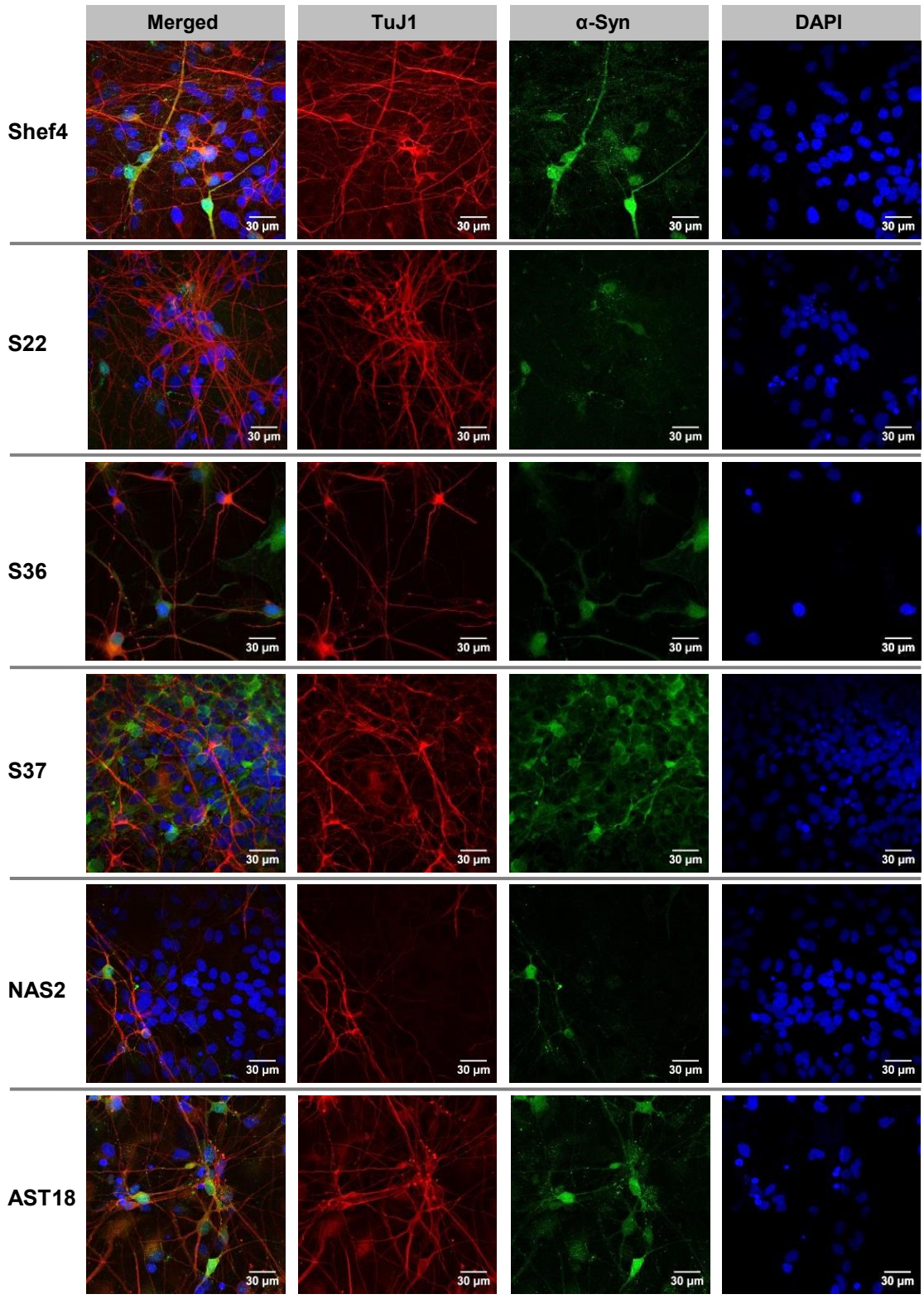

Figure 4.10 Immunocytochemistry for αSyn and TuJ1 in day 72 neurons. The expression of αSyn is heterogeneous between neurons derived from each cell line (n=1).

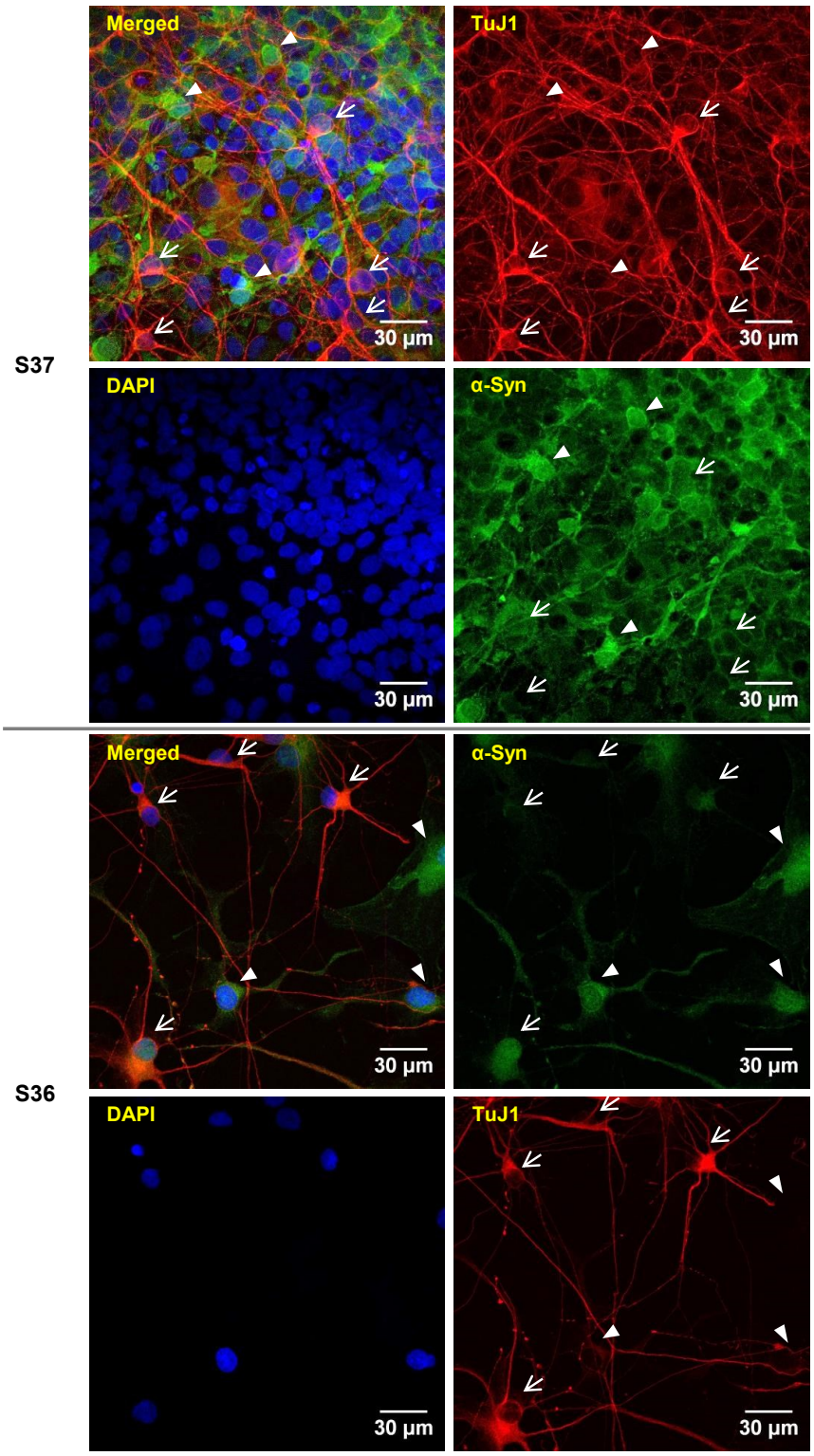

Figure 4.11 Magnified images of Figures 4.10 shows reduced αSyn in a number of day 72 neurons derived from S36 and S37 while the expression remain high in glia-like cells. Arrows and arrowheads indicate TuJ1-positive and TuJ1- negative cells, respectively. The TuJ1-negative cells have flat morphology similar to glia.

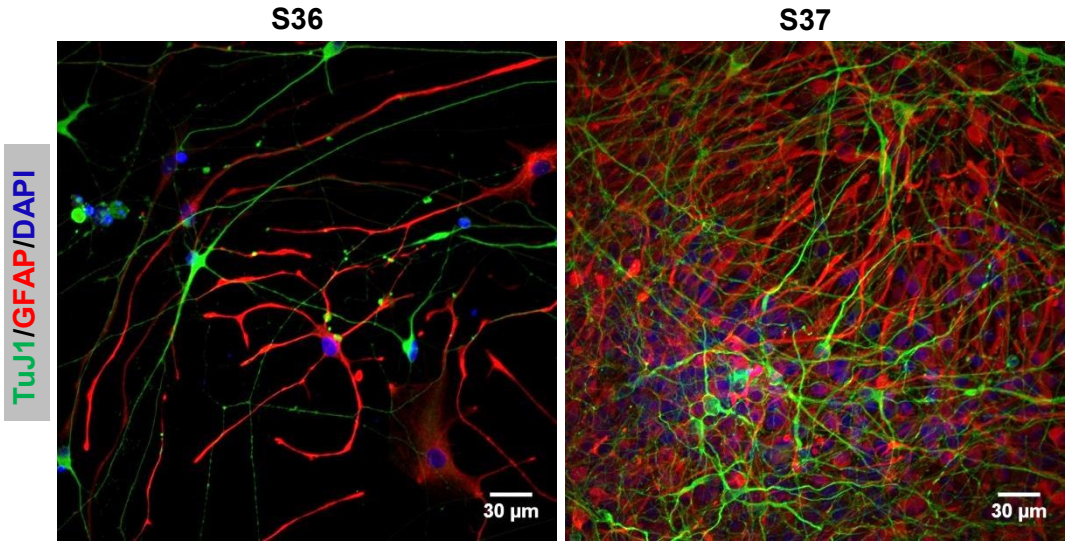

Figure 4.12 Immunocytochemistry shows a glia-neuron mixed population of day 72 neuronal differentiated S36 and S37. Immunocytochemistry for TuJ1 and GFAP in differentiated cortical neuronal cells (day 72) revealed enrichment of GFAP-positive cells instead of neurons (n=1).

4.4.4 Data analysis of ROS production rate

I then investigated ROS production in day 72 differentiated population of S37 and Shef4. Analysis showed no significant difference in ROS production rate between these two cell lines (Figure 4.13). This result might be due to a drawback of the assay, which cannot distinguish cell types within the population; thus data from neurons and non-neuronal cells were pooled. In an attempt to distinguish sub-populations within each cell line, and then to compare the data from the same sub-population of these two cell lines, I filtered the data based on the initial value of blue fluorescent intensity, which is the value detected at the beginning of the assay. Using this method, the data were separated into two sub-populations; one is that with the blue intensity lower than or equal to 30 and the other with a greater intensity. However, when the same sub-populations of each cell line were compared, the results showed no difference in ROS production rate between S37 and Shef4 (Figure 4.13).

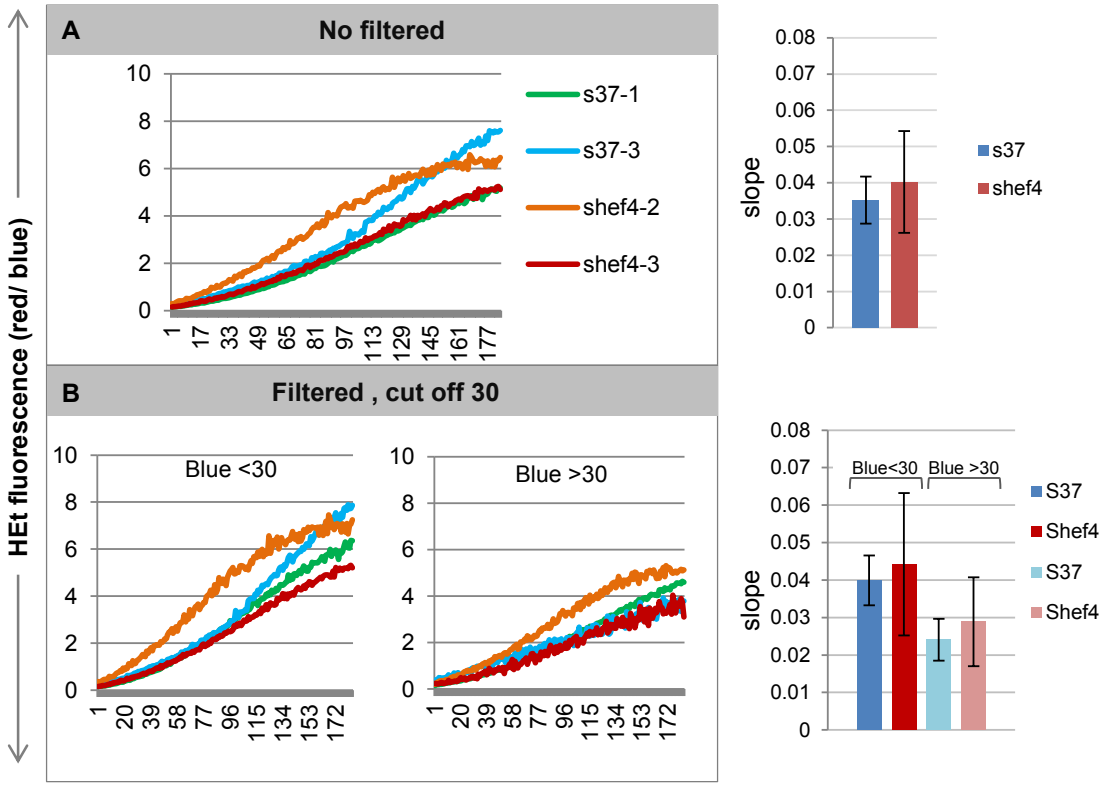

Figure 4.13 No significant difference in rate of ROS production in day 72 neurons. The assay for ROS production was performed in neurons derived from a pair of hESC lines; wild-type Shef4 (control) and transgenic Shef4 cell line over-expressing αSyn (S37). The data was processed in 2 different methods prior to analysis as usual. A) No data filtering, and B), data filtering based on the intensity of the blue fluorescent signal at the first experimental time point with an arbitrary cut-off value of 30 fluorescent units. Histograms show the ROS production rates for both unfiltered and filtered data. Note that there is no significant difference in ROS production rate in neurons derived from wild-type Shef4 and S37 hES cells in all analyses (n=1).

4.5 Discussion

In this chapter I described a set of transgenic Shef4 hESC lines over-expressing *SNCA*. The cell lines were characterised for stable *SNCA* transgene expression, neural differentiation potential and cytosolic ROS production when differentiated into the neural lineage.

4.5.1 Transgene silencing during neural differentiation

I provided evidences supporting that most of the transgenic lines (Figure 4.2) stably expressed *SNCA* transgene during neural differentiation while gene silencing was observed in a few cell lines. The low frequency of developmental transgene silencing could considerably due to a promoter of choice, pCAGs, which has been reported for stably driving the expression of transgenes during differentiation of ES cells (Alexopoulou et al., 2008; Hadjantonakis et al., 1998). Theoretically, transgene silencing can occur through multiple mechanisms, including removing of the transgene, transcriptional silencing and enhanced mRNA degradation. However, the most common mechanism related to developmental gene silencing is transcriptional silencing, which involves changes of chromatin structure by DNA methylation and histone deacetylation to restrict access of transcription factors to the promoter (Cherry et al., 2000; Wang et al., 2007).

4.5.2 Different differentiation potential among transgenic *SNCA*-Shef4 hESC lines

I showed that a few transgenic cell lines exhibited considerably different differentiation potential from others. As this variation is not correlated with *SNCA* expression in the undifferentiated state, it is unlikely that it is a result of the differences in *SNCA* expression level. Rather, it is most likely to be caused by clonal variation of the hESC lines. It is well documented that hESC populations are heterogenous, and they can have different transcriptional profiles, thus affecting their differentiation properties (Stewart et al., 2006). To avoid this effect, one should use the lines with similar neural differentiation potential for further phenotypic analysis.

Over-expression of *SNCA* in human foetal cortical progenitor cells has been reported to impair gliogenesis without affecting cell death (Schneider et al., 2007). The direct effect of elevated *SNCA* on gliogenesis has not been investigated in this study. However, I observed considerable GFAP+ cells in the differentiated population from S37 and S36 lines (Figure 4.12), which over-express *SNCA*. As increased cell death due to elevated αSyn is suspected for these cell lines, enrichment of glia-like cells in this study could be the result of selective

neuronal cell death rather than cell fate change. The contradictory results between these two studies may be due to differences in transgene expression systems and experimental cell types. Work reported by Schneider and colleagues used viral infection at the stage of neural progenitors whereas present study employed constitutive expression in transgenic hESC lines.

4.5.3 Increased ROS production rate may be increased in young neurons, but not in more mature neurons

The contradictory results of the two ROS production analyses could be due to selective cell death of neurons that have very high αSyn expression as differentiation progresses. Although cell death has not been observed by the Hoechst 33342/PI assay in S37 neurons, the increased ROS production without change in cell death may imply the very early stages of phenotypic manifestation. The ROS production may get more severe over time, which could lead to cell death. Thus, by the time that second analysis took place in more mature neurons, there would be fewer neurons with high αSyn expression present. This is consistent with the finding that the differentiated population of S37 at day 34 exhibited robust and homogenous αSyn expression (Figure 4.6), whereas those at day 72 exhibited heterogeneous αSyn expression, and were composed mainly with glia-like cells and neurons with low level αSyn (Figure 4.10, Figure 4.11, and Figure 4.12).

Further evidence supporting that selective cell death due to elevated *SNCA* exists for the S36 line. This line exhibited very high αSyn expression in hES cells and at day 11 of differentiation (Figure 4.3), but by day 72 of differentiation the level of αSyn expression was undistinguishable from control lines (Figure 4.9). Similar to S37, the differentiated αSyn expressing S36 cells were mostly glial-like and very little neurons remained (Figure 4.10).

In addition to cell death, phenotypic analysis at late differentiation is also complicated by the heterogeneity of cell types within the differentiated population. Obviously, this is not due to exogenous *SNCA* expression as it is also observed in the cell populations derived from the control hESC lines, such as, the parental Shef4 line. Rather, it is due the nature of the differentiation protocol used in this study that sequentially produces complex classes of cortical neurons as differentiation progresses (Shi et al., 2012) As a result, cells in later stages of differentiation may exhibit differences in maturity, neural subtype and importantly, *SNCA* expression.

Due to limitations discussed above, future phenotypic analysis should be performed in young neurons or possibly at time points before day 72 of differentiation, to capture the phenotypes, such as changes in ROS production and cell death. I would wish to replicate these experiments at least three times to ensure that the results are robust. I would also like to assess the amount of cell death using different assays, for example using TUNEL staining. The ROS production differences suggest that mitochondria may be involved, and so assays to determine whether these are dysfunctional would be very interesting. Finally, it would be interesting to examine the localisation of αSyn (especially the overexpressed a-synuclein) in cells by both confocal microscopy and immuno-electron microscopy using immuno-gold labelling.

Furthermore, investigation of the effect of αSyn on glial cells would be very interesting to investigate further. Quantification of double staining of αSyn and glial fibrillary acidic protein (GFAP) would be very important to help the interpretation of these results. This would help address the problem which I have had with using mixed cell cultures, but actually also add to the data. After all, there are other neurodegenerative disease in which the major effect of the mutation is in the supporting cells (e.g. astrocytes) (e.g. vanishing white matter disease).

Chapter 5

Discussion and conclusion

Understanding the mechanisms underlying the disease process of synucleinopathies has been hampered by the lack of appropriate disease models. Most currently available models are devoid of either neuronal aspects or human genetic background, which may contribute to failures in manifesting disease phenotypes.

The present research is aimed to establish a novel disease model that has neuronal aspects combined with a normal human genetic background. The hESC system was employed due to their genetic stability and ability to be genetically manipulated, thus giving an opportunity to model genetic forms of synucleinopathies. Additionally, their self-renewal and capacity to differentiate into neurons *in vitro* provides an unlimited access to human neurons. The focus is on increased expression of WT-*SNCA*, which represents one of the genetic forms of PD.

5.1 Establishment of *SNCA*-transgenic Shef4 hESC lines and their characteristics.

Employing random insertional transgenesis using a plasmid vector, a set of transgenic Shef4 hESC lines constitutively expressing *SNCA* at different levels has been established. Instead of relying on the Venus reporter protein as expected, they required other approaches to detect the *SNCA* transgene expression, such as, RT-qPCR and western blotting, which were used successfully in this study. Failure in detecting Venus protein made it more complicated to identify hESC clones with differing levels of expression, not only during clonal selection but also in down-stream experiments. However, directly assessing *SNCA* expression became essential and highly recommended in this model system, in which the transgene could be silenced during hES cell propagation and neural differentiation.

The transgenic *SNCA* hESC lines were able to propagate and self-renew as ES cells, and differentiate into neuronal cell types as well as control hESC lines. This shows that they are not significantly affected by *SNCA* expression level.

However, some transgenic lines exhibited variable neural differentiation potential, which is likely to be due to hESC clonal variation as discussed in Chapter 4. Thus, it is recommended

that one should pair hESC lines with comparable efficiency of neural differentiation for further analysis.

5.2 Phenotypic analyses revealed promising results indicating they are suitable to study early events of the disease process.

The models were tested whether they were able to recapitulate disease phenotypes by mean of ROS production and cell death. Cortical neurons derived from a pair of transgenic hESC lines, one with high (S37) and the other with normal *SNCA* (S9, control) expression were subjected to analyses, which were performed in two time points, between day 34 to day 38 and by day 72 of differentiation. The analyses revealed significantly increased ROS production in the S37 neurons compared to the control. This phenotype was observed only observed in young neurons, but absent in more mature neurons. The contradictory results are likely to be caused by selective cell death of neurons with high αSyn expression as differentiation progresses. The stress from elevated αSyn and heterogenous expression of the transgene in later differentiation might have a negative effect on neuronal survival, leading to selective cell death before the second analysis took place. The unchanged cell death in young neurons could be due to insensitive assay used in this study. Employing more sensitive approach, such as using a longitudinal videomicroscopy to track neurons for extended periods of time (Bilican et al., 2012), would have assisted in detecting dynamic changes.

Back to the research question of whether *SNCA*-transgenic hESC lines can be use as tools to model a genetic form of synucleinopathies, I would say that the models are not a panacea for all of the disease features. Due to cell death in prolong culture and the embryonic characteristics of the neurons produced from hES cells, the present model has limitations to recapitulate the late stage of the disease. Rather, increased ROS production in young neurons may represent an early event of the disease in human. If so, the model system should have an advantage to provide insights into early pathogenic changes in neurons, which are essential for developing effective approach to prevent the disease progression.

In addition to recapitulating some major disease characteristics demonstrated in this study, there are promising reasons supporting that these transgenic *SNCA*-hESC lines have a potential to be extremely useful tools in studying synucleinophaties. Firstly, the models system was capable to derive neurons with up to 10-fold difference in αSyn compared to the control. It is worth noting that current iPS cell lines with *SNCA* triplication produced neurons with only 2-fold increased αSyn (Devine et al., 2011). Secondly, this set of transgenic hESC

lines expresses different levels of *SNCA*, which should be beneficial to study allelic effect on disease phenotypes *in vitro*. The positive correlation between *SNCA* expression level and the severity of the disease was observed in human (Fuchs et al., 2007); however, this has not been demonstrated *in vitro*. Finally, the transgenic hESC lines have identical genetic background, which may help minimise the phenotypic interference contributed by genetic variation.

For these reasons, even though the present cell lines are not perfect models of synucleinopathies, it is hoped that they will be used in concert with other models to accelerate the research in this field.

5.3 Future research

Following are suggestions for future experiments to make more out of the model system and to over-come the limitations that exist in the current models.

5.3.1 ROS assay and cell death in young neurons.

Although the results provided in this study are statistically significant, the models have not been reassessed due to time limitation. To confirm the current results, it is recommended to repeat the experiments using the same transgenic Shef4 hESC lines with young neurons.

5.3.2 Employing other protocols to generate a pure population of neurons.

The current study employed a directed cortical differentiation to generate neurons to model the disease. This protocol produces complex classes of cortical neurons in a temporal manner as the differentiation progresses (Shi et al., 2012). The heterogeneity of the cell population caused difficulty when two cell lines are phenotypically compared. The example is ROS and cell death assays in this study, where cells have been analysed as a pooled population without separating neurons from glia. As differential analysis is very difficult as demonstrated previously, producing a pure population of neuronal subtype, such as dopaminergic neurons, instead of a complex neuronal population should make phenotypic comparison between cell lines more interpretable.

5.3.3 Mitochondrial assays in pure population of neurons when they are still young.

This should be performed only after the experiments in this study (ROS and cell death assays in young cortical neurons) have been reassessed. The purpose is to further evaluate the models. As the phenotypes have been observed in young cortical neurons, the same results are expected in other neuronal subtypes that are affected in synucleinopathies. In addition, as mitochondria are closely associated with ROS production, it is interesting to investigate its function in the current models, which suffer from increase ROS.

5.3.4 Establish a DOX-inducible system to permit *SNCA* induction at later times.

Even though this study has provided initial results showing that over-expression of αSyn in transgenic hESC lines does not perturb their ability to propagate and differentiate into neural lineages, it is not ensure that the elevated protein does not have other impacts on cell biology. Changes of cell fate and differentiation due to over-expression of αSyn in neural progenitors have been reported (Schneider et al., 2007), however, this has not been observed in this study. With the DOX-inducible system, the *SNCA* expression would be controllable, allowing the expression to occur at a time point similar to natural developmental process. Thus there should not then be a problem with ES differentiation, but SNCA could be overexpressed in mature neurons, isolating this effect from an earlier developmental defect.

5.3.5 Instead of pCAGS promoter, use a neuronal promoter, of knock-in a mutant *SNCA* gene into the human *SNCA* locus with CRISPR/Cas9 technology.

Instead of being controlled by a constitutive promoter, the *SNCA* expression can be controlled under the neuronal promoter, which allows the expression to occur in relation to neuronal development. The knock-in approach allows integration of the transgene in a precise location in the chromosome without disturbing other genomic area. This minimises the risk of phenotypes being due to random integrations. The level of gene expression can be adjusted during plasmid design, for example, two *SNCA* genes can be constructed bicistronically.

5.3.6 How would I tackle the project if starting again

Five years later, I would tackle this project in a different way as technologies have developed further. I would consider whether insertion of the genes would be better in a defined position – either using a locus such as the Rosa 26 or HPRT locus, or by positioning repeats into the endogenous SNCA locus, using Crispr-Cas9 technology. If I chose the Rosa26 or HPRT locus, then I would reconsider the promoter to be used, picking one with expression only after the NS cell stage, so that I could examine the effect on neuron development rather than NS cell development. I would very much like to over express αSyn in dopaminergic neurons specifically, and there are now established protocols to efficiently grow dopaminergic neurons in culture – both in mouse and humans. It may well remain difficult to model a disease of ageing such as Parkinson's disease in a dish where we keep cells alive for weeks to months rather than decades, and this is a possible limitation of this type of experiment, although I tried to overcome this by overexpressing the αSyn which leads to earlier disease in humans. Inducing stress in these cells may accelerate "ageing" in these cell cultures, bypassing the problem. An alternative is to take iPS cells from patients with genetic α-synucleinopathies, and convert these into dopaminergic neurons. This is indeed being done already, and would be interesting, but the variability between clones even from the same patient, and the variability with passage number, still means that this is not without its problems.

References

Abeliovich, A., Schmitz, Y., Farinas, I., Choi-Lundberg, D., Ho, W.H., Castillo, P.E., Shinsky, N., Verdugo, J.M., Armanini, M., Ryan, A.*, et al.* (2000). Mice lacking alpha-synuclein display functional deficits in the nigrostriatal dopamine system. Neuron *25*, 239-252.

Aflatoonian, B., Ruban, L., Shamsuddin, S., Baker, D., Andrews, P., and Moore, H. (2010). Generation of Sheffield (Shef) human embryonic stem cell lines using a microdrop culture system. In Vitro Cell Dev Biol Anim *46*, 236-241.

Alam, Z.I., Jenner, A., Daniel, S.E., Lees, A.J., Cairns, N., Marsden, C.D., Jenner, P., and Halliwell, B. (1997). Oxidative DNA damage in the parkinsonian brain: an apparent selective increase in 8-hydroxyguanine levels in substantia nigra. J Neurochem *69*, 1196-1203.

Alderson, T.R., and Markley, J.L. (2013). Biophysical characterization of alpha-synuclein and its controversial structure. Intrinsically Disord Proteins *1*, 18-39.

Alexopoulou, A.N., Couchman, J.R., and Whiteford, J.R. (2008). The CMV early enhancer/chicken beta actin (CAG) promoter can be used to drive transgene expression during the differentiation of murine embryonic stem cells into vascular progenitors. In BMC Cell Biol, pp. 2.

Alexopoulou, A.N., J. R. Couchman, et al. Analysis of Different Promoter Systems for Efficient Transgene.pdf>.

Appel-Cresswell, S., Vilarino-Guell, C., Encarnacion, M., Sherman, H., Yu, I., Shah, B., Weir, D., Thompson, C., Szu-Tu, C., Trinh, J.*, et al.* (2013). Alpha-synuclein p.H50Q, a novel pathogenic mutation for Parkinson's disease. Mov Disord *28*, 811-813.

Baba, M., Nakajo, S., Tu, P.H., Tomita, T., Nakaya, K., Lee, V.M., Trojanowski, J.Q., and Iwatsubo, T. (1998). Aggregation of alpha-synuclein in Lewy bodies of sporadic Parkinson's disease and dementia with Lewy bodies. Am J Pathol *152*, 879-884.

Bartels, T., Choi, J.G., and Selkoe, D.J. (2011). alpha-Synuclein occurs physiologically as a helically folded tetramer that resists aggregation. Nature *477*, 107-110.

Ben Gedalya, T., Loeb, V., Israeli, E., Altschuler, Y., Selkoe, D.J., and Sharon, R. (2009). Alpha-synuclein and polyunsaturated fatty acids promote clathrin-mediated endocytosis and synaptic vesicle recycling. Traffic *10*, 218-234.

Bilican, B., Serio, A., Barmada, S.J., Nishimura, A.L., Sullivan, G.J., Carrasco, M., Phatnani, H.P., Puddifoot, C.A., Story, D., Fletcher, J.*, et al.* (2012). Mutant induced pluripotent stem cell lines recapitulate aspects of TDP-43 proteinopathies and reveal cell-specific vulnerability. Proc Natl Acad Sci U S A *109*, 5803-5808.

Braak, H., and Del Tredici, K. (2009). Neuroanatomy and pathology of sporadic Parkinson's disease. Adv Anat Embryol Cell Biol *201*, 1-119.

Burre, J., Sharma, M., Tsetsenis, T., Buchman, V., Etherton, M.R., and Sudhof, T.C. (2010). Alpha-synuclein promotes SNARE-complex assembly in vivo and in vitro. Science *329*, 1663-1667.

Cabin, D.E., Shimazu, K., Murphy, D., Cole, N.B., Gottschalk, W., McIlwain, K.L., Orrison, B., Chen, A., Ellis, C.E., Paylor, R.*, et al.* (2002). Synaptic vesicle depletion correlates with attenuated synaptic responses to prolonged repetitive stimulation in mice lacking alpha-synuclein. J Neurosci *22*, 8797-8807.

Cao, F., Xie, X., Gollan, T., Zhao, L., Narsinh, K., Lee, R.J., and Wu, J.C. (2010). Comparison of gene-transfer efficiency in human embryonic stem cells. Mol Imaging Biol *12*, 15-24.

Carlson, S.S., and Kelly, R.B. (1980). An antiserum specific for cholinergic synaptic vesicles from electric organ. J Cell Biol *87*, 98-103.

Chambers, I., Colby, D., Robertson, M., Nichols, J., Lee, S., Tweedie, S., and Smith, A. (2003). Functional expression cloning of Nanog, a pluripotency sustaining factor in embryonic stem cells. Cell *113*, 643-655.

Chambers, S.M., Fasano, C.A., Papapetrou, E.P., Tomishima, M., Sadelain, M., and Studer, L. (2009). Highly efficient neural conversion of human ES and iPS cells by dual inhibition of SMAD signaling. Nat Biotechnol *27*, 275-280.

Chambers, S.M., Qi, Y., Mica, Y., Lee, G., Zhang, X.J., Niu, L., Bilsland, J., Cao, L., Stevens, E., Whiting, P.*, et al.* (2012). Combined small-molecule inhibition accelerates developmental timing and converts human pluripotent stem cells into nociceptors. Nat Biotechnol *30*, 715-720.

Chandra, S., Fornai, F., Kwon, H.B., Yazdani, U., Atasoy, D., Liu, X., Hammer, R.E., Battaglia, G., German, D.C., Castillo, P.E.*, et al.* (2004). Double-knockout mice for alpha- and beta-synucleins: effect on synaptic functions. Proc Natl Acad Sci U S A *101*, 14966-14971.

Chandra, S., Gallardo, G., Fernandez-Chacon, R., Schluter, O.M., and Sudhof, T.C. (2005). Alpha-synuclein cooperates with CSPalpha in preventing neurodegeneration. Cell *123*, 383-396.

Chen, X., de Silva, H.A., Pettenati, M.J., Rao, P.N., St George-Hyslop, P., Roses, A.D., Xia, Y., Horsburgh, K., Ueda, K., and Saitoh, T. (1995). The human NACP/alpha-synuclein gene: chromosome assignment to 4q21.3-q22 and TaqI RFLP analysis. Genomics *26*, 425-427.

Cheng, F., Vivacqua, G., and Yu, S. (2011). The role of alpha-synuclein in neurotransmission and synaptic plasticity. J Chem Neuroanat *42*, 242-248.

Cherry, S.R., Biniszkiewicz, D., van Parijs, L., Baltimore, D., and Jaenisch, R. (2000). Retroviral expression in embryonic stem cells and hematopoietic stem cells. Mol Cell Biol *20*, 7419-7426.

Conway, K.A., Lee, S.J., Rochet, J.C., Ding, T.T., Harper, J.D., Williamson, R.E., and Lansbury, P.T., Jr. (2000a). Accelerated oligomerization by Parkinson's disease linked alpha-synuclein mutants. Ann N Y Acad Sci *920*, 42-45.

Conway, K.A., Lee, S.J., Rochet, J.C., Ding, T.T., Williamson, R.E., and Lansbury, P.T., Jr. (2000b). Acceleration of oligomerization, not fibrillization, is a shared property of both alpha-synuclein mutations linked to early-onset Parkinson's disease: implications for pathogenesis and therapy. Proc Natl Acad Sci U S A *97*, 571-576.

Conway, K.A., Rochet, J.C., Bieganski, R.M., and Lansbury, P.T., Jr. (2001). Kinetic stabilization of the alpha-synuclein protofibril by a dopamine-alpha-synuclein adduct. Science *294*, 1346-1349.

Cremades, N., Cohen, S.I., Deas, E., Abramov, A.Y., Chen, A.Y., Orte, A., Sandal, M., Clarke, R.W., Dunne, P., Aprile, F.A.*, et al.* (2012). Direct observation of the interconversion of normal and toxic forms of alpha-synuclein. Cell *149*, 1048-1059.

Dawson, T.M., Ko, H.S., and Dawson, V.L. (2010). Genetic animal models of Parkinson's disease. Neuron *66*, 646-661.

Devi, L., Raghavendran, V., Prabhu, B.M., Avadhani, N.G., and Anandatheerthavarada, H.K. (2008a). Mitochondrial import and accumulation of alpha-synuclein impair complex I in human dopaminergic neuronal cultures and Parkinson disease brain. J Biol Chem *283*, 9089-9100.

Devi, L., Raghavendran, V., Prabhu, B.M., Avadhani, N.G., and Anandatheerthavarada, H.K. (2008b). Mitochondrial import and accumulation of alpha-synuclein impair complex I in human dopaminergic neuronal cultures and Parkinson disease brain. J Biol Chem *283*, 9089-9100.

Devine, M.J., Ryten, M., Vodicka, P., Thomson, A.J., Burdon, T., Houlden, H., Cavaleri, F., Nagano, M., Drummond, N.J., Taanman, J.W.*, et al.* (2011). Parkinson's disease induced pluripotent stem cells with triplication of the alpha-synuclein locus. Nat Commun *2*, 440.

Dias, V., Junn, E., and Mouradian, M.M. (2013). The role of oxidative stress in Parkinson's disease. J Parkinsons Dis *3*, 461-491.

Ellis, C.E., Murphy, E.J., Mitchell, D.C., Golovko, M.Y., Scaglia, F., Barcelo-Coblijn, G.C., and Nussbaum, R.L. (2005). Mitochondrial lipid abnormality and electron transport chain impairment in mice lacking alpha-synuclein. Mol Cell Biol *25*, 10190-10201.

Farrer, M., Kachergus, J., Forno, L., Lincoln, S., Wang, D.S., Hulihan, M., Maraganore, D., Gwinn-Hardy, K., Wszolek, Z., Dickson, D.*, et al.* (2004). Comparison of kindreds with parkinsonism and alpha-synuclein genomic multiplications. Ann Neurol *55*, 174-179.

Ferreon, A.C., Gambin, Y., Lemke, E.A., and Deniz, A.A. (2009). Interplay of alpha-synuclein binding and conformational switching probed by single-molecule fluorescence. Proc Natl Acad Sci U S A *106*, 5645-5650.

Floor, E., and Wetzel, M.G. (1998). Increased protein oxidation in human substantia nigra pars compacta in comparison with basal ganglia and prefrontal cortex measured with an improved dinitrophenylhydrazine assay. J Neurochem *70*, 268-275.

Fornai, F., Schluter, O.M., Lenzi, P., Gesi, M., Ruffoli, R., Ferrucci, M., Lazzeri, G., Busceti, C.L., Pontarelli, F., Battaglia, G.*, et al.* (2005). Parkinson-like syndrome induced by continuous MPTP infusion: convergent roles of the ubiquitin-proteasome system and alpha-synuclein. Proc Natl Acad Sci U S A *102*, 3413-3418.

Fuchs, J., Nilsson, C., Kachergus, J., Munz, M., Larsson, E.M., Schule, B., Langston, J.W., Middleton, F.A., Ross, O.A., Hulihan, M., *et al.* (2007). Phenotypic variation in a large Swedish pedigree due to SNCA duplication and triplication. Neurology *68*, 916-922.

Fujioka, S., Ogaki, K., Tacik, P.M., Uitti, R.J., Ross, O.A., and Wszolek, Z.K. (2014). Update on novel familial forms of Parkinson's disease and multiple system atrophy. Parkinsonism Relat Disord *20 Suppl 1*, S29-34.

Fujishiro, H., Ferman, T.J., Boeve, B.F., Smith, G.E., Graff-Radford, N.R., Uitti, R.J., Wszolek, Z.K., Knopman, D.S., Petersen, R.C., Parisi, J.E., *et al.* (2008). Validation of the neuropathologic criteria of the third consortium for dementia with Lewy bodies for prospectively diagnosed cases. J Neuropathol Exp Neurol *67*, 649-656.

Georgieva, E.R., Ramlall, T.F., Borbat, P.P., Freed, J.H., and Eliezer, D. (2010). The lipid-binding domain of wild type and mutant alpha-synuclein: compactness and interconversion between the broken and extended helix forms. J Biol Chem *285*, 28261-28274.

Giasson, B.I., Murray, I.V., Trojanowski, J.Q., and Lee, V.M. (2001). A hydrophobic stretch of 12 amino acid residues in the middle of alpha-synuclein is essential for filament assembly. J Biol Chem *276*, 2380-2386.

Golovko, M.Y., Faergeman, N.J., Cole, N.B., Castagnet, P.I., Nussbaum, R.L., and Murphy, E.J. (2005). Alpha-synuclein gene deletion decreases brain palmitate uptake and alters the palmitate metabolism in the absence of alpha-synuclein palmitate binding. Biochemistry *44*, 8251-8259.

Golovko, M.Y., Rosenberger, T.A., Feddersen, S., Faergeman, N.J., and Murphy, E.J. (2007). Alpha-synuclein gene ablation increases docosahexaenoic acid incorporation and turnover in brain phospholipids. J Neurochem *101*, 201-211.

Groppe, J., Greenwald, J., Wiater, E., Rodriguez-Leon, J., Economides, A.N., Kwiatkowski, W., Affolter, M., Vale, W.W., Izpisua Belmonte, J.C., and Choe, S. (2002). Structural basis of BMP signalling inhibition by the cystine knot protein Noggin. Nature *420*, 636-642.

Hadjantonakis, A.K., Gertsenstein, M., Ikawa, M., Okabe, M., and Nagy, A. (1998). Generating green fluorescent mice by germline transmission of green fluorescent ES cells. Mech Dev *76*, 79-90.

Hashimoto, M., Hsu, L.J., Xia, Y., Takeda, A., Sisk, A., Sundsmo, M., and Masliah, E. (1999). Oxidative stress induces amyloid-like aggregate formation of NACP/alpha-synuclein in vitro. Neuroreport *10*, 717-721.

Heins, N., Lindahl, A., Karlsson, U., Rehnstrom, M., Caisander, G., Emanuelsson, K., Hanson, C., Semb, H., Bjorquist, P., Sartipy, P., *et al.* (2006). Clonal derivation and characterization of human embryonic stem cell lines. J Biotechnol *122*, 511-520.

Hsu, L.J., Mallory, M., Xia, Y., Veinbergs, I., Hashimoto, M., Yoshimoto, M., Thal, L.J., Saitoh, T., and Masliah, E. (1998). Expression pattern of synucleins (non-Abeta component of Alzheimer's disease amyloid precursor protein/alpha-synuclein) during murine brain development. J Neurochem *71*, 338-344.

Ibanez, P., Bonnet, A.M., Debarges, B., Lohmann, E., Tison, F., Pollak, P., Agid, Y., Durr, A., and Brice, A. (2004). Causal relation between alpha-synuclein gene duplication and familial Parkinson's disease. Lancet *364*, 1169-1171.

Ibanez, P., Lesage, S., Janin, S., Lohmann, E., Durif, F., Destee, A., Bonnet, A.M., Brefel-Courbon, C., Heath, S., Zelenika, D.*, et al.* (2009). Alpha-synuclein gene rearrangements in dominantly inherited parkinsonism: frequency, phenotype, and mechanisms. Arch Neurol *66*, 102-108.

Ikeuchi, T., Kakita, A., Shiga, A., Kasuga, K., Kaneko, H., Tan, C.F., Idezuka, J., Wakabayashi, K., Onodera, O., Iwatsubo, T.*, et al.* (2008). Patients homozygous and heterozygous for SNCA duplication in a family with parkinsonism and dementia. Arch Neurol *65*, 514-519.

Inman, G.J., Nicolas, F.J., Callahan, J.F., Harling, J.D., Gaster, L.M., Reith, A.D., Laping, N.J., and Hill, C.S. (2002). SB-431542 is a potent and specific inhibitor of transforming growth factor-beta superfamily type I activin receptor-like kinase (ALK) receptors ALK4, ALK5, and ALK7. Mol Pharmacol *62*, 65-74.

Jakes, R., Spillantini, M.G., and Goedert, M. (1994). Identification of two distinct synucleins from human brain. FEBS Lett *345*, 27-32.

James, D., Levine, A.J., Besser, D., and Hemmati-Brivanlou, A. (2005). TGFbeta/activin/nodal signaling is necessary for the maintenance of pluripotency in human embryonic stem cells. Development *132*, 1273-1282.

Jankovic, J. (2008). Parkinson's disease: clinical features and diagnosis. J Neurol Neurosurg Psychiatry *79*, 368-376.

Ji, H., Liu, Y.E., Jia, T., Wang, M., Liu, J., Xiao, G., Joseph, B.K., Rosen, C., and Shi, Y.E. (1997). Identification of a breast cancer-specific gene, BCSG1, by direct differential cDNA sequencing. Cancer Res *57*, 759-764.

Jiang, H., Wu, Y.C., Nakamura, M., Liang, Y., Tanaka, Y., Holmes, S., Dawson, V.L., Dawson, T.M., Ross, C.A., and Smith, W.W. (2007). Parkinson's disease genetic mutations increase cell susceptibility to stress: mutant alpha-synuclein enhances H2O2- and Sin-1-induced cell death. Neurobiol Aging *28*, 1709-1717.

Junn, E., and Mouradian, M.M. (2002). Human alpha-synuclein over-expression increases intracellular reactive oxygen species levels and susceptibility to dopamine. Neuroscience letters *320*, 146-150.

Kamp, F., Exner, N., Lutz, A.K., Wender, N., Hegermann, J., Brunner, B., Nuscher, B., Bartels, T., Giese, A., Beyer, K.*, et al.* (2010). Inhibition of mitochondrial fusion by alpha-synuclein is rescued by PINK1, Parkin and DJ-1. Embo J *29*, 3571-3589.

Kiely, A.P., Asi, Y.T., Kara, E., Limousin, P., Ling, H., Lewis, P., Proukakis, C., Quinn, N., Lees, A.J., Hardy, J.*, et al.* (2013). alpha-Synucleinopathy associated with G51D SNCA mutation: a link between Parkinson's disease and multiple system atrophy? Acta Neuropathol *125*, 753-769.

Kim, K.J., Kim, H.E., Lee, K.H., Han, W., Yi, M.J., Jeong, J., and Oh, B.H. (2004). Two-promoter vector is highly efficient for overproduction of protein complexes. Protein Sci *13*, 1698-1703.

Kruger, R., Kuhn, W., Leenders, K.L., Sprengelmeyer, R., Muller, T., Woitalla, D., Portman, A.T., Maguire, R.P., Veenma, L., Schroder, U.*, et al.* (2001). Familial parkinsonism with

synuclein pathology: clinical and PET studies of A30P mutation carriers. Neurology *56*, 1355-1362.

Kruger, R., Kuhn, W., Muller, T., Woitalla, D., Graeber, M., Kosel, S., Przuntek, H., Epplen, J.T., Schols, L., and Riess, O. (1998). Ala30Pro mutation in the gene encoding alpha-synuclein in Parkinson's disease. Nat Genet *18*, 106-108.

Lamb, T.M., Knecht, A.K., Smith, W.C., Stachel, S.E., Economides, A.N., Stahl, N., Yancopolous, G.D., and Harland, R.M. (1993). Neural induction by the secreted polypeptide noggin. Science *262*, 713-718.

Lee, H.J., Shin, S.Y., Choi, C., Lee, Y.H., and Lee, S.J. (2002). Formation and removal of alpha-synuclein aggregates in cells exposed to mitochondrial inhibitors. J Biol Chem *277*, 5411-5417.

Lesage, S., Anheim, M., Letournel, F., Bousset, L., Honore, A., Rozas, N., Pieri, L., Madiona, K., Durr, A., Melki, R.*, et al.* (2013). G51D alpha-synuclein mutation causes a novel parkinsonian-pyramidal syndrome. Ann Neurol *73*, 459-471.

Li, W.W., Yang, R., Guo, J.C., Ren, H.M., Zha, X.L., Cheng, J.S., and Cai, D.F. (2007). Localization of alpha-synuclein to mitochondria within midbrain of mice. Neuroreport *18*, 1543-1546.

Liew, C.G., Draper, J.S., Walsh, J., Moore, H., and Andrews, P.W. (2007). Transient and stable transgene expression in human embryonic stem cells. Stem Cells *25*, 1521-1528.

Liu, G., Zhang, C., Yin, J., Li, X., Cheng, F., Li, Y., Yang, H., Ueda, K., Chan, P., and Yu, S. (2009a). alpha-Synuclein is differentially expressed in mitochondria from different rat brain regions and dose-dependently down-regulates complex I activity. Neuroscience letters *454*, 187-192.

Liu, J., Jones, K.L., Sumer, H., and Verma, P.J. (2009b). Stable transgene expression in human embryonic stem cells after simple chemical transfection. Mol Reprod Dev *76*, 580-586.

Loeb, V., Yakunin, E., Saada, A., and Sharon, R. (2010). The transgenic overexpression of alpha-synuclein and not its related pathology associates with complex I inhibition. J Biol Chem *285*, 7334-7343.

Maroteaux, L., Campanelli, J.T., and Scheller, R.H. (1988). Synuclein: a neuron-specific protein localized to the nucleus and presynaptic nerve terminal. J Neurosci *8*, 2804-2815.

McKeith, I.G., Dickson, D.W., Lowe, J., Emre, M., O'Brien, J.T., Feldman, H., Cummings, J., Duda, J.E., Lippa, C., Perry, E.K.*, et al.* (2005). Diagnosis and management of dementia with Lewy bodies: third report of the DLB Consortium. Neurology *65*, 1863-1872.

McMahon, A.P., and Bradley, A. (1990). The Wnt-1 (int-1) proto-oncogene is required for development of a large region of the mouse brain. Cell *62*, 1073-1085.

Merdes, A.R., Hansen, L.A., Jeste, D.V., Galasko, D., Hofstetter, C.R., Ho, G.J., Thal, L.J., and Corey-Bloom, J. (2003). Influence of Alzheimer pathology on clinical diagnostic accuracy in dementia with Lewy bodies. Neurology *60*, 1586-1590.

Miller, D.W., Hague, S.M., Clarimon, J., Baptista, M., Gwinn-Hardy, K., Cookson, M.R., and Singleton, A.B. (2004). Alpha-synuclein in blood and brain from familial Parkinson disease with SNCA locus triplication. Neurology *62*, 1835-1838.

Moore, J.C., Atze, K., Yeung, P.L., Toro-Ramos, A.J., Camarillo, C., Thompson, K., Ricupero, C.L., Brenneman, M.A., Cohen, R.I., and Hart, R.P. (2010). Efficient, high-throughput transfection of human embryonic stem cells. Stem Cell Res Ther *1*, 23.

Muenter, M.D., Forno, L.S., Hornykiewicz, O., Kish, S.J., Maraganore, D.M., Caselli, R.J., Okazaki, H., Howard, F.M., Jr., Snow, B.J., and Calne, D.B. (1998). Hereditary form of parkinsonism--dementia. Ann Neurol *43*, 768-781.

Murphy, D.D., Rueter, S.M., Trojanowski, J.Q., and Lee, V.M. (2000). Synucleins are developmentally expressed, and alpha-synuclein regulates the size of the presynaptic vesicular pool in primary hippocampal neurons. J Neurosci *20*, 3214-3220.

Nakamura, K. (2013). alpha-Synuclein and mitochondria: partners in crime? Neurotherapeutics *10*, 391-399.

Nakamura, K., Nemani, V.M., Azarbal, F., Skibinski, G., Levy, J.M., Egami, K., Munishkina, L., Zhang, J., Gardner, B., Wakabayashi, J.*, et al.* (2011). Direct membrane association drives mitochondrial fission by the Parkinson disease-associated protein alpha-synuclein. J Biol Chem *286*, 20710-20726.

Nishioka, K., Ross, O.A., Ishii, K., Kachergus, J.M., Ishiwata, K., Kitagawa, M., Kono, S., Obi, T., Mizoguchi, K., Inoue, Y.*, et al.* (2009). Expanding the clinical phenotype of SNCA duplication carriers. Mov Disord *24*, 1811-1819.

Niwa, H., Yamamura, K., and Miyazaki, J. (1991). Efficient selection for high-expression transfectants with a novel eukaryotic vector. Gene *108*, 193-199.

Papp, M.I., Kahn, J.E., and Lantos, P.L. (1989). Glial cytoplasmic inclusions in the CNS of patients with multiple system atrophy (striatonigral degeneration, olivopontocerebellar atrophy and Shy-Drager syndrome). J Neurol Sci *94*, 79-100.

Papp, M.I., and Lantos, P.L. (1994). The distribution of oligodendroglial inclusions in multiple system atrophy and its relevance to clinical symptomatology. Brain *117 (Pt 2)*, 235-243.

Parihar, M.S., Parihar, A., Fujita, M., Hashimoto, M., and Ghafourifar, P. (2009). Alpha-synuclein overexpression and aggregation exacerbates impairment of mitochondrial functions by augmenting oxidative stress in human neuroblastoma cells. Int J Biochem Cell Biol *41*, 2015-2024.

Parker, W.D., Jr., Parks, J.K., and Swerdlow, R.H. (2008). Complex I deficiency in Parkinson's disease frontal cortex. Brain Res *1189*, 215-218.

Pasanen, P., Myllykangas, L., Siitonen, M., Raunio, A., Kaakkola, S., Lyytinen, J., Tienari, P.J., Poyhonen, M., and Paetau, A. (2014). A novel alpha-synuclein mutation A53E associated with atypical multiple system atrophy and Parkinson's disease-type pathology. Neurobiol Aging *35*, 2180 e2181-2185.

Paxinou, E., Chen, Q., Weisse, M., Giasson, B.I., Norris, E.H., Rueter, S.M., Trojanowski, J.Q., Lee, V.M., and Ischiropoulos, H. (2001). Induction of alpha-synuclein aggregation by intracellular nitrative insult. J Neurosci *21*, 8053-8061.

Polymeropoulos, M.H., Lavedan, C., Leroy, E., Ide, S.E., Dehejia, A., Dutra, A., Pike, B., Root, H., Rubenstein, J., Boyer, R.*, et al.* (1997). Mutation in the alpha-synuclein gene identified in families with Parkinson's disease. Science *276*, 2045-2047.

Poon, H.F., Frasier, M., Shreve, N., Calabrese, V., Wolozin, B., and Butterfield, D.A. (2005). Mitochondrial associated metabolic proteins are selectively oxidized in A30P alpha-synuclein transgenic mice--a model of familial Parkinson's disease. Neurobiol Dis *18*, 492-498.

Porte, L., Khatibi, S., Hajj, L.E., Cassaing, S., Berry, A., Massip, P., Linas, M.D., Magnaval, J.F., Sans, N., and Marchou, B. (2006). Scedosporium apiospermum mycetoma with bone involvement successfully treated with voriconazole. Trans R Soc Trop Med Hyg *100*, 891-894.

Protter, D., Lang, C., and Cooper, A.A. (2012). alphaSynuclein and Mitochondrial Dysfunction: A Pathogenic Partnership in Parkinson's Disease? Parkinsons Dis *2012*, 829207.

Proukakis, C., Dudzik, C.G., Brier, T., MacKay, D.S., Cooper, J.M., Millhauser, G.L., Houlden, H., and Schapira, A.H. (2013). A novel alpha-synuclein missense mutation in Parkinson disease. Neurology *80*, 1062-1064.

Raghavan, R., Kruijff, L., Sterrenburg, M.D., Rogers, B.B., Hladik, C.L., and White, C.L., 3rd (2004). Alpha-synuclein expression in the developing human brain. Pediatr Dev Pathol *7*, 506-516.

Scherzer, C.R., Grass, J.A., Liao, Z., Pepivani, I., Zheng, B., Eklund, A.C., Ney, P.A., Ng, J., McGoldrick, M., Mollenhauer, B.*, et al.* (2008). GATA transcription factors directly regulate the Parkinson's disease-linked gene alpha-synuclein. Proc Natl Acad Sci U S A *105*, 10907-10912.

Schneider, B.L., Seehus, C.R., Capowski, E.E., Aebischer, P., Zhang, S.C., and Svendsen, C.N. (2007). Over-expression of alpha-synuclein in human neural progenitors leads to specific changes in fate and differentiation. Hum Mol Genet *16*, 651-666.

Seguin, C.A., Draper, J.S., Nagy, A., and Rossant, J. (2008). Establishment of endoderm progenitors by SOX transcription factor expression in human embryonic stem cells. Cell Stem Cell *3*, 182-195.

Shi, Y., Kirwan, P., Smith, J., Robinson, H.P., and Livesey, F.J. (2012). Human cerebral cortex development from pluripotent stem cells to functional excitatory synapses. Nat Neurosci *15*, 477-486, S471.

Singleton, A.B., Farrer, M., Johnson, J., Singleton, A., Hague, S., Kachergus, J., Hulihan, M., Peuralinna, T., Dutra, A., Nussbaum, R.*, et al.* (2003). alpha-Synuclein locus triplication causes Parkinson's disease. Science *302*, 841.

Spillantini, M.G., Crowther, R.A., Jakes, R., Hasegawa, M., and Goedert, M. (1998). alpha-Synuclein in filamentous inclusions of Lewy bodies from Parkinson's disease and dementia with lewy bodies. Proc Natl Acad Sci U S A *95*, 6469-6473.

Spillantini, M.G., Schmidt, M.L., Lee, V.M., Trojanowski, J.Q., Jakes, R., and Goedert, M. (1997). Alpha-synuclein in Lewy bodies. Nature *388*, 839-840.

Stewart, M.H., Bosse, M., Chadwick, K., Menendez, P., Bendall, S.C., and Bhatia, M. (2006). Clonal isolation of hESCs reveals heterogeneity within the pluripotent stem cell compartment. Nat Methods *3*, 807-815.

Thomson, J.A., Itskovitz-Eldor, J., Shapiro, S.S., Waknitz, M.A., Swiergiel, J.J., Marshall, V.S., and Jones, J.M. (1998). Embryonic stem cell lines derived from human blastocysts. Science *282*, 1145-1147.

Turrens, J.F. (2003). Mitochondrial formation of reactive oxygen species. J Physiol *552*, 335-344.

Uchiyama, T., Ikeuchi, T., Ouchi, Y., Sakamoto, M., Kasuga, K., Shiga, A., Suzuki, M., Ito, M., Atsumi, T., Shimizu, T.*, et al.* (2008). Prominent psychiatric symptoms and glucose hypometabolism in a family with a SNCA duplication. Neurology *71*, 1289-1291.

Ueda, K., Fukushima, H., Masliah, E., Xia, Y., Iwai, A., Yoshimoto, M., Otero, D.A., Kondo, J., Ihara, Y., and Saitoh, T. (1993). Molecular cloning of cDNA encoding an unrecognized component of amyloid in Alzheimer disease. Proc Natl Acad Sci U S A *90*, 11282-11286.

Vargas, K.J., Makani, S., Davis, T., Westphal, C.H., Castillo, P.E., and Chandra, S.S. (2014). Synucleins regulate the kinetics of synaptic vesicle endocytosis. J Neurosci *34*, 9364-9376.

Wang, S., Hu, C., and Zhu, J. (2007). Transcriptional silencing of a novel hTERT reporter locus during in vitro differentiation of mouse embryonic stem cells. Mol Biol Cell *18*, 669-677.

Watanabe, K., Ueno, M., Kamiya, D., Nishiyama, A., Matsumura, M., Wataya, T., Takahashi, J.B., Nishikawa, S., Muguruma, K., and Sasai, Y. (2007). A ROCK inhibitor permits survival of dissociated human embryonic stem cells. Nat Biotechnol *25*, 681-686.

Weisman, D., Cho, M., Taylor, C., Adame, A., Thal, L.J., and Hansen, L.A. (2007). In dementia with Lewy bodies, Braak stage determines phenotype, not Lewy body distribution. Neurology *69*, 356-359.

Winslow, A.R., Chen, C.W., Corrochano, S., Acevedo-Arozena, A., Gordon, D.E., Peden, A.A., Lichtenberg, M., Menzies, F.M., Ravikumar, B., Imarisio, S.*, et al.* (2010). alpha-Synuclein impairs macroautophagy: implications for Parkinson's disease. J Cell Biol *190*, 1023-1037.

Wurtele, H., Little, K.C., and Chartrand, P. (2003). Illegitimate DNA integration in mammalian cells. Gene Ther *10*, 1791-1799.

Yoshida, M. (2007). Multiple system atrophy: alpha-synuclein and neuronal degeneration. Neuropathology *27*, 484-493.

Yu, S., Li, X., Liu, G., Han, J., Zhang, C., Li, Y., Xu, S., Liu, C., Gao, Y., Yang, H.*, et al.* (2007). Extensive nuclear localization of alpha-synuclein in normal rat brain neurons revealed by a novel monoclonal antibody. Neuroscience *145*, 539-555.

Zarranz, J.J., Alegre, J., Gomez-Esteban, J.C., Lezcano, E., Ros, R., Ampuero, I., Vidal, L., Hoenicka, J., Rodriguez, O., Atares, B.*, et al.* (2004). The new mutation, E46K, of alpha-synuclein causes Parkinson and Lewy body dementia. Ann Neurol *55*, 164-173.

Zhang, J., Perry, G., Smith, M.A., Robertson, D., Olson, S.J., Graham, D.G., and Montine, T.J. (1999). Parkinson's disease is associated with oxidative damage to cytoplasmic DNA and RNA in substantia nigra neurons. Am J Pathol *154*, 1423-1429.

Zhong, S.C., Luo, X., Chen, X.S., Cai, Q.Y., Liu, J., Chen, X.H., and Yao, Z.X. (2010). Expression and subcellular location of alpha-synuclein during mouse-embryonic development. Cell Mol Neurobiol *30*, 469-482.

Zwaka, T.P., and Thomson, J.A. (2003). Homologous recombination in human embryonic stem cells. Nat Biotechnol *21*, 319-321.